The structural design of the tailplane of the JS1 glider.

G.C. Kühn, B.Eng.

Thesis submitted in the School for Mechanical and Material Engineering at the Potchefstroom University for Christian Higher Education in partial fulfilment of the requirements for the degree of Master in Engineering.

Study leader: **Mr. A.S. Jonker**

POTCHEFSTROOM
November 2003

ABSTRACT

A new technique was developed with which to accurately predict the mechanical properties of composite materials without the influence of fluctuating thickness of the composite due to the matrix material. Using this technique a new tailplane was designed for the JS1 18m-class glider.

The designing of the tailplane was done by means of classical analytical methods with the use of LAP (Laminate Analysis Program). The methods used by LAP are based on classical lamination theory. Due to the complex shape of the new tailplane various limitations existed on the accurate analysis of the complex three dimensional structure of the tailplane.

A finite element analysis program (ANSYS) was used to model the tailplane which was designed. Using the finite element model a more accurate analysis could be done taking into account the complex shape and material lay-up of the tailplane.

To verify the analysis process of the tailplane a physical model was built from available material which was also analysed with ANSYS. The deflections obtained from the finite element modelling of the tailplane were compared with deflections of the model under similar loading conditions. The values fell within 3,5% of each other. The analysis technique used could therefore be accepted as accurate.

UITTREKSEL

'n Nuwe tegniek was ontwikkel om die meganiese eienskappe van saamgestelde materiale akkuraat te voorspel sonder dat die dikte van die matriks material 'n invloed daarop het nie. Hierdie tegniek sal gebruik word om 'n nuwe vertikale stertvlerk vir die JS1 18m-klas sweeftuig te ontwerp.

Die ontwerp van die stertvlerk is gedoen deur gebruik te maak van klassieke analitiese metodes en LAP (Laminaat Analise Program). Die metodes wat gebruik word deur LAP is gebaseer op die klassieke laminaat teorie. Weens die komplekse drie dimensionele vorm van die stertvlerk is daar sekere beperkings op die akkurate analyse van die struktuur.

'n Eindige element analise program (ANSYS) is gebruik vir die modeleering van die ontwerpte stertvlerk. Deur gebruik te maak van die eindige element analise program kon 'n meer akkurate analise gedoen word waarin die komplekse vorm en materiaal opleggings in ag geneem kon word.

Om die analise proses te verifier was 'n stertvlerk vervaardig van beskikbare materiale. Hierdie stertvlerk is ook in ANSYS gemodelleer en die defleksies van die model is vergelyk met die defleksies van die vervaardigde stertvlerk onder dieselfde belastings. Die waardes van die defleksies het binne 3,5% van mekaar geval. Die analise tegniek wat gebruik is kan dus aanvaar word as akkuraat.

ACKNOWLEDGEMENTS

I would like to thank God without Whom nothing would have been possible. I would like to express my sincerest gratitude to my promoter, Attie Jonker, for all the guidance and assistance throughout my studies. My wife, Ria, thank you for all the support and motivation during my times in need. Lastly I would like to thank my parents and friends for all their assistance and encouragement.

TABLE OF CONTENTS

LIST OF FIGURES

LIST OF TABLES

1. INTRODUCTION

1.1. History

More than one hundred and ten years have passed since Otto Lilienthal's first gliding flight and 80 years since the actual begging of glider development at the Wasserkuppe. That the sport of soaring has progressed enormously is evident by comparing the first flight of Lilienthal's of 100m with world records of today which include flights of over 3000 km and speed records in excess of 200 km/h.

These new records were possible due to a number of advancements in the aero dynamical design of the gliders. The most significant of these advancements was the advent of laminar airfoils which during the 1950's presented the manufacturers of gliders with considerable challenges. This was due to the extreme sensitivity of laminar airfoils to surface quality and profile accuracy. Standard materials used for sailplane manufacturing at the time posed the problem of increased manufacturing effort. A new manufacturing technology that made use of fibreglass was developed at about this time. The idea to manufacture these newly designed laminar airfoils with this new technology was thought up by R. Eppler and H. Nägele (1956). This idea marked the beginning of a new era in sailplane design.

Together Eppler and Nägele designed a new glider the Phoenix (Figure 1.1). It featured a laminar airfoil specifically designed by Eppler for glider applications. The Phoenix flew for the first time on 27 November 1957. (Thomas 1999:179) Performance increases due to the use of this newly designed laminar airfoil was immediately noticeable. Eight of these gliders were built in total of which some are still flying today. The Phoenix provided the first practical experience in the design and construction of fibreglass gliders.

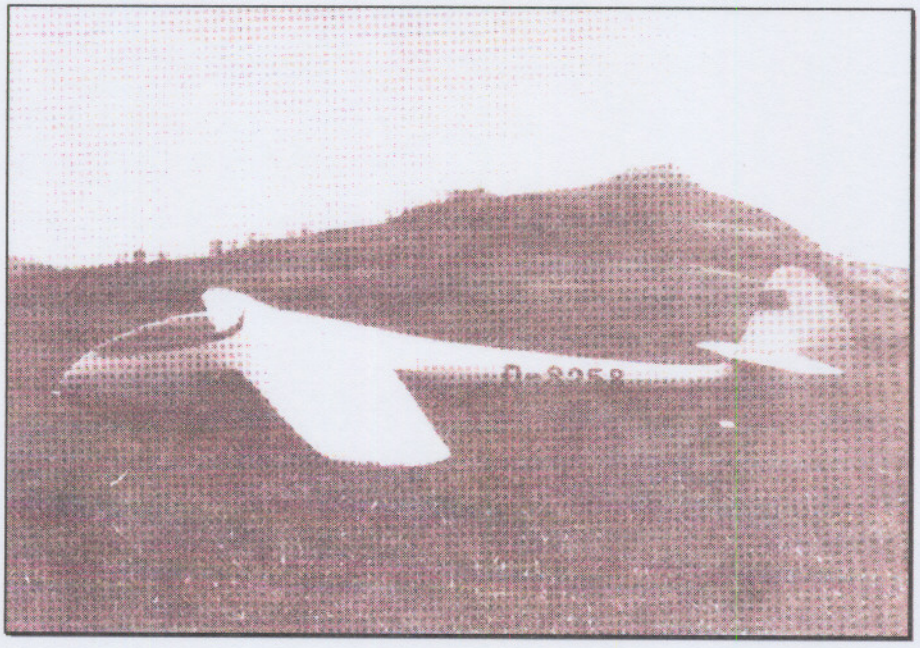

Figure 1.1: The Phoenix

1.2. Production fibreglass sailplanes

It took seven years after the first flight of the Phoenix before the first commercially produced fibreglass gliders became available. These were the Glasflügel "Libelle" and the Bolkow "Phoebus".

The series of Open Class gliders that followed on these first two fibreglass gliders dispelled all doubts regarding the superiority over gliders designed and built from traditional materials like wood and canvas. This group of gliders with wingspans of between 17 and 18 meters included the ASW 12 (1966), Cirrus (1967), Phoebus C (1967) and the Kestrel (1968). (Thomas 1999:181)

1.3. Composite materials

Since the start of the production of gliders from composite materials the industry has grown dramatically. In the past 10 years it has been showing growth of 30% per annum. (Thomas 1999:184) It is these sailplanes that have sparked most of the technological advances as well as the various manufacturing techniques associated with composite materials.

Composite materials are defined as materials that consist of a combination of two or more distinct constituents. This encompasses materials like fibreglass, fibre reinforced concrete and wood. Examples of engineering use of composites date back to the use of straw in clay as a construction material by Egyptians. (Swanson 1997:1) Fibre reinforced plastics, which form part of this group of materials known as composite materials have become increasingly important over the past fifty years, and is now the first choice for fabricating structures where low weight in combination with high strength and stiffness are required. Such materials are sometimes referred to as "high performance" composites, and would often be composed of carbon fibres and epoxy resin. (Matthews et al. 1997:2)

Materials and structures have largely been responsible for major performance improvements in many aerospace systems. The development of computational structures and the development of advanced composite materials ("high performance") over the past 30 years have improved structural performance, reduced operational risk and shortened development time. (Noor et al. 1999)

Figure 1.2 shows the projected reduction in subsonic operating costs by the year 2020 due to the use of these new technologies in a range of different aerospace applications.

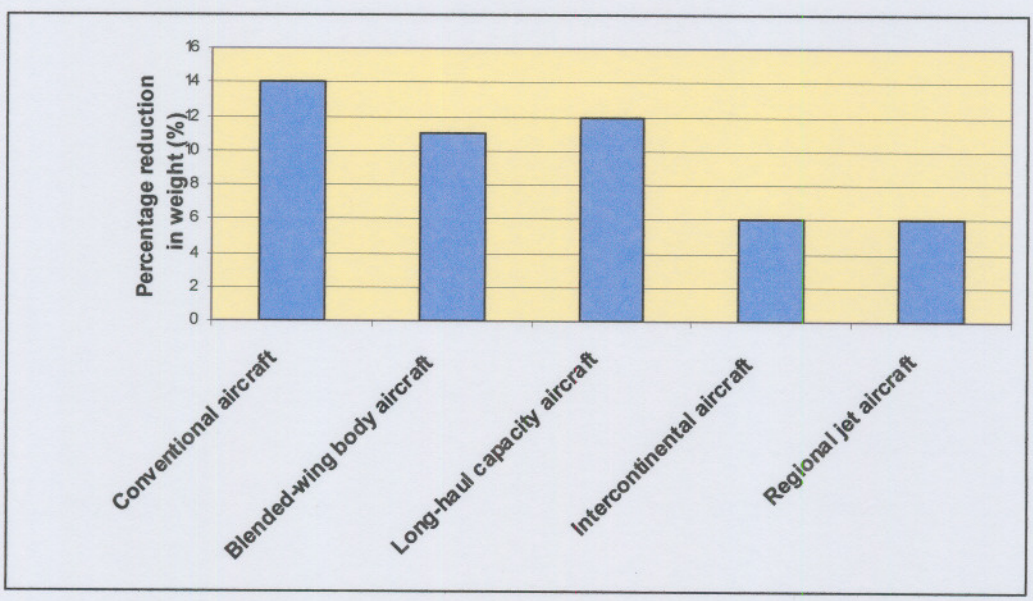

Figure 1.2: Percentage reduction in operating costs due to the use of new manufacturing techniques

It can be seen from Figure 1.2 that advances in structural technologies, which include advances in the material technologies will play a major role in the reduction of operating cost in all the major aerospace industries.

Besides these reductions of both the weight and operating costs, composite materials offer another major advantage over classical materials. Due to the manufacturing techniques used for composite materials, any complex three-dimensional shape can be produced. This gives the designer of new aerospace geometries total freedom in the design process. This is also one of the major reasons why composite materials are used in the manufacturing of gliders.

The structural analysis of composite materials are however extremely complex. This is mostly due to the anisotropic properties of composite materials. Various analytical techniques have been developed over the years. All these techniques are however only capable of analysing extremely simple geometries, limiting the shape of the structure being designed.

Numerical analyses methods provided the answer to these limited analytical techniques.

1.4. Numerical methods

The numerical method used predominantly throughout the industry with which to analyse composite material structures is the finite element method. The finite element method is merely an alternative approach to solving the governing equations of a structural problem. The finite element method and the classical analytical methods will produce identical results for the same problem.

With the finite element method the structure which is to be analyzed is imagined as being composed of discrete parts (i.e. finite elements). These finite elements represent the structure, its composition and the loadings imposed thereon. The major advantage which numerical analysis methods have over the classical analytical methods is the possibility to analyse complex three dimensional structures.

1.5. Problem identification

The Akavlieg PUK is currently developing a new 18m-class glider. This glider will have an all composite structure. The purpose of this study is to structurally design the horizontal tailplane for the JS1 glider.

1.6. Objectives of study

There are four main objectives for this study. The first is to clarify the analysis methods that will be used in the design of the rest of the glider. Various analysis methods will be investigated and compared to obtain the best possible technique for the designing of the composite structures of the glider.

The second objective is the development of a method for obtaining the material properties of the materials used throughout the glider. This includes the actual mechanical testing of the various composite materials used in the manufacturing of the sailplane as well as the development of a technique which simplifies the design process.

Thirdly is the actual designing of the new composite tailplane for the 18m sailplane. This designing will be done using classical lamination theory as well as theory developed for the calculation of the properties of composite laminate beams. This design will then be analyzed using numerical methods using a commercial finite element code (ANSYS).

Lastly the tailplane which was designed will then be manufactured and statically tested in order to obtain actual data to compare to the values obtained using the design techniques described.

1.7. Outline of Study

Chapter 2 discusses the relevant literature on the subject, including composite materials as well as discussing the various techniques used in literature for the analytical and numerical analysis of composite materials.

The techniques used for the calculation of the mechanical properties of the composite materials are discussed in chapter 3. The chapter also includes technique used for the description of the mechanical properties of the composite materials used in the design process of the tailplane of the glider.

In chapter 4 the calculations of the aero dynamical loads acting on the tailplane for the various flight conditions are shown.

Chapter 5 discusses the analytical design of the tailplane of the glider. The primary lay-up schedule as calculated using the analytical methods is also given.

Chapter 6 focuses on the numerical analysis methods used in the analysis of the tailplane. All assumptions and reasoning made for the method is discussed. The techniques used for the creation of the tailplane model in ANSYS as well as the different analyses done are also discussed.

In chapter 7 the verification of the numerical model is done. The technique used for the loading of the manufactured tailplane is discussed. The actual values obtained through mechanical testing is compared to the values obtained using the finite element model to quantify the accuracy of the design and analysis techniques.

Chapter 8 consists of a brief conclusion and recommendations for further studies.

2. LITERATURE STUDY

2.1. Introduction

A complete composite structure is proposed for the new 18m glider, called the JS1. The orthotropic nature of the materials from which this composite structure will be manufactured sets them apart from normal engineering materials and therefore requires different analysis and design methods.

This chapter will look at the basic design methods used for composite materials. It will be divided into three sections namely Composite materials, Analytical design and Numerical analysis.

2.2. Composite materials

2.2.1. Description

Composite materials are defined as materials which consist of two distinct constituents. Composite materials are therefore also heterogeneous materials. These materials are being used increasingly in the manufacturing of high performance structures such as gliders due to their advantages over classic metal materials in strength, stiffness and weight.

Swanson (1997:1) describes the use of composites in structural applications not merely as structural designing but also as material designing. This is due to the orthographic properties which composite materials possess. The designer has the freedom to select the optimum fibre orientation for best possible material performance.

Military aircraft designers were the first to realize the tremendous potential of composites over traditional metallic materials with high specific strength and stiffness properties. The performance and manoeuvrability of these vehicles depends heavily on weight. Composite construction also leads further to smooth surfaces which reduces the overall drag of the aircraft.

According to Thomas the first composite material glider was manufactured in the late 1950's (Thomas, 1999:177). It was designed by Eppler and Nägele and was built solely from fibreglass. This was the first step into a new era in glider design, opening the door to what was unimaginable performance increases.

Composite materials offered far superior characteristics when compared to classic materials used in aircraft design. This is largely due to the possibility to orientate the reinforcement fibres of the composite material in the direction in which the forces act upon the structure. This therefore minimises the amount of material needed to support the structure in the directions in which no or little forces exist.

A number of problems however also arose with the use of these materials. The first of these involved the obtaining of the properties of the different composite materials. The mechanical properties of the various constituents of the composite structure each contributes to the final properties of the structure which is manufactured. The reinforcement materials used in the structure however plays the most important role in the final mechanical properties.

2.2.2. Reinforcement materials

Although there are a large number of different reinforcement fibre materials available on the market today only three fibre materials are used predominantly in the glider manufacturing industry today. These are

- E-glass glass fibres,
- Carbon fibres and
- Kevlar fibres.

These fibres are used in different applications in the manufacturing of gliders. This is due to the large differences in the physical properties of these materials.

2.2.2.1. E-glass glass fibers

Glass fibres are the most widely used fibres in the composite industry. This is mainly due to the low cost of the fibres as well as the low cost of the manufacturing techniques used.

Glass fibres are used widely in the manufacturing of glider parts. All components that do not require high stiffness are manufactured from glass fibres. Three reasons are given for the use of glass fibres in glider manufacturing. The first and most important is to minimize the overall price off the glider. The second reason is that glass fibres are the easiest of all the different types of reinforcement materials to use in the manufacturing process. The third reason is the good corrosion resistance that glass fibres possess.

2.2.2.2. Carbon fibres

Carbon fibres are used extensively throughout the different parts of gliders. This is due to the relatively high stiffness-to-weight and high strength-to-weight ratios of these fibres. Carbon fibres are also the second least expensive reinforcement material used in composite materials manufacturing today.

Carbon fibres are however not as workable as glass fibres. The main reason for this is the fact that it is extremely difficult to physically see whether carbon fibres are wetted out properly. It is therefore customary not to aim for an extremely high fibre-resin ratio when working with these fibres. This however negatively influences the overall strength to weight ratio of the material.

2.2.2.3. Kevlar fibres

The most expensive of all the different reinforcement fibres used in modern glider manufacturing are Kevlar fibres. Kevlar possesses higher tensile strength and stiffness to glass. Due to the low density of Kevlar the specific tensile strength thereof even surpasses that of carbon fibres. The major disadvantage of Kevlar fibres are the low compressive strength properties.

Due to its light weight and high mechanical properties Kevlar is slowly replacing glass fibres as reinforcement material in modern gliders. A number of factors

however keep them from totally replacing glass fibres. The first is the high cost of Kevlar fibres compared to glass fibres. The second is the difficulty working with Kevlar fibres which become fluffy whenever there are any alterations made to the reinforcing material. Thirdly, Kevlar is known to mechanically degrade when subjected to ultra-violet light.

2.2.3. Core materials

According to Loken et al. (1988:2) a core structure is one in which a low density, shear rigid material is used to separate two thin face sheets. The face sheets carry all the in-plane compressive and tensile loads. The resulting structure is extremely stiff while still being very light.

The advantage that cored structures provide to the manufacturing of glider parts is the fact that fewer parts are needed for the final structure. This is evident from the fewer number of ribs needed in wing structures to prevent buckling of the skins. According to Loken et al. (1988:5) small aircraft wing skins consist of up to 48 ribs without the use of cored materials. Using cored materials the number of ribs falls to a mere 12.

2.2.4. Mechanical testing

Due to the major influence of the manufacturing process on the material properties of the composite materials the properties need to be obtained with experimental testing. According to Gibson the testing methods used for conventional metallic materials are usually not applicable to composite materials due to their special characteristics such as anisotropy, coupling effects and the variety of possible failure modes (Gibson, 1994:374). A large number of testing methods have been developed over the years to accurately obtain the mechanical properties of the composite materials.

The American Society for Testing and Materials (ASTM) has adopted some of these testing methods as standards to which the mechanical testing needs to comply. Several different types of tests are prescribed for testing the different properties. The methods available for the testing are described briefly below.

2.2.4.1. Tensile testing

The ASTM standards describing the tensile testing of composite specimens are detailed in the D3039M-93 standard. Dog bone specimens which are used for isotropic materials are not acceptable for laminate tensile testing (Gibson, 1994:375). Flat coupons therefore need to be made to ensure that the values obtained using tensile testing is correct.

The values obtainable using tensile testing methods are E_{11}, E_{22}, ν_{12}, and ν_{21}. According to Gibson (1994:377) the tensile testing works well for the orthographic composite materials as uniform stresses are produced throughout the specimen. If nonuniformities in the stress distribution arise it is due to off-axis fibres which exhibit shear coupling effects. If the data extracted therefore produces non-linear stress-strain relations it is due to the off-axis fibre orientation of the specimen.

2.2.4.2. Compressive testing

According to Gibson (1994:378) compression testing of composite laminates still is a part of mechanical testing of composite laminates which leads to a lot of different opinions. Even in the light of the ASTM D3410M-93 standard which describes the method for compression testing of laminates. According to Tarnopol'skii et al. (1998:787) the main problem with compression testing of flat specimens is the selection of a loading method that ensures compressive failure.

In compression testing, great care needs to be taken to ensure stability of the specimen. Buckling of the specimen side faces are not always detectable and leads to erroneous strain measurements. Special test fixtures are used to prevent overall buckling of the specimen (Tarnopol'skii et al., 1998:787).

Another method of compression testing of laminates is by manufacturing a beam comprising of laminate skins attached to a core material. The beam is than simply supported and subjected to bending loads. Values calculated with the use of this method are according to Gibson returns good compression values for the laminates (Gibson, 1994:389). The manufacturing of the specimens used for this testing is however expensive.

The compression testing done on the laminates used in the glider design are done with the ASTM D3410M-93 standard as basis. A specimen is made according to the standard and is then placed in special test fixture which prevents the specimen from buckling. This method was chosen over the beam bending because it is relatively inexpensive.

2.2.4.3. In-plane shear testing

Various types of in-plane shear testing exist. Four of the most widely used methods according to Whitney et al. (1982) are the $[\pm 45]_S$ lamina test method, the off-axis tensile test method, the rail shear test and the torsion test method.

The ASTM has adopted two of these methods in its standards. The first is the rail shear test method and the second is the $[\pm 45]_S$ lamina test method. These methods are described in the D3518M-91 and D4255-83 standards.

Lee and Munro (1986) evaluated the different in-plane shear test methods taking into account different criterion including reproducibility, testing cost, fabrication cost and accuracy. The $[\pm 45]_S$ lamina tensile test was rated best along with the Iosipescu shear test method.

The Iosipescu testing method is however more complex than the $[\pm 45]_S$ lamina test and is not specified in the ASTM standards. The $[\pm 45]_S$ lamina test will therefore be used on the analysis of the in-plane shear testing.

2.2.5. Composite material analysis method

Laminate analysis theory as presented by Swanson (1997:187) and Gibson (1994:190) was developed to calculate the stress and strain in orthographic materials.

Laminate analysis theory is basically a lower order version of the theory describing the properties of fully orthographic materials. The theory characterizing orthographic materials involves the depiction of the stress-strain relations of the materials in all three major axis directions. These relations are then written in matrix forms to model

the material. The stress-strain stiffness matrix characterizing three-dimensional orthographic materials is a 6X6 matrix.

Many engineering structures like the tailplane skins are thin in the through-the-thickness direction of the lay-up. According to Swanson the theory used for orthographic materials can then be simplified to a two-dimensional subset. This is done by assuming that the tensile stresses and the shear stresses in the through-the-thickness direction of the laminate are zero. A 3X3 matrix is then used to describe the stress-strain stiffness relations of the laminate.

It can be seen that the number of equations governing the stress-strain stiffness relations are significantly less using the composite lamination theory compared to the theory describing orthographic materials. It is thus sensible to design the tailplane using laminate analysis theory.

2.3. Tailplane design methods

2.3.1. Force analysis

The first step in the design process of the tailplane of the new glider is to calculate the aero dynamical forces acting thereon.

The calculation of the air loads acting on the tailplane is done according to the JAR22. The JAR22 is regulations complied by the Joint Aviation Authority (JAA) specifying the structural characteristics to which any new glider must comply.

The loads specified by the JAR22 which the tailplane of the glider must carry are divided into three classes. These classes are the loads acting on the tailplane to firstly balance the overall moment generated by the glider, the manoeuvring loads and finally the gust loads.

The final force acting on the tailplane needs to be multiplied by a safety factor specified by the JAR22. The JAR22 specifies a safety factor of 1.5. According to Weber et al. (2002:3) a further 15% is added to this factor if the structure is to be only

statically tested. This raises the safety factor to 1.725. This safety factor will be used for the designing of the tailplane.

2.3.2. Structural design

According to Hollmann the wing is divided into three basic structures. Each of these three structures fulfils a different role in the final structure, the wing. These three structures are the wing spar flanges, wing spar shear web and lastly the wing skins (Hollmann, 1996:85).

The wing spar, consisting of the spar flange and shear web, must transfer the wing bending moments and the corresponding shear loads along the wings length to where it attaches to the fuselage and along to the centre of the aircraft. According to Hollmann most aircraft usually use only a single main spar to carry all the bending loads. Another rear spar is sometimes added to aid in the carrying of the wing twisting moment.

Designing using this technique is conservative and the final structure consisting of the different substructures should be stronger due to the influences of all the separate parts on one another.

2.3.3. Composite beam design

The technique used by Cremer (1995:48) for the structural sizing of the composite components of the wing structures are based on classic metal stress analysis methods. The spar of the structure is designed using the equations of normal beam theory for isotropic materials.

According to Swanson the use of these equations for the analysis of composite beam structures do not hold. This is due to the fact that the formula is based on uniformly varying stress distributions. Stresses in composite beams can be very nonuniform due to changes in the material properties from layer to layer. The basic principle behind the theory of composite beam analysis are that the moments found by integrating the axial stress times a moment arm over the entire area and the axial strain varies linearly with distance from the neutral axis. These principles are then added separately to the

web and flanges of the composite beam to obtain the governing equations for the composite beam.

Swanson has developed four different sets of governing equations for the different laminated I-beam structure used. These cases are symmetric narrow flanges, symmetric wide flanges, nonsymmetric narrow flanges and nonsymmetric wide flanges. The major difference between wide and narrow flange theory involves the "anti-elastic" effect that distinguishes beam bending from plate bending. Usual beam bending theory assumes that there is no moment in the transverse direction of the flanges. In wide flanges there can however be a build up of transverse moment within the flanges.

In the case of the I-beam characterising the tailplane only wide flange theory will be used. This is due to the relatively wide flanges compared to the overall thickness of the beam. The flanges therefore will react to the bending forces in a manor reflecting that of plate bending. The wide flange theories are therefore used in the analytical designing I-beam characterising the tailplane.

2.4. Numerical analysis methods

Analysis of complex three dimensional composite structures is virtually impossible using only analytical methods. This is mainly due to the difficulty in constructing approximation functions for these geometries. The use of numerical methods facilitates the solution of these equations for problems of practical importance (Ochoa et al., 1992:37).

Several types of finite element analysis models have been developed for composite plate theories. These methods can be divided into the following three major categories namely displacement models, hybrid models and equilibrium models. The displacement models are based on the principle of virtual displacement. The hybrid model is based on modified variational statements of the plate theories in which both displacements and stresses are independently approximated. The equilibrium model is based on the principle of virtual forces. According to Ochoa et al. the displacement finite element models are the most natural and commonly used in commercial finite

element programs. The finite element code used for the numerical analysis of the tailplane is ANSYS.

2.5. Conclusion

In this chapter the various methods used in the design process of composite materials were discussed. These included the methods used for the obtaining of the mechanical properties of the composite materials as well as the various techniques used in the design process of the composite material structures. The limitations of the techniques were also discussed. The design mythology of the composite tailplane was based on a combination of the methods discussed in this chapter.

3. COMPOSITE MATERIAL PROPERTY DATABASE

3.1. Introduction

The mechanical properties of composite materials are not only characterized by the constituting components but it is also affected by the process which is used in the manufacturing of the product. It is thus necessary that the specific process used for the manufacturing of composite components be qualified and the material properties obtained by this process be verified by experimental testing (Gibson, 1994:374.)

Due to of the orthotropic nature of composite materials many of the conventional metallic material mechanical testing methods are usually not applicable. The technologies involved with the testing of composites has become as sophisticated as that of the analytical methods.

In this chapter the basic techniques, methods and assumptions that will be used in the calculation of the composite material mechanical characteristics from the experimental data will be discussed.

3.2. Literature material data

The composite materials used in the design and analysis of the new tailplane first needs to be identified. Three major types of composite materials are used throughout modern gliders. These three different types are listed below:

- Carbon fibre,
- Glass fibre and
- Kevlar fibre.

Calculation of the composite material properties of these three fibres needed to be done before any design of the tailplane could be done.

The first step in the calculation of the material characteristics is the evaluation of data as collected from literature. An extensive study was made using information from various sources. These sources are listed below:

- Hanover University Akaflieg
- Hollmann, M. 1996. Modern Aircraft Design, Volume 1 4th Edition. California: Aircraft Designs, Inc. 236p.
- Swanson, S.R. 1997. Advanced Composite Materials. Saddle River: Prentice-Hall, Inc. 249p.
- GIBSON, R.F. 1994. Principles of composite materials mechanics. Singapore: McGraw-Hill, Inc. 425p.
- V.d. Walt, J.P. 1999. Mechanical testing of composite materials. Potchefstroom

A material property database was set-up in a spreadsheet. The data obtained from the literature did not take into account the manufacturing processes of the composite materials. The data was therefore expected to be scattered over a wide area.
Figure 3.1 illustrates the normalized tensile strength and Poisson ratio of woven carbon fabric. The other properties and materials showed similar results.

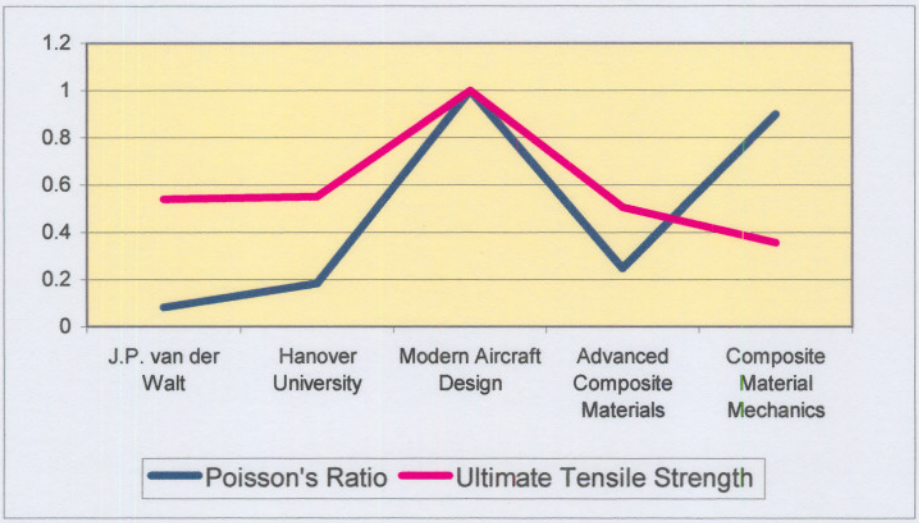

Figure 3.1: Normalized mechanical properties for woven carbon fabric

It is thus clear that mechanical properties from literature are not suitable. This as well as the fact that aircraft certification requires a proof of mechanical properties,

prompted a detail investigation into the process of experimental testing to obtain mechanical properties for the various composite materials used.

3.3. Experimental testing

Having decided upon the different types of composite reinforcement materials which will be used in the design of the tailplane a list of the material properties needed, had to be compiled. This list serves as the basis upon which the types of mechanical tests used for the calculations are chosen. The different material properties needed are listed below:

- Ultimate tensile strength, $\sigma 11$ and $\sigma 22$
- Ultimate compression strength, $\sigma 11$ and $\sigma 22$
- Ultimate shear strength, $\tau 12$
- Moduli of elasticity, E11 & E22
- Shear moduli, G12
- Ultimate bearing strength.

Due to the orthotropic nature of composite materials various testing procedures need to be used for the calculation of the mechanical properties of the composite laminates. These include tensile and compression testing as well as bearing stress testing. The American Society for Testing and Materials (ASTM) prescribes various standards that need to be adopted for the testing of these composites. These standards where used as a basis in all of the procedures described below.

3.3.1. Tensile testing

The ASTM standard specifies the dimensions of the tensile test specimens to be: length 229mm with a length to width ratio of 18 and a length to thickness ratio of between 100 and 225. To prevent damage to the specimen during testing, the loads are transferred to the specimens by aluminium sheet metal bonded to the ends of the specimen.

A typical tensile test specimen is shown in Figure 3.2.

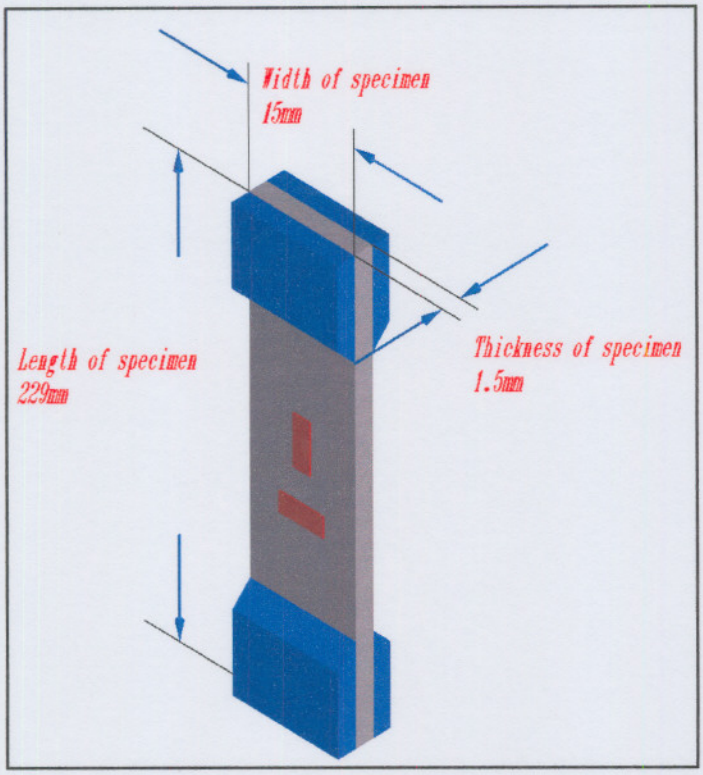

Figure 3.2: Tensile specimen size and strain gauge mounting

For the calculation of E11, E22, υ12 and σten specimens are prepared with fibre orientations axially along the specimen. A variable force is then applied over the specimens, which slowly increases the internal stresses. The elongations, ε11 and ε22, can then both be measured by means of the strain gauges mounted directly onto the specimen surfaces. These strain gauges are mounted axially and longitudinally on the specimens as illustrated in Figure 3.2. The data of the experiment is then stored for later manipulation.

The ultimate tensile strength is the easiest of the mechanical properties to obtain. It is simply the stress value at failure. This is merely done by slowly increasing the force applied over the specimen until it ultimately fails. From the data logged and the geometry of the specimen the ultimate tensile stresses of the composite specimens are then obtained. No strain gauges are applied to these specimens as there is no need for strain values.

Using the values of the ultimate tensile strengths of the various materials we know at what tensile force they will fail. To ensure that the specimens fitted with strain

gauges do not break they will only be subjected to a maximum of 80% of their ultimate tensile stresses. The data obtained from these test are then represented on a graph producing a straight line though the origin from which the Young's modulus can then be calculated.

As example the tensile test data obtained for woven carbon fibres is discussed. The stress-strain relation for the fabric is shown in Figure 3.3. The linear elastic deformation is illustrated clearly in the data.

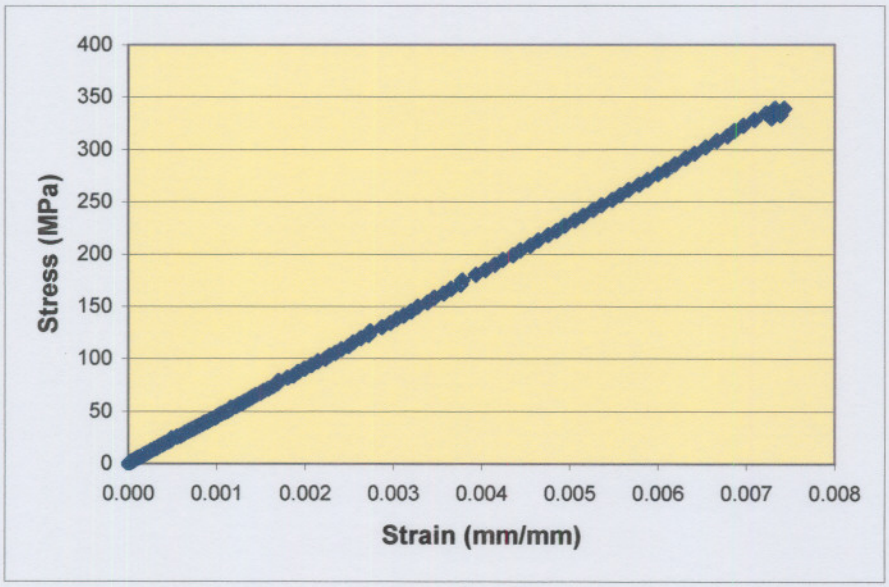

Figure 3.3: Stress-strain relation for carbon fabric

The Young's modulus in this example is 46 GPa.

3.3.2. Compressive testing

Compression testing of composite materials are one of the most interesting and difficult challenges in the process of composite testing. Even though an ASTM standard for compression testing has been published, there is still much discussion regarding the alternative test methods as discussed by Berg et al. and Schoeppner et al. The most important aspect in the compressive testing of composites is to ensure that no buckling occurs in the specimen.

Special test fixtures are used to ensure specimen stability. The fixture designed for the compression testing of the composites, is based on that of the ASTM standard for compression testing as explained in procedure A of the standard D 3410-87. The specimens are firstly inserted into the test fixture and then clamped to ensure that buckling of the specimen side face is prevented. Compression loading is then applied over the fixture.

Figure 3.4 illustrates the compression fixture manufactured for use in the compression testing of the composite materials.

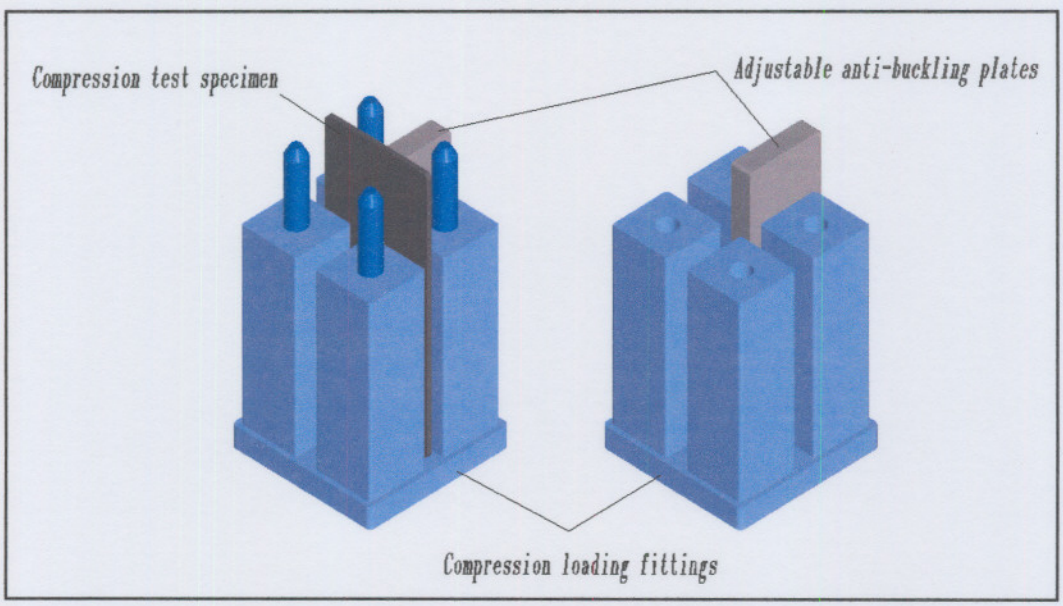

Figure 3.4: Compression testing fixtures

The data of the compression test can then be logged in real-time and can then be used to obtain the maximum compression strength of the different composite materials. The data obtained from the compression testing of woven carbon is shown in Figure 3.5.

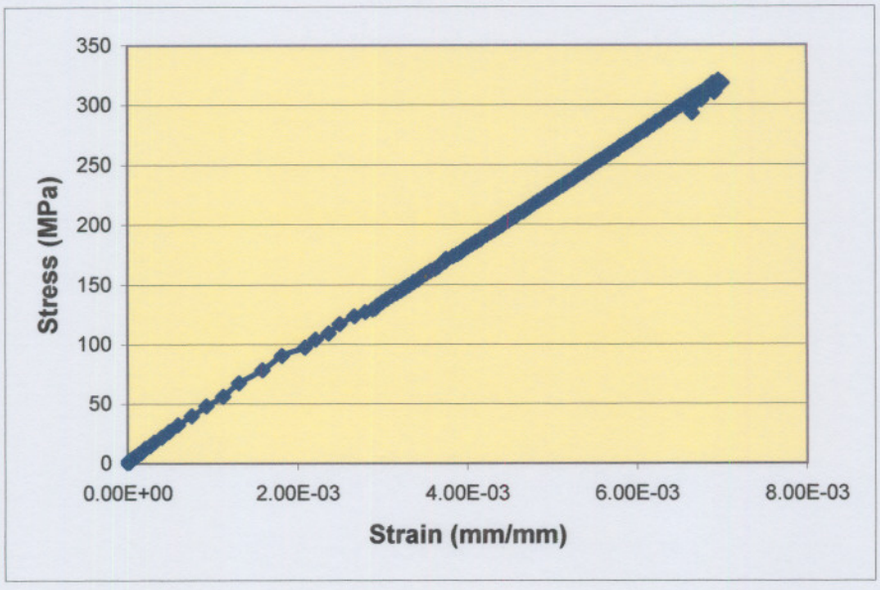

Figure 3.5: Stress-strain diagram for compression testing of bi-directional carbon

3.3.3. In-Plane Shear Test

There are four widely used methods for testing in-plane shear of composites. (Whitney 1982:67) These are the $[\pm 45]_s$ laminate tensile test, the off-axis tensile test, the rail shear test and the torsion test methods. Only two of these methods have been adopted as ASTM standards. (Gibson, 1994:382) The two methods are the $[\pm 45]_s$ laminate test method, described in D3518/D3518M of the ASTM standards, and the rail shear test, described in D4255/D4255M of the ASTM standards. It was decided that the $[\pm 45]_s$ laminate tensile test method is the most efficient way of measuring the in-plane shear stresses and that it would be used for the obtaining of the data.

The test specimen is manufactured so that all the layers used are orientated at ±45 degrees to the specimen axial direction and the strain gauges are applied to the specimen as shown in Figure 3.2. The axial and lateral strain can therefore be measured for different stress conditions.

The axial strain of the specimen is then used to obtain the shear modulus G_{12}. This is done with the use of equation 3.1 where c = cosθ and s = sinθ with θ the angle of the plies i.e. 45°. (Gibson, 1994:52)

$$E_x = \frac{1}{\frac{1}{E_1}c^4 + \left[-\frac{2\upsilon_{12}}{E_1} + \frac{1}{G_{12}}\right]c^2 s^2 + \frac{1}{E_2}s^4} \qquad \text{...(3.1)}$$

The shear stress τ_{12}, is also obtainable from this experiment as it is related to the uniaxial tensile stress σ_x acting on the laminate specimen. The relationship of these two stresses is given by equation 3.2 . (Gibson, 1994:390)

$$\tau_{12} = \frac{\sigma_x}{2} \qquad \text{...(3.2)}$$

A typical stress-strain relationship obtained using this method on woven carbon fabric is illustrated in Figure 3.6.

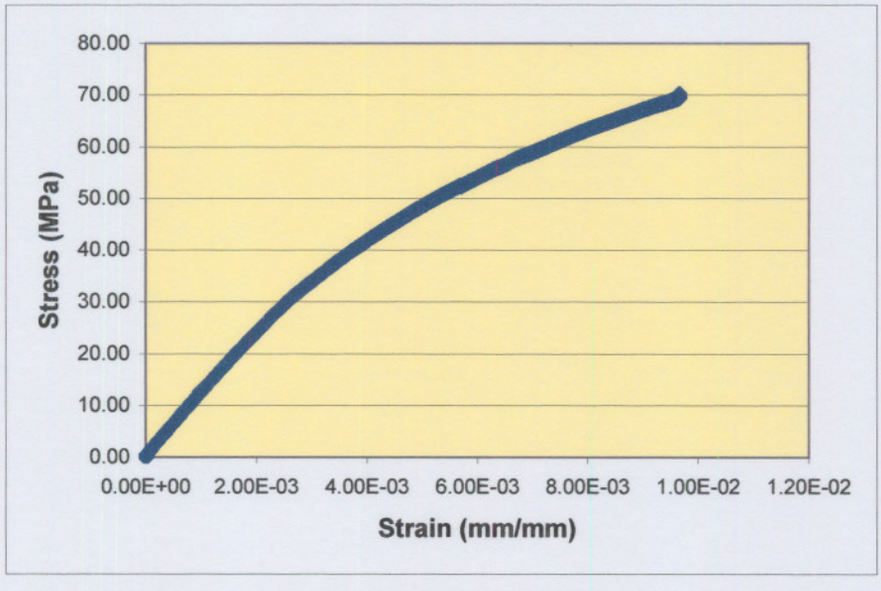

Figure 3.6: Stress-strain relation for in-plane shear test of woven carbon

3.3.4. Bearing stresses

Composite materials are also used in the manufacturing of bearing fittings in the gliders. An example of this is the main pins that connect the two wings of the gliders together or any other butted connection throughout the composite skin. It is thus necessary to calculate the ultimate bearing stresses for the various materials that will be used for these applications.

A test procedure was designed for this reason. The instrumentation used was the Tinus Olsen tensile testing machine as well as a specially designed fixture. The fixture consists of four mild steel plates of which the thickness was calculated to withstand the forces involved. Two of these plates where then fitted to the top of the testing bed and two where fitted to the bottom of the bed.

Three holes where reamed into the composite material test sections. Great care was taken to ensure that the holes where correctly positioned. The test sections as well as the fixture are illustrated in Figure 3.7. The test was designed so that the bearing area in the composite specimen was the weakest. This ensures that other failures will not affect the test.

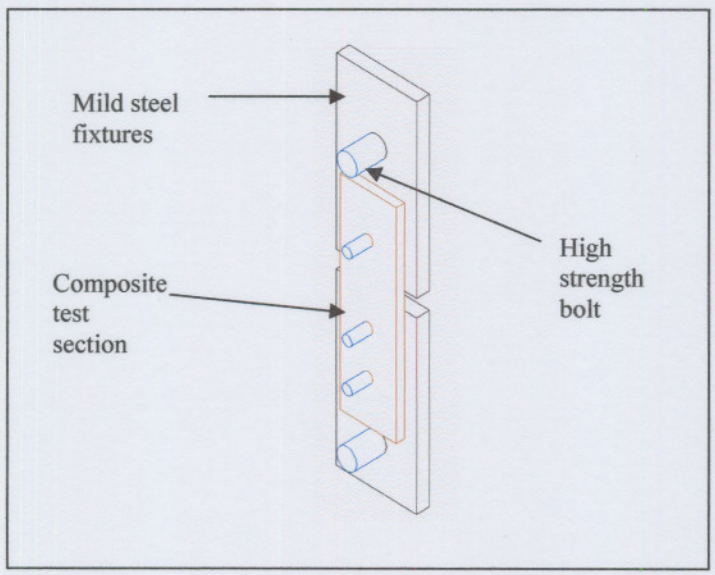

Figure 3.7: Testing fixture for obtaining bearing stresses

By slowly applying the load, the single bolt in the specimen will overload the bearing area. This will show up as a linear region in the stress-strain relationship from which the maximum bearing stress can be calculated.

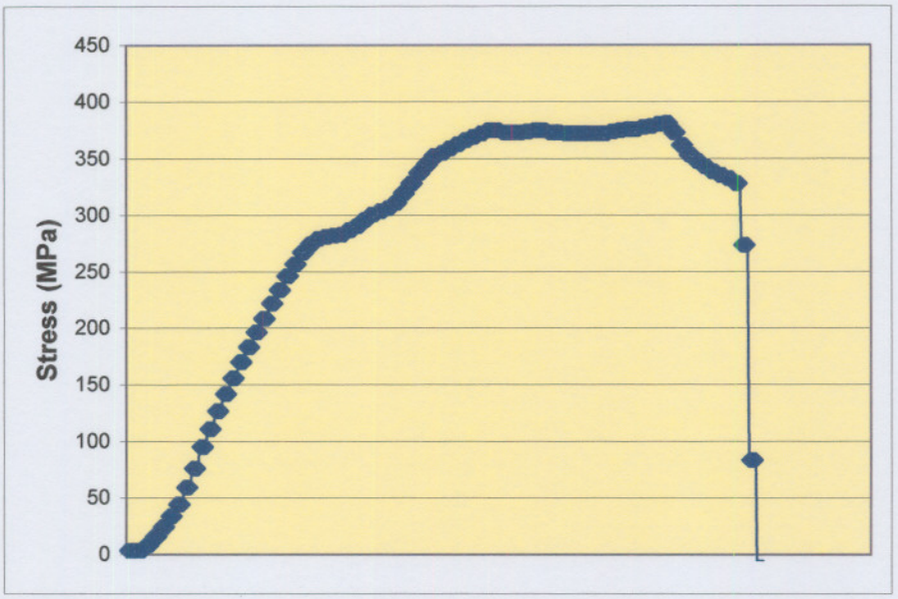

Figure 3.8: Typical behaviour of woven glass fibre to bearing stresses

In Figure 3.8 it can be seen how the force applied over the test section was slowly increased, increasing the internal bearing stresses. This is a typical diagram illustrating the reaction of the composite materials to bearing stresses. It can be seen that the stresses increase slowly up to 275 MPa where the material starts to give way for the first time. If one however continues applying more load to the section the stress increase again. This is due to the increase of the area. The diagonal fibres start to displace to the sides of the section.

Once the composite material starts deforming plastically it is of no use. In the design we therefore only worked with the maximum stresses that the composite material could withstand while only deforming elastically. In the case of the glass fibres as shown above the maximum bearing stresses which could be used is 275 MPa.

3.3.5. Experimental Test Results

To ensure that representative data is obtained for the various materials which are tested, a minimum of 5 tests were done for each material. The data obtained from the mechanical testing was then compared to the data found in literature. From the comparison it could be seen that the value fell within acceptable ranges of the literature data. Table 3.1 shows the material property database which will be used in the design of the tailplane.

	σ_{11} Tension (MPa)	σ_{22} Tension (MPa)	σ_{11} Comp (MPa)	σ_{22} Comp (MPa)	τ_{12} (MPa)	E_{11} (GPa)	E_{22} (GPa)	Poisson	G_{12} (GPa)
Glass fibre	223	223	174	174	82.5	23.8	23.8	0.28	5.4
Kevlar fibre	485	485	207.5	207.5	52.5	49.5	49.5	0.185	2.2
UD Carbon	1180	89	689	48.5	121	107	5.8	0.05	0.98
Woven carbon fibre	525	525	327.5	327.5	60	48.2	48.2	0.08	2.2

Table 3.1: Experimental composite material mechanical properties

3.4. Lamina theoretical design values

Traditional design techniques used for composites do not differ from those used in the design with isotropic materials. The only difference between the two is that composite material analysis takes into account the orthographic properties of the composite material.

Using these traditional methods we however assume that the magnitude of the forces acting on a composite can increase if the composite area increases. This assumption only holds ground in the case of traditional metallic materials. Composite materials are heterogeneous.

In heterogeneous materials the strength of the material is not the same throughout its volume. The material properties are influenced by the composite constituents. For

instance the tensile strength of a composite does not increase with the addition of matrix material.

A need arose for a technique which could simplify the final designing of the composite materials for the tailplane. This technique has to accurately describe the mechanical properties of the composite material with the use of certain known governing parameters.

The first step in the creation of this technique is defining of the governing parameters. These are the parameters by which the composite materials are differentiated from one another. The first parameter is the type of composite reinforcement used. The second is the type of weave of the fibre reinforcement used in the composite. Thirdly is the type and amount of matrix material used in the composite (volume fraction).

The type of reinforcement material used is the largest contributing factor to the mechanical properties of the composite. This can be seen from data obtained from literature regarding the strength of the different fibres used in reinforcement materials as illustrated in Figure 3.9.

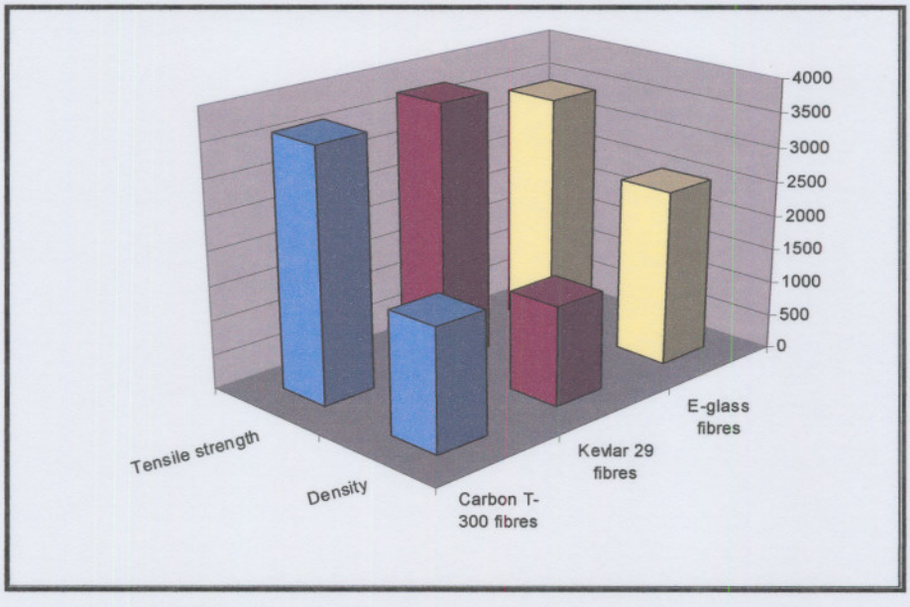

Figure 3.9: Tensile strength and density of various reinforcement fibres

The weave pattern of the reinforcement material also plays an important role in the final mechanical properties of the composite material. The reason for this is the angles at which the fibres are woven and the thickness of the reinforcement material. This is illustrated in Figure 3.10. The overall fibre density of the twill woven fabric is higher than that of the plain woven fabric. The strength of the twill woven material will therefore be higher for the twill woven fabric when used in a composite structure.

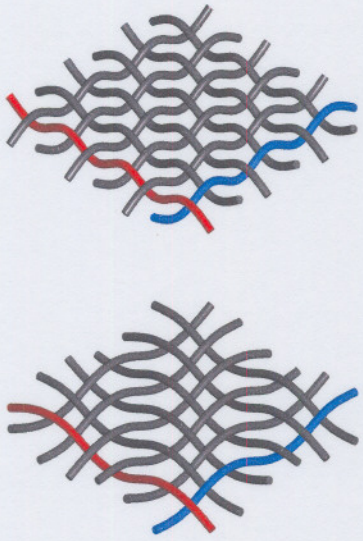

Plain woven fabric

Twill woven fabric

Figure 3.10: Weave patterns of reinforcement material

The volume fraction of the reinforcement material to matrix material is the last of the major contributing factors to the final strength of the composite material. All the composite structures which are manufactured for the glider are manufactured using hand lay-up techniques. The best possible volume fraction which can be obtained using this technique is 40% (resin in final structure per volume). If the volume fraction were to be decreased the possibility of the fibres not being wetted out properly exists and the mechanical properties of the composite material would be adversely affected. It was therefore assumed that all the materials would have the properties of composites with this 40% resin volume fraction.

The technique had to take into account all these different factors to ensure that the mechanical properties of the composites used would reflect a conservative estimate of

the true composite system. Different values needed to be obtained for different reinforcement materials used and the different weave patterns.

Figure 3.11 illustrates the approach used. On the right the composite material is illustrated as it is found in its manufactured state. With the new technique the fibres are extracted from the composite structure and compressed until no empty spaces are found throughout the fibres.

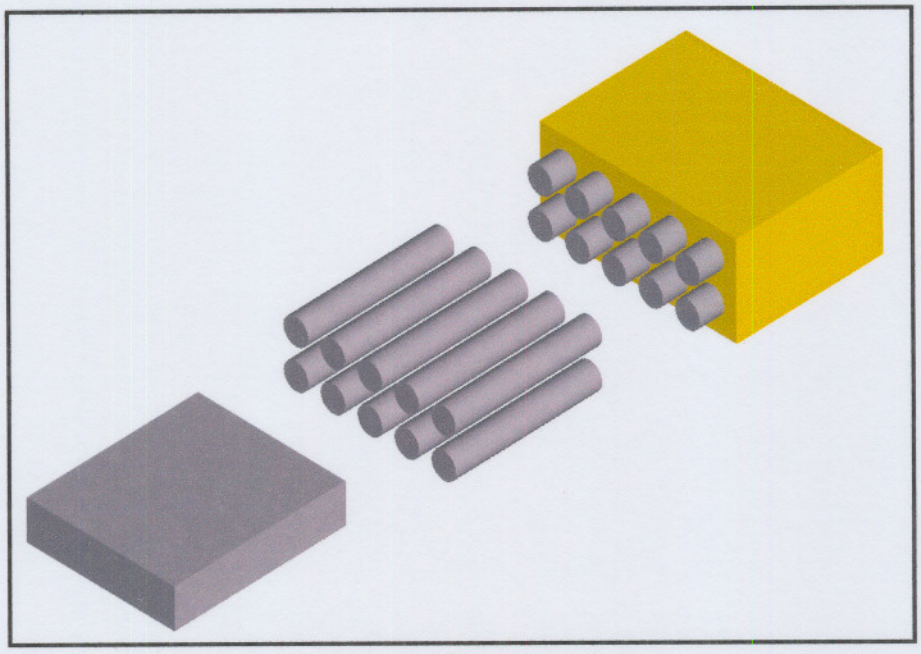

Figure 3.11: Composite material breakdown

The new volume of the reinforcement material is calculated using the mass per square meter of the reinforcement fabric and the density of the specific fibres used. If the mass per square meter of the fabric used is divided by the density of the fibres used in the fabric we could calculate the thickness of the reinforcement fabric assuming that there are no air pockets in the reinforcement fabric.

The new thickness obtained using this technique is then used for the description of the mechanical properties of the composite. All the mechanical properties obtained experimentally can then be transformed to this new thickness. The new values of the

mechanical properties are noticeably higher than that calculated using traditional techniques.

As an example the calculations will be done for MDL9001 unidirectional carbon fabric. The weight of MDL9001 is supplied by the manufacturer as being $135g/m^2$. The density of carbon fibres are $1760kg/m^3$. Using equation 3.3 the thickness of the fabric related to its density, t_ρ, is given as being 0.0767mm. This value is almost half that of the thickness of the fabric as specified by the manufacturer (0.13mm).

$$t_\rho = \frac{w}{\rho} \qquad \text{...(3.3)}$$

The cross-sectional areas of the specimens can then be calculated by using this new thickness. The internal stresses present in the specimens therefore increase due to this decrease in cross-sectional area. As illustration the stress-strain diagram for woven carbon fabric for the two scenarios are shown in Figure 3.12.

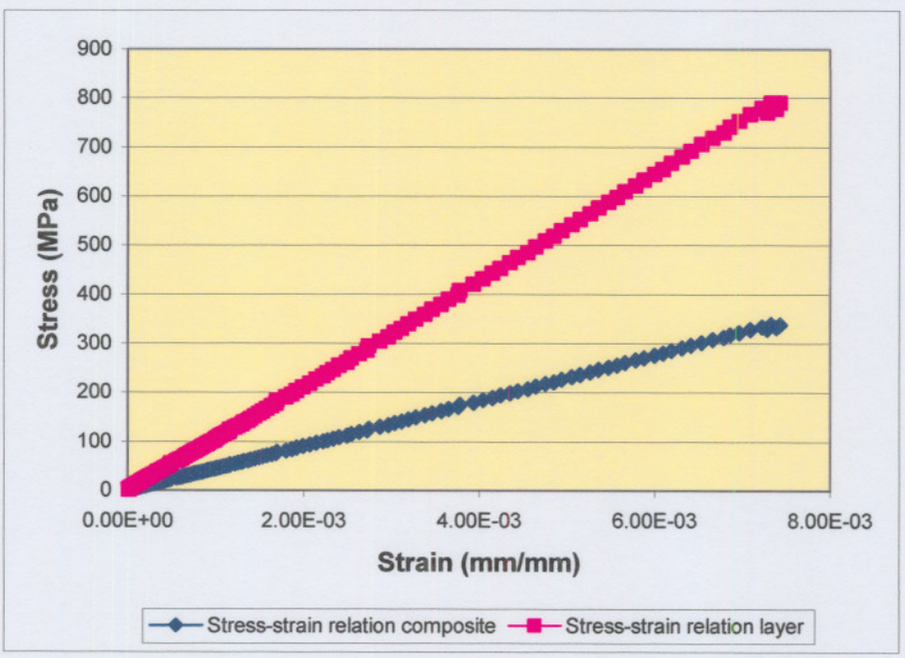

Figure 3.12: Stress-stain relation for manufactured carbon and for transformed layers

The material properties for all the composite materials tested where transformed in a similar manner. In Table 3.2 the newly calculated mechanical properties of the various materials tested are given.

	σ_{11} Tension (MPa)	σ_{22} Tension (MPa)	σ_{11} Comp (MPa)	σ_{22} Comp (MPa)	τ_{12} (MPa)	E_{11} (GPa)	E_{22} (GPa)	Poisson	G_{12} (GPa)
Glass fibre	746	746	540	540	165	45.3	45.3	0.28	10.8
Kevlar fibre	1086	1086	753	753	297	86	86	0.185	4.43
UD Carbon	2150	180	1280	100	250	188	18	0.05	0.5
Woven carbon fibre	1190	1190	655	655	121	102	102	0.08	4.46

Table 3.2: Transformed mechanical properties of composite materials

The transformed thickness of a number of the different types of reinforcements used are given in Table 3.3.

Material Type	Material Thickness (mm)
Woven Glass Fibre – 92110	0.06417
Woven Glass Fibre – 92125	0.19444
Unidirectional Carbon Fibre – MDL9001	0.0767
Woven Kevlar Fibre – 98605	0.04236

Table 3.3: Transformed thickness of various reinforcement materials

These newly obtained values are then used in conjunction with the thickness relative to the density of the various reinforcement fabrics in the designing of the new tailplane for the glider. This technique simplifies the design process as the influence of the matrix material thickness can be ignored.

3.5. Conclusion

The mechanical properties used further in this study in the designing of the composite tailplane for the glider was obtained using the methods described above. The method of rewriting the properties of the composite lay-ups to the reinforcement material used is also described. This was mainly done to aid in the simplification of the design process by being able to neglect volume fractions of the reinforcement material and the epoxy in the composite materials used in the initial design.

4. AIR LOAD CALCULATION

4.1. Introduction

The calculation of the forces acting on the tailplane of the glider is done using the JAR22 as guideline. The JAR22 is the regulatory legislation to which all newly designed gliders need to comply.

The JAR22 specifies three different types of loads acting on the tailplane of the glider. These three different types are:

- balancing loads,
- manoeuvring loads and
- gust loads.

Each of these load types will be discussed briefly in this chapter.

4.2. Balancing loads

The tail balancing loads are defined in the JAR22 as the loads necessary to maintain equilibrium in any specified flight condition with no pitching acceleration (JAA, 2001:C7). The balancing loads acting on the tailplane can be divided into two categories, namely free flight balancing loads and towing balancing loads. These two different load conditions will be analyzed separately.

The techniques used in the calculation of the balancing loads on the tailplane of the glider are based on the techniques described by Thomas (1999:130).

4.2.1. Free flight balancing loads

The balancing loads acting on the tailplane of the glider are calculated taking the moment around the aerodynamic centre of the glider.

Figure 4.1 illustrates the aerodynamic moments around the aerodynamic centre of the tailplane. The equation describing the load on the tailplane can therefore be derived as being:

$$L_T = \frac{0.5C_{M0}\rho_0 V_i^2 S\bar{c} + (h - h_0)\bar{c}L}{l_{T'}} \qquad \text{...(4.1)}$$

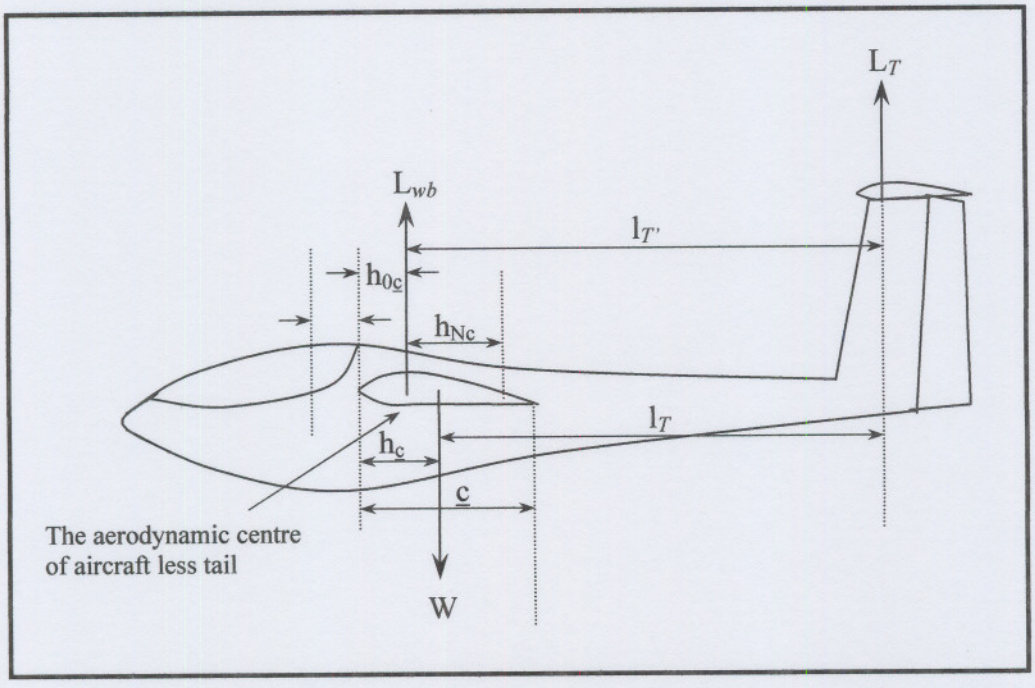

Figure 4.1: Aerodynamic moments around glider

This relationship is then rewritten to nondimensional form by normalizing the dynamic pressure, the wing area, and the mean aerodynamic chord.

$$C_{LT} = \frac{C_{M0} + (h - h_0)C_L}{\overline{V'}} \qquad \text{...(4.2)}$$

Equation 4.2 illustrates this nondimensional lifting coefficient acting on the tailplane. In equation 4.2 h_0 is given as the distance from the reference point on the mean aerodynamic centre to the centre of pressure is taken as 0.25 of the chord length. h_c is given as the distance from the reference point to the centre of gravity on the mean aerodynamic chord.

The modified tail volume coefficient, V', as found in equation 4.2 is given by equation 4.3.

$$V' = \frac{l_{T'} S_T}{cS} \qquad \text{...(4.3)}$$

Using the equations described above the balancing loads acting on the tailplane of the glider can be calculated for the two outer most centres of gravity positions as well as for different flap settings. These different scenarios are illustrated in Figure 4.2.

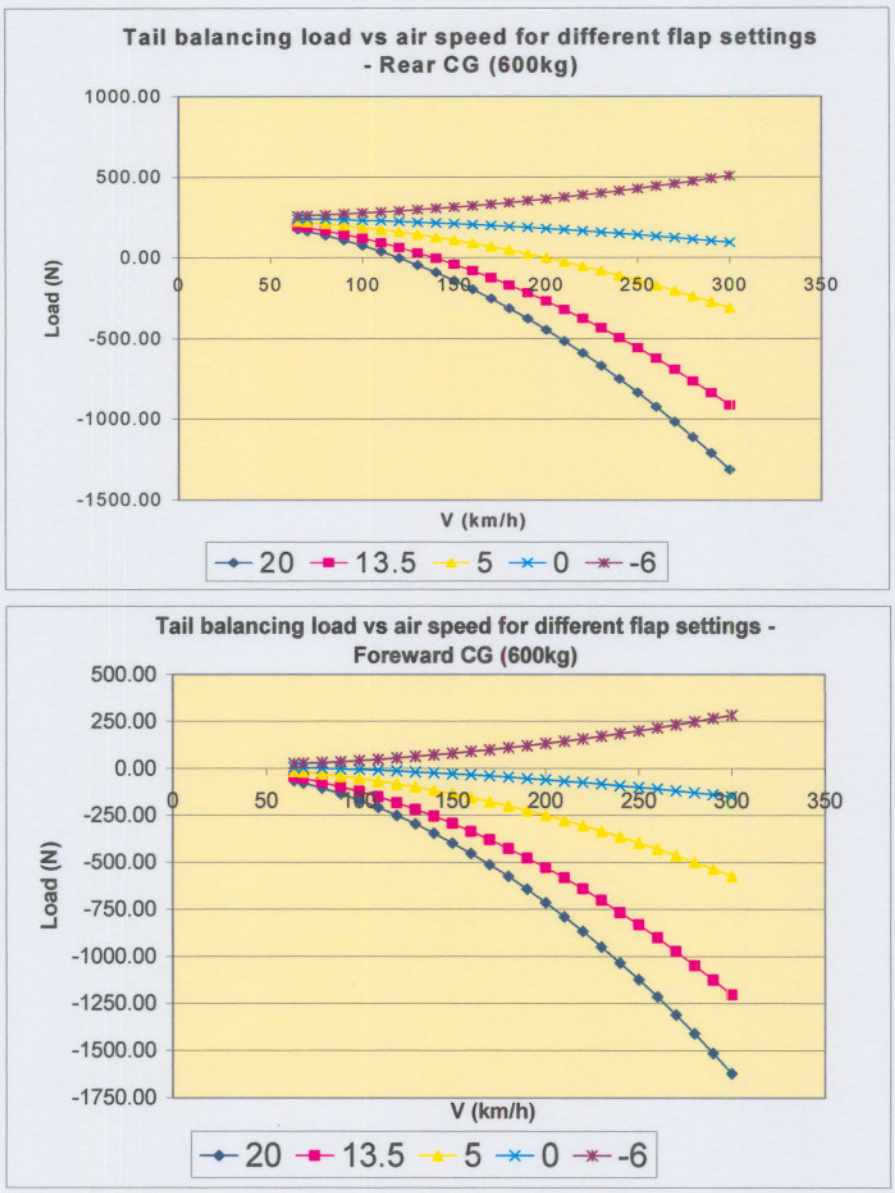

Figure 4.2: Balancing loads on tailplane

The maximum balancing loads can be taken directly from these diagrams. The maximum balancing load on the tailplane due to normal flight conditions is therefore calculated as -1620N.

4.2.2. Towed flight balancing loads

The loads acting on the tailplane of the glider during towed flight can be subdivided into two sub categories. The first hereof is aero towing balancing loads and the second is winch launching balancing loads.

4.2.2.1. Aero towing loads (JAR 22.581)

The JAR22 stipulates the loads acting on the glider during aero towing in section JAR 22.581. It specifies that the forces acting on the launching hook acts in the following directions:

1. horizontally forwards,
2. upwards at a 20° angle to the horizontal,
3. downwards at a 40° angle to the horizontal,
4. impulse loading in cable of 1.2 QNom, where QNom is the ultimate tensile strength of the cable used (or weak link if employed).
5. QNom is specified as being $1.3M_{Max}$ where M_{Max} is the maximum glider weight.

The load conditions acting on the glider during aero towing are illustrated in Figure 4.3.

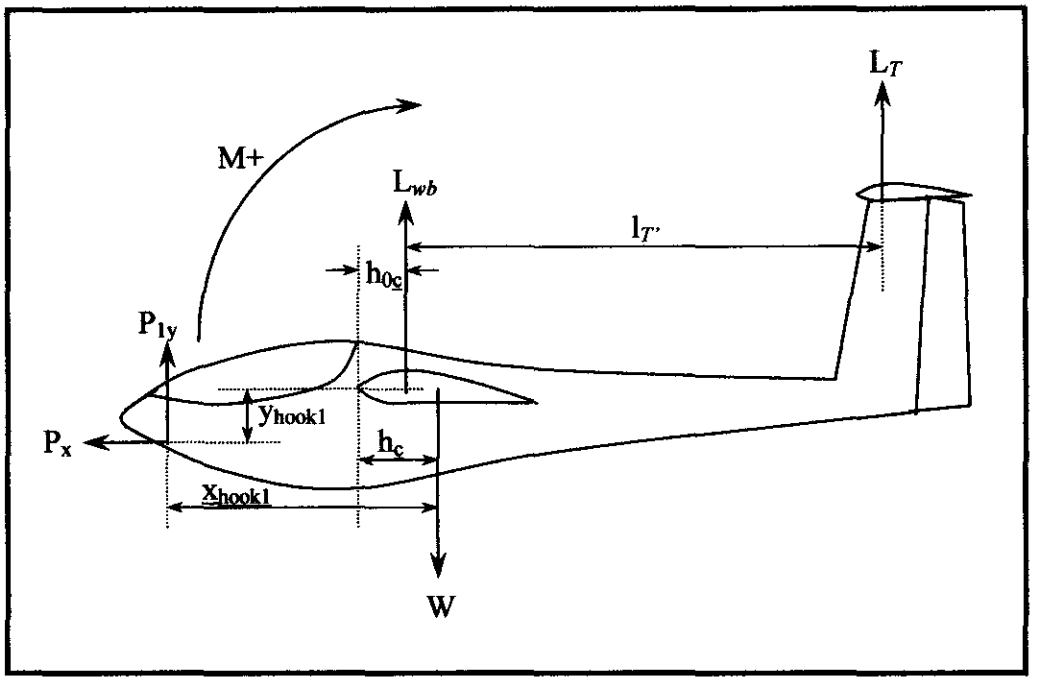

Figure 4.3: Load conditions during aero towing

Calculating the tail loads due to aero towing of the glider can then be calculated by taking the moments around the centre of gravity of the glider. The equation describing these moment calculations are given below.

$$L_T = \frac{0.5 \;\; C_{M0} \;\; \rho_0 \;\; V_i^2 S \;\; \underline{c} + (h - h0)\underline{c}L + P_{1y}x_{hook1} + P_x y_{hook1}}{l_T'} \qquad \text{...(4.4)}$$

Using this equation the maximum tail load due to aero towing is calculated as being 1855N.

4.2.2.2. Winch launching loads

The load configuration on the glider is virtually the same during winch launching as aero towing with the only differences being:

1. the hook position differs, for winch launching the hook position is situated more towards the centre of gravity of the glider and
2. the angle of the cable can vary between 0° and 75° with the horizontal.

The same equation can therefore be used for the calculation of the loads acting on the tailplane of the glider under winch launching conditions as for aero towing conditions taking into account the differences stipulated above.
The outermost situations are showed in Table 4.1.

Flap	CG front	CG rear
20	1409.95	-1133.43
13.5	1499.57	-1043.81
-6.6	***1818.72***	-724.66

Table 4.1: Winch launching conditions

The maximum load acting on the tailplane of the glider due to winch launching is thus 1818.72N.

4.3. Manoeuvring loads (JAR 22.423)

According to JAR22.423 the tailplane must be designed for the most severe loads likely to occur in pilot-induced pitching manoeuvres. This must be done at all speeds up to V_D the design speed of the glider. There are however two methods described by the JAR22 with which to calculate these values.

The first method is to calculate the load due to an instantaneous deflection of the elevator. This can be done by using the maximum cl and angle of attack of the elevator and calculate the maximum possible load at the required airspeed. The following table gives the load on the tailplane.

V	η	alpha	cl_{max}	P
55	20	3	1.2	2219.789
55	-20	3	1.2	2219.789
90.00	7	2	0.75	***3714.937***
90.00	-7	2	0.75	***3714.937***

Table 4.2: Load on tailplane

The maximum load due with this method is 3715 N.

The second method, the manoeuvring load is given as:

$$\Delta P = \Delta n \quad mg \left[\frac{x_{cg}}{l_t} - \frac{S_t}{S} \frac{a_h}{a} \left(1 - \frac{d\varepsilon}{d\alpha} \right) - \frac{\rho_0}{2} \left(\frac{S_t a_h l_t}{m} \right) \right] \qquad \text{...(4.5)}$$

This can be calculated with the previous equation using the following values for the load increments delta n.

Load case	V	Load increment	Description
1	V_A	4.3	Positive deflection to max load
2	V_A	-4.3	Max positive load to zero load
3	V_A	-3.65	Negative elevator deflection to max negative load
4	V_A	3.65	Max negative load to zero
5	V_D	3	Positive deflection to max load at V_D
6	V_D	-3	Max positive load to zero load at V_D
7	V_D	-2.5	Negative elevator deflection to max negative load
8	V_D	2.5	Max negative load to zero at V_D

Table 4.3: Manoeuvring load cases for tailplane

Table 4.4 gives the manoeuvre load increments.

M	δ = 20°		δ = 13.5°		δ = 5°		δ = 0°		δ = –6°	
600.00	CG_{front}	CG_{back}	CG_{front}	CG_{back}	CG_{front}	CG_{back}	CG_{front}	CG_{back}	CG_{front}	CG_{back}
4.30	-2128.96	-1382.72	***-2032.99***	-1286.76	-1988.64	-1242.40	-1980.46	-1234.22	-2026.54	-1280.30
-4.30	2128.96	1382.72	***2032.99***	1286.76	1988.64	1242.40	1980.46	1234.22	2026.54	1280.30
-3.65	1807.14	1173.71	1725.68	1092.25	1688.03	1054.60	1681.08	1047.65	1720.20	1086.77
3.65	-1807.14	-1173.71	-1725.68	-1092.25	-1688.03	-1054.60	-1681.08	-1047.65	-1720.20	-1086.77
3.00	-1485.32	-964.69	-1418.37	-897.74	-1387.42	-866.79	-1381.71	-861.08	-1413.86	-893.23
-3.00	1485.32	964.69	1418.37	897.74	1387.42	866.79	1381.71	861.08	1413.86	893.23
-2.50	1237.77	803.91	1181.97	748.11	1156.19	722.33	1151.43	717.57	1178.22	744.36
2.50	-1237.77	-803.91	-1181.97	-748.11	-1156.19	-722.33	-1151.43	-717.57	-1178.22	-744.36
M	**δ = 20°**		**δ = 13.5°**		**δ = 5°**		**δ = 0°**		**δ = –6°**	
350.00	CG_{front}	CG_{back}	CG_{front}	CG_{back}	CG_{front}	CG_{back}	CG_{front}	CG_{back}	CG_{front}	CG_{back}
4.30	***-1241.89***	-806.59	-1185.91	-750.61	-1160.04	-724.74	-1155.27	-719.96	-1182.15	-746.84
-4.30	***1241.89***	806.59	1185.91	750.61	1160.04	724.74	1155.27	719.96	1182.15	746.84
-3.65	1054.17	684.66	1006.65	637.14	984.69	615.18	980.63	611.13	1003.45	633.95
3.65	-1054.17	-684.66	-1006.65	-637.14	-984.69	-615.18	-980.63	-611.13	-1003.45	-633.95
3.00	-866.44	-562.74	-827.38	-523.68	-809.33	-505.63	-806.00	-502.30	-824.75	-521.05
-3.00	866.44	562.74	827.38	523.68	809.33	505.63	806.00	502.30	824.75	521.05
-2.50	722.03	468.95	689.48	436.40	674.44	421.36	671.67	418.58	687.30	434.21
2.50	-722.03	-468.95	-689.48	-436.40	-674.44	-421.36	-671.67	-418.58	-687.30	-434.21

Table 4.4: Manoeuvre load increments

The load increment must be combined with the balancing load to get the total maximum load seen by the tailplane. To get the maximum load on the tailplane the maximum of the combined load of method 2, or the total load of method 1 must be used. This will be discussed under combined loads.

4.4. Gust loads (JAR 22.425)

During normal flight conditions variations in vertical wind directions are encountered frequently and are the basis of gliding. These variations can however occur extremely fast generating impulse loading on the tailplane of the glider. The JAR 22.425 describes this impulse loading as gust loads.

These gust loads are calculated using the following equation:

$$P = P_0 + \frac{\rho}{2} S_t a_h U \quad kH \quad V(1 - \frac{d\varepsilon}{d\alpha}) \qquad \text{...(4.6)}$$

The gust speed U need to be the same as that of the main wing, therefore $15m/s^2$ at V_A and $7.5m/s^2$ at V_D. The gust loads are calculated for altitudes up to 9000m and for all possible flap configurations. The gust loads for the different flight conditions are shown in Table 4.5.

M	V	-6	0	5	13.5
600	V_B+	1783.855	1781.315	1781.777	*1784.199*
	V_B-	-1783.855	-1781.315	-1781.777	*-1784.199*
	V_D+	1496.802	1494.670	1495.058	1497.090
	V_D-	-1496.802	-1494.670	-1495.058	-1497.090
350	V_B+	1728.990	1724.903	1725.647	1729.544
	V_B-	-1728.990	-1724.903	-1725.647	-1729.544
	V_D+	1450.766	1447.336	1447.960	1451.230
	V_D-	-1450.766	-1447.336	-1447.960	-1451.230

Table 4.5: Gust loads for all possible flight configurations

It must be kept in mind that these are loadings additional to the balancing loads. It can therefore be seen that the maximum additional loading caused by gusts are 1785N.

4.5. Resulting forces

According to the JAR22 these different loadings do not act onto the tailplane separately but must be combined to give the worst possible load case. It does however specify that all three of these loadings need not to be added together but rather the balancing load needs to be combined with the manoeuvring loads and the balancing loads need to be combined with the gust loads. Either of there two load scenarios will produce the maximum force acting on the tailplane of the glider.

The following tables lay out the different load cases for the various flap configurations, weight configurations and different centre of gravity positions.

M	δ = 20°		δ = +13.5°		δ = 5°		δ = 0°		δ = –6°	
600	CG_{back}	CG_{front}	CG_{back}	CG_{front}	CG_{back}	CG_{front}	CG_{back}	CG_{front}	CG_{back}	CG_{front}
V_B+	354.01	86.23	1542.29	1274.50	1815.79	1548.01	2001.43	1733.64	2193.27	1925.48
V_B-	-1203.61	-1471.39	-2026.11	-2293.90	-1747.76	-2015.54	-1561.20	-1828.99	-1374.44	-1642.23
V_B-2	-1203.61	-1471.39	-2026.11	-2293.90	-1747.76	-2015.54	-1561.20	-1828.99	-1374.44	-1642.23
V_B+2	354.01	86.23	1542.29	1274.50	1815.79	1548.01	2001.43	1733.64	2193.27	1925.48
V_D+	-485.21	-753.00	589.41	321.63	1208.23	1261.29	1626.55	1358.76	2054.61	1786.82
V_D-	-2100.28	-2368.07	-2404.77	***-2672.55***	-1781.89	-1728.83	-1362.79	-1630.58	-939.00	-1206.78
V_D-2	-2100.28	-2368.07	-2404.77	***-2672.55***	-1781.89	-1728.83	-1362.79	-1630.58	-939.00	-1206.78
V_D+2	-485.21	-753.00	589.41	321.63	1208.23	1261.29	1626.55	1358.76	2054.61	1786.82

Table 4.6: Gust & Balancing Loads m=600kg

M	δ = 20°		δ = +13.5°		δ = 5°		δ = 0°		δ = –6°	
350	CG back	CG front	CG back	CG front	CG back	CG front	CG back	CG front	CG back	CG front
V_B+	992.36	813.18	1383.59	1212.31	1642.64	1483.28	1819.23	1667.90	2003.71	1860.56
V_B-	-2032.82	-2212.00	-2075.50	-2246.78	-1808.65	-1968.02	-1630.58	-1781.90	-1454.27	-1597.42
V_B-2	992.36	813.18	1383.59	1212.31	1642.64	1483.28	1819.23	1667.90	2003.71	1860.56
V_B+2	-2032.82	-2212.00	-2075.50	-2246.78	-1808.65	-1968.02	-1630.58	-1781.90	-1454.27	-1597.42
V_D+	-1476.48	-1699.00	393.45	189.91	1021.90	846.99	1447.33	1291.72	1884.15	1748.18
V_D-	-1476.48	-1699.00	-2509.01	***-2712.55***	-1874.02	-2048.93	-1447.35	-1602.95	-1017.38	465.42
V_D+2	-1476.48	-1699.00	-2509.01	***-2712.55***	-1874.02	-2048.93	-1447.35	-1602.95	-1017.38	465.42
V_D-2	-1476.48	-1699.00	393.45	189.91	1021.90	846.99	1447.33	1291.72	1884.15	1748.18

Table 4.7: Gust & Balancing Loads m=350kg

M	δ = 20°		δ = +13.5°		δ = 5°		δ = 0°		δ = −6°	
600	CG_{back}	CG_{front}	CG_{back}	CG_{front}	CG_{back}	CG_{front}	CG_{back}	CG_{front}	CG_{back}	CG_{front}
4.3	-1882.38	-2872.49	-1597.87	-2587.98	-1274.97	-2265.08	-1080.21	-2070.32	-939.71	-1929.82
-4.3	1032.79	1487.33	1114.04	1568.58	1343.00	1797.54	1520.43	1974.97	1758.53	2213.07
-3.65	812.46	1157.81	909.07	1254.42	1145.13	1490.48	1323.87	1669.22	1554.60	1899.95
3.65	-1662.05	-2542.97	-1392.90	-2273.82	-1077.10	-1958.02	-883.65	-1764.57	-735.77	-1616.69
3	-2336.09	***-3107.82***	-1853.69	-2625.42	-1200.08	-1650.96	-775.32	-1547.05	-383.44	-1155.17
-3	-302.25	-66.08	38.34	274.50	626.41	1183.43	1039.08	1275.24	1499.05	1735.21
-2.5	-471.73	-319.56	-119.33	32.84	474.21	947.23	887.88	1040.05	1342.18	1494.35
2.5	-2166.60	-2854.34	-1696.02	-2383.76	-1047.87	-1414.76	-624.12	-1311.86	-226.57	-914.31

Table 4.8: Balance & Manoeuvre Load m=600kg

M	δ = 20°		δ = +13.5°		δ = 5°		δ = 0°		δ = −6°	
350	CG_{back}	CG_{front}	CG_{back}	CG_{front}	CG_{back}	CG_{front}	CG_{back}	CG_{front}	CG_{back}	CG_{front}
4.3	-1370.49	-1971.02	-1136.93	-1729.56	-846.58	-1427.30	-664.19	-1236.87	-512.27	1076.77
-4.3	330.03	572.21	445.02	695.10	680.57	942.56	852.85	1122.88	1061.71	1339.91
-3.65	201.50	379.99	325.46	511.84	565.14	763.44	738.19	944.52	942.74	1157.25
3.65	-1241.96	-1778.80	-1017.36	-1546.30	-731.16	-1248.18	-549.53	-1058.52	-393.30	-894.12
3	-2069.69	***-2586.17***	-1609.62	-2107.13	-958.78	-1427.66	-529.21	-978.78	-115.68	-545.61
-3	-883.28	-811.82	-505.94	-415.51	106.67	225.73	529.19	667.55	982.44	1140.45
-2.5	-982.15	-959.69	-597.91	-556.48	17.88	87.94	440.99	530.36	890.93	999.94
2.5	-1970.82	-2438.31	-1517.65	-1966.16	-870.00	-1289.88	-441.01	-841.59	-24.17	-405.11

Table 4.9: Balance & Manoeuvre Load m=350kg

The maximum symmetric load from the combination of loads is +3108 N. The maximum manoeuvre load by method 1 is however 3715N. This will be used as the maximum symmetric load on the tailplane.

4.6. Asymmetric loads on tailplane and attachment fittings

The asymmetric load on the tailplane can be calculated from three sources. The first is the balancing load, the second is the moment induced due to sideslip while the last is the moment induced due to a gust.

4.6.1. Asymmetric balancing load (JAR 22.447)

The asymmetric loads on the tailplane can be calculated according to JAR 22.447 a by multiplying the maximum balancing load by (1+x) and (1-x) with x = 0.34 for V_A and 0.15 for V_D.

The maximum moment on the tailplane due to the balancing load is

V	F_{total}	M_{total}
55	710.26	-159.13
90	1392.55	-137.64

Table 4.10: Maximum moment on tailplane due to balancing load

4.6.2. Asymmetric loads due to sideslip (JAR 22.441)

The maximum rolling moment induced by the horizontal tail due to sideslip can be calculated with the following equation:

$$M_{RST} = 0.2St\frac{\rho_0}{2}\beta V^2 b_h \qquad \text{...(4.7)}$$

with:
- St - area of horizontal tail
- β - Sideslip angle
- b_h - Span of horizontal tail.
- V - Flight speed

The sideslip angle is taken as 6° at V_D and 15° at V_B. The following table gives the resultant moments.

V (m/s)	B (°)	M (Nm)
90	6	304.6422
55	15	284.4268

Table 4.11: Resulting moments due to sideslip

4.6.3. Asymmetric gust loads. (JAR 22.443)

The gust load on the vertical tail can be calculated with the following equation:

$$P_{VT} = \frac{\partial Cl_{VT}}{\partial \alpha} S_{VT} V U k \qquad \text{...(4.8)}$$

with:

	P_{VT}	-	Gust load on vertical tail
	S_{VT}	-	Vertical tail surface area
	U	-	Gust speed
	K	-	gust factor =1.2

The gust loads and resulting moment on the fuselage are shown in the following table:

V	v	U	Mr
VD	90	7.5	305.714
VB	55	15	373.651

Table 4.12: Resulting moments due to gust loads

4.6.4. Ground handling loads (JAR 22.593)

JAR 22.593 specifies that 3% of the maximum weight of the sailplane can be applied at the tip of the tailplane. This creates and asymmetric load. The load for this condition is P = 177N at 1.5 m which result in moment M = 265Nm.

4.6.5. Maximum asymmetric loads on tailplane (JAR 22.447)

The maximum asymmetric load on the tailplane is a combination of moments and direct loads. As JAR 22.447 (3) prescribes that the induced rolling moment must not be combined with the asymmetric loads due to balancing, they will only be used on their own to obtain the maximum asymmetric load. The following table gives a summary of the asymmetric loads.

Loads	V	P	M
1. Balancing loads	VB	710.26	-159.13
	VD	1392.55	-137.64
2. Sideslip induced	VB	0.00	284.43
	VD	0.00	304.64
3. Gust induced	VB	0.00	373.65
	VD	0.00	305.71
4. Hand loads on tail lane	GND	176.58	264.87

Table 4.13: Asymmetric loads on tail lane.

4.7. Conclusion

The various load cases as specified by the JAR22 were all calculated as shown above. The maximum load acting on the tailplane as calculated above is due to flight at a load of 600kg with a flap setting of 3° with the centre of gravity in the forward position.

It is shown that this load can also be applied asymmetrically to the tailplane causing larger forces on a single half of the tailplane. This unsymmetrical load was calculated as being 3715N.

A safety factor of 1.725 is used. To simplify further calculations the force is also multiplied by this safety factor. The maximum load used in the design and analysis of the tailplane of the glider is therefore 6408N.

5. TAILPLANE STRUCTURAL DESIGN

5.1. Introduction

Having calculated the forces acting on the forces acting on the tailplane of the glider the next step is the detail structural design of the tailplane. This process can be subdivided into two sub steps. The first sub step involves the calculation of the force distribution over the tailplane. The second of the sub steps is the analytical design of the tailplane. These different sub steps are discussed in detail in this chapter.

5.2. Force analysis

5.2.1. Shear force and bending moment diagrams

The first step in the analysis of the tailplane is the calculation of the shear force and bending moment diagrams for the tailplane. This requires that the load distribution of the tailplane to be known.

The load distribution can be calculated from the lift distribution by using:

$$L_i = \frac{Cl_i S_i}{\sum_{i=1}^{50} Cl_i S_i} L_{Total} \qquad \text{where I is the different station ID's.} \qquad \text{...(5.1)}$$

This equation merely distributes the total load L_{total}, which was calculated in the previous chapter, according to the lift distribution over the tailplane. This load distribution is illustrated in Figure 5.1.

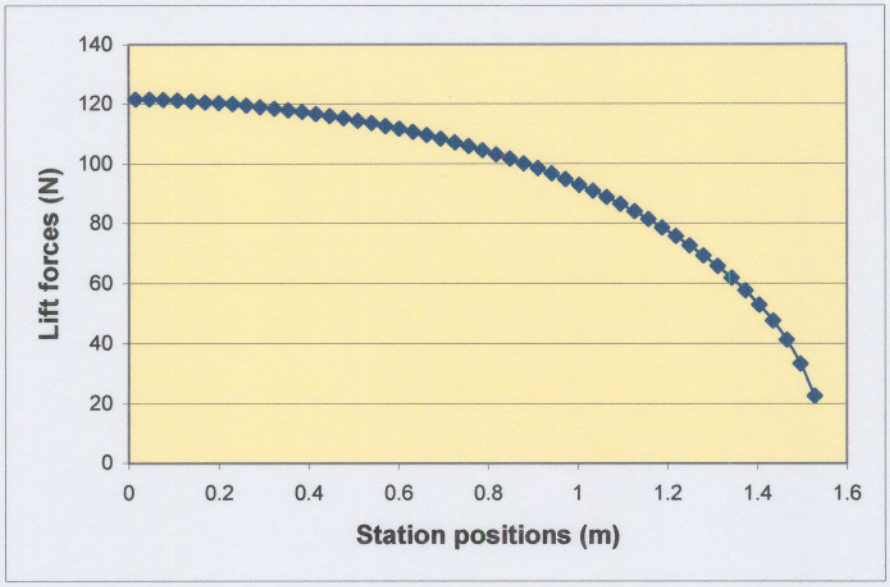

Figure 5.1: Tailplane load distribution

Using this information the shear force and bending moment diagrams are calculated. These are illustrated in Figure 5.2 and Figure 5.3 respectively.

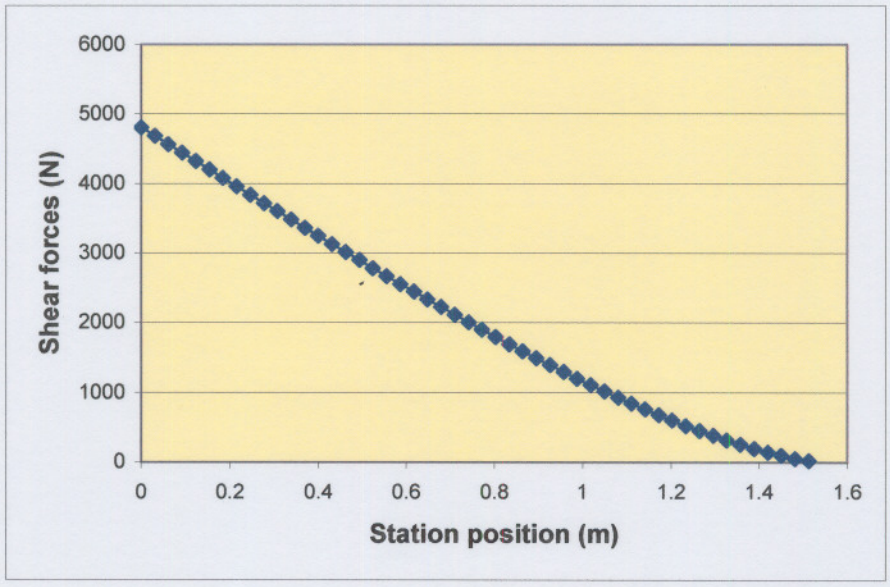

Figure 5.2: Shear force diagram for tailplane

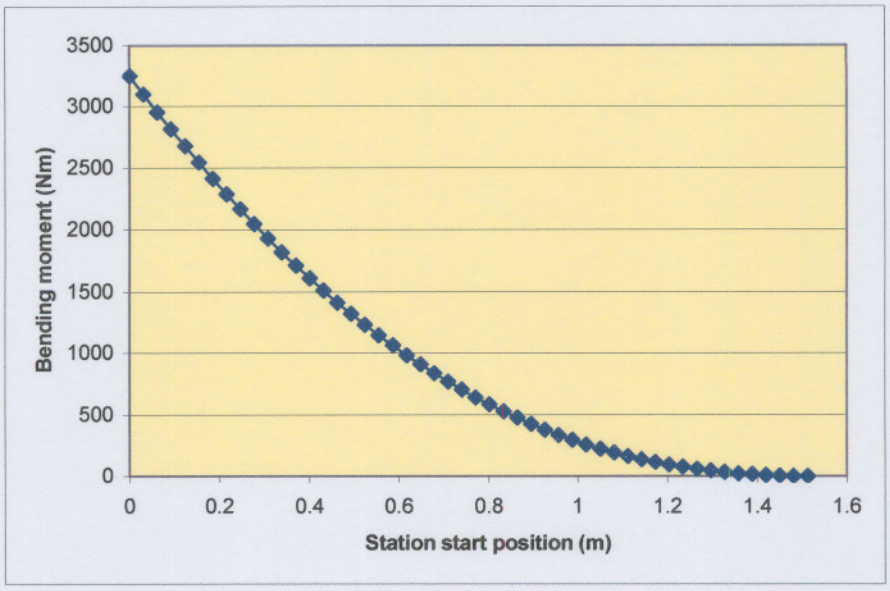

Figure 5.3: Bending moment diagram for tailplane

5.2.2. Twisting moment calculations

Another aero dynamic force that needs to be analysed is the twisting moment generated during flight. The magnitude of this force is calculated using equation 5.2 (Anderson, 1991:20) and the moment coefficient distribution calculated aero dynamically.

$$C_M = \frac{M}{q_\infty Sl} \qquad \text{...(5.2)}$$

The twisting moment, M, is calculated for each of the stations along the length of the tailplane and is then summed from the outside of the tailplane to the centre. This process gives us a twisting moment diagram for the tailplane as illustrated in Figure 5.4.

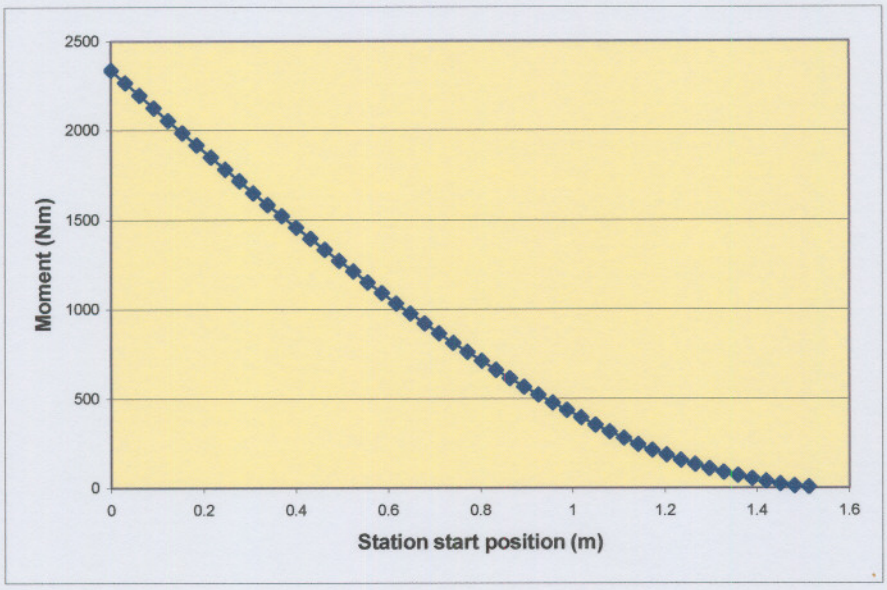

Figure 5.4: Twisting moment diagram for tailplane

5.3. Analytical design

Having calculated the different force diagrams for the tailplane the process of design can begin. The first step in this process is the simplification of the problem. Three simplifications were made which will be discussed briefly below.

The first of these simplifications made to the problem was assuming that the forces acting on the tailplane is symmetrical around the centre of the tailplane. Using this assumption only one half of the tailplane need be designed as it would be structurally symmetrical around the centre. All the calculations shown are for only one half of the tailplane.

The second simplification made the division of the tailplane into 50 stations of equal length. This was done to simplify the whole design process; the forces acting on the tailplane could be calculated at the different stations and then merely summed to calculate the full effect of the forces on the tailplane as a whole, secondly the structural designing of the tailplane could also be done for the different stations and then transformed to the full tailplane. Figure 5.5 illustrates the divisions made on the tailplane. The width of the stations was made 0.03086m.

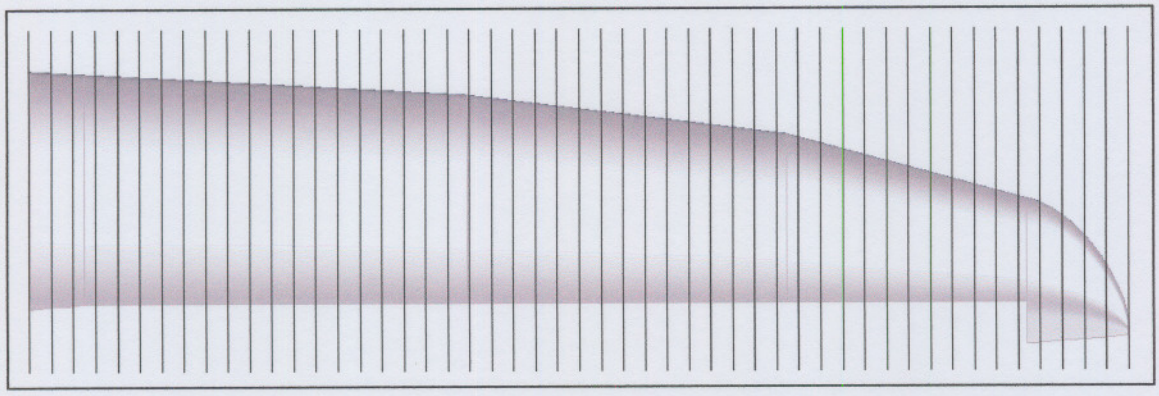

Figure 5.5: Elevator stations

The third of the simplifications made concerns the actual aero dynamical shape of the tailplane. To simplify the structural sizing of the tailplane the cross-section is transformed to an I-beam section. Figure 5.6 illustrates this simplification.

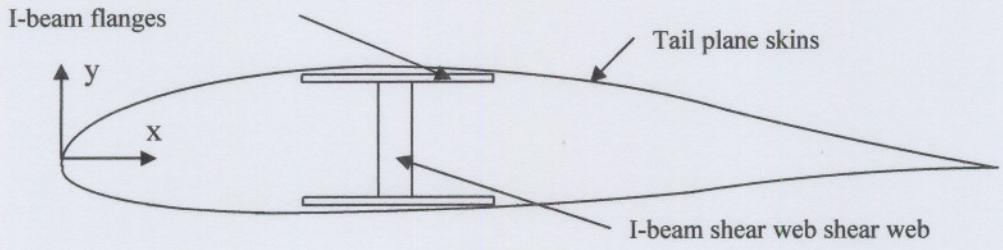

Figure 5.6: Cross-sectional simplification

The process of the transformation firstly involved the calculation of the cross-sectional moment of inertia of the tailplane. This was done using a CAD package which numerically calculates the moment of inertia for the complex section around the x-axis. Equation 5.3 was then used to calculate the height of an I-beam section with equal flange thickness to that of the actual tailplane and with of equal width. This was done for four major sections of the tailplane. The values of the sections between these major sections were calculated by means of interpolation.

$$I_{xx} = \frac{bh^3}{12} \qquad \text{...(5.3)}$$

Using this I-beam model and the load conditions the lay-up schedules of the tailplane could be calculated.

There are three lay-up schedules which needed to be calculated. The first is the lay-up of the I-beam flanges which carry the tailplane bending moments. Secondly the I-beam shear web which carries the shear forces of the tailplane and lastly the tailplane skin lay-up to withstand the twisting moment generated by the tailplane during flight conditions.

5.3.1. Design of beam flanges

As discussed before the flanges of the I-beam will be the part that has to overcome the bending moments generated by the force acting on each of the stations. It is assumed that pure bending is caused. In the case of pure bending the maximum stresses in the flanges can be calculated using equation 5.4 (Shigley, 1989:44).

$$\sigma_{max} = \frac{Mc}{I} \quad \text{where} \quad c = y_{max} \qquad \text{...(5.4)}$$

y_{max} is the distance from the centre of the I-beam section to the outer most point on the flanges i.e. the half the height of the beam. The moment, M, was calculated for the different stations as shown previously. These values were used directly in the calculation of the moment of inertia needed to comply with the strength of the composite materials.

The value obtained for each station is then transformed back to geometric values by using Equation 5.5 (Shigley, 1989:754). This is done by firstly calculating the moment of inertia for the total outside dimensions of the I-beam. The difference between this outside geometry and the actual inertia needed could then be used in the calculation of the flange thickness.

$$I = \frac{bh^3}{12} \qquad \text{...(5.5)}$$

This process then gives us a value for the thickness of the flanges. This will be refined by using laminate analysis theory.

The basic procedure involves the calculation of the effective EI product for the lay-up using the lamination theory relationships. The maximum curvature and moment is then found using the usual procedure for statically determinate beams. The two-dimensional strain distributions are then obtained. These strain values are then used in conjunction with LAP for the calculation of the stresses exerted on each individual ply in the lay-up.

The equations used for the calculation of the curvature and the moment are derived from the following basic equations as described in Swanson (1997:193).

$$EI\frac{d^2w}{dx^2} = -M_{beam} \quad \text{and} \quad \kappa_x = -\frac{\partial^2 w}{\partial x^2}. \qquad \text{...(5.6)}$$

The moment-curvature relation for a composite beam is derived as being:

$$EI\kappa_x = M_{beam} \qquad \text{...(5.7)}$$

The application of composite materials in the tailplane of a glider exposes the material to moisture and thermal varying environments. These environments can introduce stresses into the individual plies. This problem can however be overcome easily by ensuring that the lay-up is symmetrical. In the case of the tailplane the skins are unsymmetrical but when the two halves are combined the final product is symmetrical around the centre of the tailplane.

The flanges are considered to be unsymmetrical plates loaded with a moment M_x. Usual beam theory assumes that there is no transverse moment acting on the flanges of the I-beam. This assumption can however not be made when we are considering flanges with width that we are using as transverse moments M_y do build up in the flanges. The proper assumption to make in this case is that the transverse curvature of the flanges is zero (Swanson, 1997:211).

The effective beam stiffness can be obtained from this as being:

$$EI_{eff} = \frac{h^3}{12A_{11,web}^{-1}} + 2b_f\left[\alpha_{11}\xi_1^2 + (\alpha_{12}+\alpha_{21})\xi_1 + \alpha_{22}\right] \qquad \text{...(5.8)}$$

where

$$\alpha_{11} = \left[A_{11} - \frac{A_{12}A_{21}}{A_{22}}\right],\ \alpha_{12} = \left[B_{11} - \frac{A_{12}B_{21}}{A_{22}}\right],$$

$$\alpha_{21} = \left[B_{11} - \frac{B_{12}A_{21}}{A_{22}}\right] \text{ and } \alpha_{22} = \left[D_{11} - \frac{B_{12}B_{21}}{A_{22}}\right].$$

After calculation of the effective beam stiffness is completed the curvature, κ_x, of the beam is calculated using equation 5.9.

$$M_{beam} = EI_{eff}\kappa_x \qquad \text{...(5.9)}$$

Obtaining the axial and lateral strain distribution through the beam is then done by using equation 5.10. It should however be noted that these formulae are derived only for nonsymmetric wide flanges and cannot be used in any other situation.

$$\varepsilon_x = \xi\kappa_x \text{ and } \varepsilon_y = -\left(\frac{A_{21}}{A_{22}}\xi_1 + \frac{B_{21}}{A_{22}}\right)\kappa_x \qquad \text{...(5.10)}$$

The axial and lateral strain values which are calculated is then transformed into fibre direction strains which can then be used in the calculation of the fibre stresses. This is done with the use of LAP which makes use of lamina stress-strain relations and classic lamination theory.

As mentioned earlier it is assumed that the flanges of the I-beam will carry only the bending moments generated in the tailplane. Unidirectional carbon was used in the

form of MDL9001. The unidirectional carbon cloth is laid in an axial direction in the tailplane. As a first iteration the number of layers of the unidirectional carbon needed is calculated using normal beam analysis techniques. This process is done for all the different stations along the length of the tailplane.

As an example we will be looking at the first station. The magnitude of the bending moment acting on this the centre section of the tailplane is 1780, 811×10^3 Nmm. The actual height of the I-beam that portrays the section of the tailplane is calculated as 47mm. We will be assuming that the flanges consist of two layers of the unidirectional carbon. The thickness of the flanges is therefore known and the moment of inertia for the beam can be calculated using equation 5.5. Stress calculation in the flanges can then be done with the use of equation 5.4. A compressive stress magnitude of 810.840 MPa was calculated. The number of layers needed using normal beam theories are two per flange.

These values now need to be tested using the classic lamination theory for composite materials. This is done with LAP. The data needed by LAP for the stress analysis of the fibres need to be calculated using a spreadsheet model and the ABD matrices for the flanges. We subsequently need to set up a model of a flange in LAP. LAP then uses this information in the calculation of the ABD matrix.

The ABD matrix values are then inserted into the spreadsheet model of the flanges which then calculates the values of the curvature of the beam using equation 5.7. Using the curvature of the beam the strain distribution in the beam is calculated with the use of equation 5.10. These values are then used in LAP as load cases for the laminate element. The value of the stresses in the fibre direction as calculated by LAP is 811,310 MPa. This value is slightly higher than that calculated using the normal beam theory. This is as a result of the coupling effects of composite materials. This occurrence is more profound in fibres of which the lay-up angles are greater out of line of the forces acting on the composite. The LAP results for the critical sections of the tailplane flanges are given in Appendix A of this report.

The calculation of the stress distribution in the flanges over the whole length showed that two layers of the MDL9001 are needed up to 220mm from the centre line of the tailplane. One layer of MDL9001 is sufficient from 200mm on to the tip.

The technique for the calculation of the flange lay-up schedule is described above. From this technique we obtained a lay-up schedule of the flanges. The lay-up schedule of the flange consists of unidirectional carbon orientated axially along the length of the tailplane.

If a full layer of carbon is lain up to this position and it is merely abruptly discontinued a large stress concentration will be created. It is better practice to let the carbon layer which will not continue throughout the length of the tailplane to taper done to minimize the effect of stress concentration as far as possible. It is for this reason that it was decided to taper the layer down from 135mm to a width of 200mm at 350mm. This is illustrated in Figure 5.7. Special care was taken to ensure that the stresses in the tapered sections of the unidirectional carbon fabric fall within the mechanical properties of the material.

Figure 5.7: Tapering of UD carbon fabric

All the different layers which do not need to continue throughout the tailplane was tapered in the same manner. This ensured that stresses concentrations throughout the tailplane was kept to a minimum.

Another design aspect that was not mentioned above is the importance of a core material in the skins of the tailplane. Core material aids in the stiffening of the structure which improves the aero elastic properties of the tailplane. Due to the low density of core materials it is a highly efficient way of increasing the total bending

strength and stiffness of a structure without adversely affecting the weight thereof (Loken, 1988:14).

Core material is added to the lay-up of the tailplane to aid in the prevention of flutter problems during flight. Two different types of core materials are commonly used in the manufacturing of modern aircraft. Honeycomb materials are the first of these. The second less expensive option is PVC foam cores. PVC foam cores do not possess the same mechanical properties of honeycomb materials. The advantages of foam cores are however financially. The forces generated within the tailplane are low enough that the use of honeycomb materials is not needed. Therefore PVC foam of 5mm thick will be added to the lay-up.

The LAP reports for the critical flange sections are given in Appendix A.

5.3.2. Design of shear web

Having calculated the first iteration of the lay-up schedules for the flanges of the I-beam, the shear web can be designed. The process of the structural sizing of the shear webs however does not involve the use of normal beam stress theories. This is mostly due the fact that it would be highly ineffective to design the shear web of the I-beam section to consist of fibres that are subjected to normal shear. The fibre orientation of the materials used in the shear web will mostly be at an angle to the shear forces acting on the tailplane.

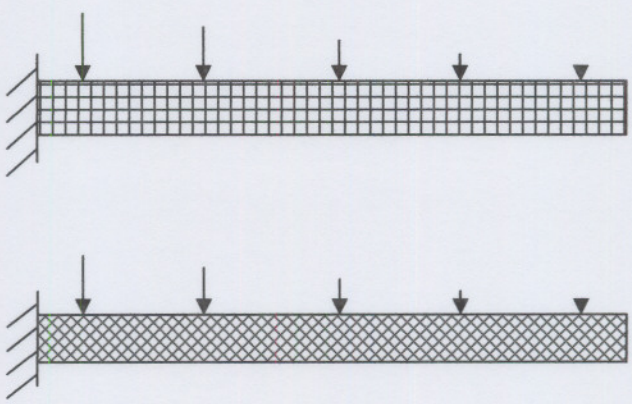

Figure 5.8: Shear web diagrams

In Figure 5.8 there can be seen that when the fibre orientation of the material used in the shear web is placed at a square angle to the forces acting on it, the stresses produced are normal shear stresses. Because of the fact that the shear stresses of composite materials are relatively low when compared to that of traditional materials it is highly inefficient to design the shear web in such a way.

The most efficient way of circumnavigating this problem is by changing the fibre orientation at an angle to the forces. Changing the angle to a 45° relative the forces minimizes the normal shear stresses produced. This is due to the fact that the forces are transferred to tensile and compression stresses within the fibres. This does not however mean that there are no shear stresses at work in the structure.

The shear web of the tailplane is therefore subjected to both tensile, compression and shear stresses. Due to this, glass fibre, or E-glass as it is better known throughout the industry, is the best possible reinforcement material that could be used. This is due to the fact that there is not such a large difference between the shear strengths of E-glass as compared to that of carbon. For that reason the first iteration of the lay-up schedule for the shear web of the tailplane will consist of two layers of 92125 at a fibre orientation of 45°.

The formulation of the equation with which the shear stress distribution in the shear web of the tailplane is derived from equation 5.11 which expresses the net axial force in the web at a location of η. The flanges of the I-beam are also subjected to the same shear forces and shear stresses are therefore induced inside the flanges.

$$F_{web} = \int_{\eta}^{h/2} \left(\frac{1}{A_{11}^{-1}} \right) \xi \kappa_x d\xi \qquad \text{...(5.11)}$$

The equation describing the shear force found in the flanges of the I-beam is

$$F_{flange} = b_f \left(D_{11}^{-1} \xi_1 - B_{11}^{-1} \right) \frac{\kappa_x}{\Delta} \quad \text{where} \quad \Delta = A_{11}^{-1} D_{11}^{-1} - B_{11}^{-1} B_{11}^{-1}. \qquad \text{...(5.12)}$$

From these two equations we can derive the equation describing the shear stress distribution through the section of I-beam.

$$\tau_{web}=\left(\frac{V}{t_w EI_{eff}}\right)\left[\left(\frac{1}{A_{11,web}^{-1}}\right)\left(\frac{h^2}{4}-\eta^2\right)/2+\frac{b_f}{\Delta}\left(D_{11}^{-1}\xi_1-B_{11}\right)\right] \quad \text{...(5.13)}$$

As described earlier we will be assuming that the shear web of the I-beam will be the sole component of the I-beam which will aid in the resistance of the shear forces. This is however not totally correct but will give us a good estimation of the initial idea of the lay-up schedule needed for the shear web. During the first iteration in the structural sizing of the shear web we will assume the last term found in equation 5.13 to be zero, as this is the term describing the shear forces absorbed in the flanges.

As in the case of the flanges of the I-beam the ABD matrix values of the shear web lay-up is inserted into a spreadsheet model using the equations above. It will be assumed that a lay-up of 2 layers of 92125 orientated at 45° angle to the shear web normal. The data obtained from the spreadsheet model can then be inserted into the LAP which then calculates the internal stresses using classic lamination theory. The Tsai-Wu failure index for the shear web is then given as 0.982. 2 layers of 92125 are therefore adequate for use in the shear web.

The strain which the shear web will be exposed to during loading is another of the design aspects which should be investigated. The maximum strain to which the shear web is exposed is the same as that calculated for the flange sections. Using LAP this loading could be applied to the shear web. The Tsai-Wu failure criteria increased to 0.988 with these additional strains.

The LAP result of the critical shear web section is given in Appendix A of this report.

5.3.3. Design of skins

As described above the tailplane generates a twisting moment around its centre line due to aerodynamic forces. These twisting moments need to be absorbed by the

tailplane skins. The moment increases from the tip of the tailplane to a maximum value at the centre thereof. The technique used for the calculation of the lay-ups for the skins are described below.

In the case of a multi-cell tube as shown in Figure 5.9 having N cells and subjected to a torque T, the torque is shared by the cells. All the cells will develop a constant shear flow (Megson, 1982:294). The total torque is the sum of the individual torques from each cell giving us equation 5.14.

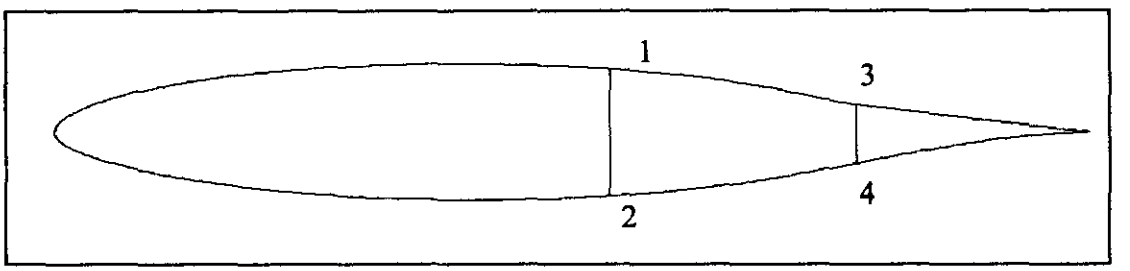

Figure 5.9: Through section of tailplane

$$T = \sum_{R=1}^{N} 2A_R q_R \qquad \text{...(5.14)}$$

Equation 5.14 is however only sufficient for the solution of the shear flow for a single cell problem. For multi-cell tubes consisting of N cells more equations are required to obtain a statically determinate system. These equations are obtained from the compatibility condition that cells must possess the same rate of twist. The rate of twist in cell R is given by equation 5.15.

$$\frac{d\theta}{dz} = \frac{1}{2A_R G_{REF}}\left(-q_{R-1}\delta_{R-1,R} + q_R\delta_R - q_{R+1}\delta_{R+1,R}\right) \qquad \text{...(5.15)}$$

Using the equations above the lay-up schedule of the skins at the centre section of the tailplane can be calculated as example. The twisting moment T which the skins need to absorb is shown in Figure 5.4 as 2339 Nm. The geometric sizes of the tailplane section are calculated with the use of a CAD package which calculates this using

numerical method. The effective mechanical properties of the skin lay-up are calculated using classical lamination theory. Using these different techniques we obtain Table 5.1.

Wall ID	**Length of wall (mm)**	**Thickness of wall (mm)**	**G_{12} of wall lay-up (N/mm^2)**
$1\text{-}2_{out}$	451.752	0.08472	43291.1
$1\text{-}2_{inside}$	52.456	0.4408	30642
1-3	87.859	0.08472	43291.1
2-4	87.6491	0.08472	43291.1
3-4	30.8018	0.4408	30642

Table 5.1: Geometrical and mechanical properties of skin sections

Due to the fact that not all the walls are geometrically and mechanically the same we will be transforming the thickness of the different walls so that there modules are the same. The weighted thickness t^* is defined by equation 5.16. The reference shear modulus used for the calculation of the weighted thickness is chosen as $43291.1N/mm^2$.

$$t^* = \frac{G}{G_{REF}} t \qquad \text{...(5.16)}$$

Wall ID	**Thickness of wall (mm)**	**G_{12} of wall lay-up (N/mm^2)**	**G_{REF}**	**t^***	**δ**
$1\text{-}2_{out}$	0.08472	43291.1	43291.1	0.08472	3804.227
$1\text{-}2_{inside}$	0.4408	30642	43291.1	0.312	168.128
1-3	0.08472	43291.1	43291.1	0.08472	739.865
2-4	0.08472	43291.1	43291.1	0.08472	738.098
3-4	0.4408	30642	43291.1	0.312	98.724

Table 5.2: Transformed geometrical and mechanical properties

The rate of twist for the different cells can then be calculated using equation 5.15 where δ is defined by equation 5.17. As described above the rate of twist of the different cells are equal.

$$\delta = \int \frac{ds}{t^*} \qquad \text{...(5.17)}$$

Substituting the values shown in Table 5.2 into equation 5.15 we obtain two equations containing the shear flow distribution in the two cells. Calculating the areas of the two different cells and substituting them into equation 5.14 we obtain a third equation. Solving these three equations simultaneously gives the values of the shear flow in the walls q_I and q_{II} as 86.18 and 79.81 respectively. The shear stresses in the different walls can then be calculated by dividing the shear flow q_I and q_{II} by the respective wall thickness. The shear stresses in the different walls are given in table 5.3.

Wall ID	**Shear stresses**	N_{xy}
$1\text{-}2_{out}$	1017.233	86.18
$1\text{-}2_{inside}$	14.45	6.37
1-3	942.044	79.81
2-4	942.044	79.81
3-4	181.057	79.81

Table 5.3: Shear stresses in skin sections

Although a thickness for the various sections of the tailplane was assumed initially to obtain the internal shear stresses in the tailplane these values can not be used in the designing of a lay-up schedule. It is for this reason that the internal shear stresses in the sections are transformed back to a shear force N_{xy} which can be used in LAP.

Two layers of 98605 Kevlar will be used in the skin lay-up of the tailplane. These Kevlar layers have a dual purpose. The first is to counteract the twisting moments and the second is to aid in the dampening of aerodynamic flutter. On the centre section of the tailplane where the shear stresses are too great for the two layers of Kevlar a layer of 92125 is also added. The internal shear stresses in the skins of the

tailplane at the centre section was calculated using LAP and was found to be inside the specifications of the material properties.

The results of the critical tailplane skin sections are presented in Appendix A of this document.

5.4. Manufacturing aspects

In the designing of the lay-up schedules of the tailplane, issues involving the manufacturing and workability of the tailplane also needed to be addressed. It is of utmost importance to ensure that workability of the final product is kept in mind. A layer of glass fibre fabric is added to the outside of the lay-up for this purpose.

Due to the mechanical properties of Kevlar fabric it is extremely difficult finishing products manufactured thereof. Attempting to sand Kevlar laminate edges creates a fine fluff which is unacceptable aerodynamically. It is for this reason that a layer of fibre glass is added to the outside of the tailplane. The glass fibres hold the Kevlar fabric together and aids in the process of finishing the product.

5.5. Final lay-up schedule

Taking into account the points discussed above the lay-up schedule for the tailplane can be compiled. The tailplane lay-up schedules are divided into three subgroups:

1. Tailplane top skin,
2. tailplane bottom skin and
3. shear web.

The tailplane top skin section lay-up starts with a layer of glass fibre fabric orientated at 0°. This layer is laid onto the gel coat layer which is applied to the inside of the mould. This layer serves as a primer for the layers which are added further.

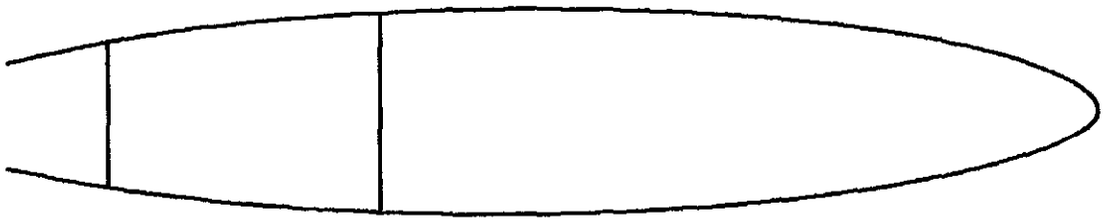

Figure 5.10: Side section of tailplane

The protruding pieces of skin at the rear of the tailplane as illustrated in Figure 5.10 are necessary to guide the air flow over the tailplane onto the elevator tab. These pieces need to be slightly flexible to ensure that full movement of the elevator tab is maintained. Structurally speaking the pieces performs no function in the load carrying abilities of the tailplane. These pieces need to be sanded down after manufacturing as a special tape is applied which seals the gap between the tailplane and the elevator tab. To help in the manufacturing of these pieces two layers of fibre glass fabric orientated at 0° are added over these sections.

A need now arises to differentiate between the procedure used for the placement of the Kevlar fabric layers absorbing the twisting moments and the unidirectional carbon fabric used for the absorbing of the bending moments. Symmetrical lay-up schedules are highly advisable for composite products. This is due to the fact that symmetrical lay-ups have an uncoupling effect on the bending end extension responses of the composite.

In the case of the Kevlar fabric layers a symmetrical lay-up poses no problem and the two layers can be placed on either side of the foam core. If we were to place a layer of each of the unidirectional carbon on either side of the foam core extremely high interlaminar shear stresses will be produced. It is therefore advisable to place the two layers of unidirectional carbon fabric on the inside of the foam core. The interlaminar shear stresses are kept to a minimum using this technique.

The fact that the skin itself is no longer symmetrically lain-up does not pose such a problem if we were to look at the tailplane as a finished product. If both the skin sections are globally symmetrical around the centre of the tailplane the final system

can be regarded as symmetrical. Uncoupled bending and extension responses can therefore be expected for the tailplane as a whole.

A layer of Kevlar fibre fabric is therefore added next to the lay-up followed by the PVC foam core. The two layers of unidirectional carbon fabric are then added followed by the second layer of Kevlar fabric. Two layers of fibre glass fabric are then added to the rear protruding sections to ensure symmetry followed by the final layer of fibre glass fabric orientated at a 45° angle.

The full lay-up procedure for the tailplane top skin is illustrated below in Figure 5.11.

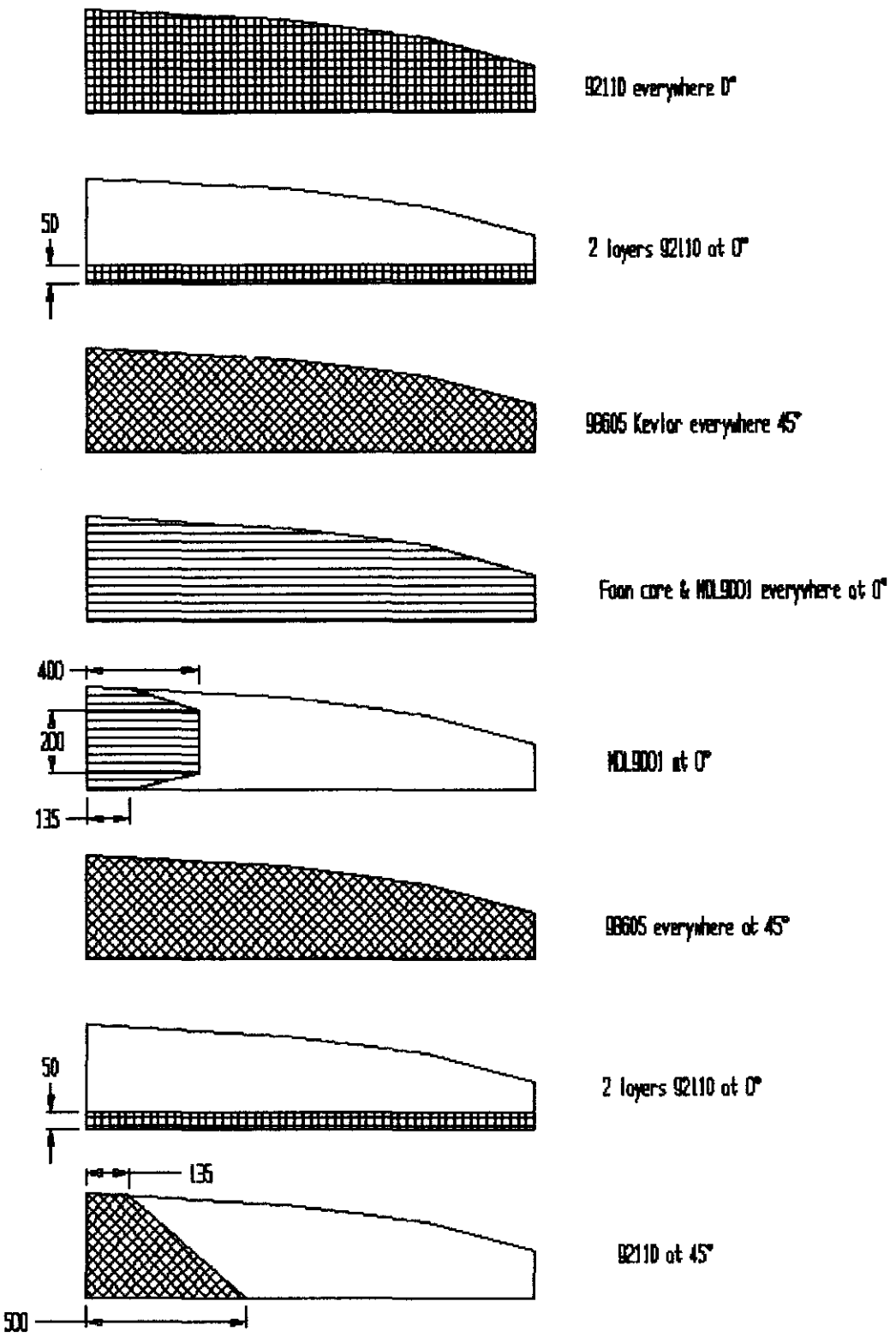

Figure 5.11: Lay-up schedule for top skin

The lay-up schedule for the bottom skin of the tailplane is similar to the top skin. The shear web lay-up was also changed to better suit the design and simplifies the manufacturing thereof in the same manner as the top and bottom skin. As the lay-up of the shear web is the same throughout the entire web the lay-up schedule is given in Table 5.4.

Layer 1	**92110 at 0°**
Layer 2	**92125 at 45°**
Layer 3	**5mm PVC foam core**
Layer 4	**92125 at 45°**
Layer 5	**92110 at 0°**

Table 5.4: Lay-up schedule for shear web

A layer of 92110 at 0° has been added to either side of the shear web. These layers of glass fibres have been added to the shear web lay-up to aid in the fixing of the shear web to the either of the two skins of the tailplane.

5.6. Conclusion

The empirical initial design of the tailplane is done for all components of the tailplane separately as shown in this chapter. As the influences of the different parts of the tailplane on one another is extremely difficult to examine empirically the next and final step in the designing of the tailplane was the numerical simulation of the tailplane as a whole using a finite element program.

Using the lay-up schedules as described in this chapter a numerical model of the tailplane will be constructed in a finite element analysis program (ANSYS). The results from this numerical analysis will then be compared to the results obtained using the empirical techniques used in this chapter.

6. NUMERICAL ANALYSIS

6.1. Introduction

An analytical design of the different parts which form the elevator was done in the previous chapter. This design was however only an approximation of what would be needed. Due to the complex shape of the elevator it is virtually impossible to calculate the true reactions of the tailplane when it is loaded.

The analytical plate theory methods used in the previous chapter is merely a representation of the composite design as rectangular plates. The Raleigh-Ritz method and the Galerkin method can also be used but these are also only of use for simple geometries as it is difficult to construct a function describing the complex geometry. A numerical method facilitates the solution of these equations for practical complex geometries. The finite element method is the most effect numerical method for the solving of the differential equations over arbitrary domains (Ochoa, 1992:3).
In this chapter the finite element analysis of the tailplane will be discussed. The finite element program used for this analysis is ANSYS.

6.2. Modelling considerations

Modelling using the finite element method involves assumptions concerning the representation of the geometry of the structure and its behaviour. These assumptions can only be made if one has a qualitative understanding of how the structure behaves. The analytic design and analysis of the structure serves as the basis in the understanding of the responses of the structure when subjected to the prescribed loads. The different aspects influencing the finite element model development will be discussed briefly. This will be done using the following guidelines as basis:

- mesh generation,
- load representation and
- imposition of boundary conditions.

6.2.1. Mesh generation

Guidelines for the generation of a finite element mesh of a structure are given by Ochoa (1992:40) as:

1. the mesh must accurately represent the geometry of the computational domain and the loads exerted thereon,
2. adequate representation of large gradients in the solution should be reflected in the mesh and
3. the mesh must not contain any elements with very large aspect ratios, especially in regions of large gradients.

If these guidelines are followed the mesh can be coarse or refined and may consist of one or more orders and types of elements. It is however good practice to firstly create a coarse mesh with which the problem can be analysed to save on computational costs. These results can also be used as a guide for subsequent mesh refinements and analysis.

There are two different types of mesh refinement employed in practice, the first thereof is h-refinement where the number of elements in a given region is increased and the second is p-refinement where the order of the elements which must be refined are increased.

6.2.2. Load representation

Special care should be taken with the representation of the loadings exerted on the structure. Suppose a body is subjected to a distributive force on its boundary. When the body is modelled by a set of finite elements the force distribution must be modelled as well. This force needs to be replaced by a set of nodal forces. This is done so that the work exerted by the distributed force on the body is the same as that of the nodal forces on the finite element representation.

Accuracy of the representation is dependant on the type of element used and the mesh used for the representation of the domain and the force itself. More accurate solutions are obtained with the use of a more refined mesh on the domain of the distributed

force. Figure 6.1 illustrates the influence of mesh refinement on the representation of distributed loading.

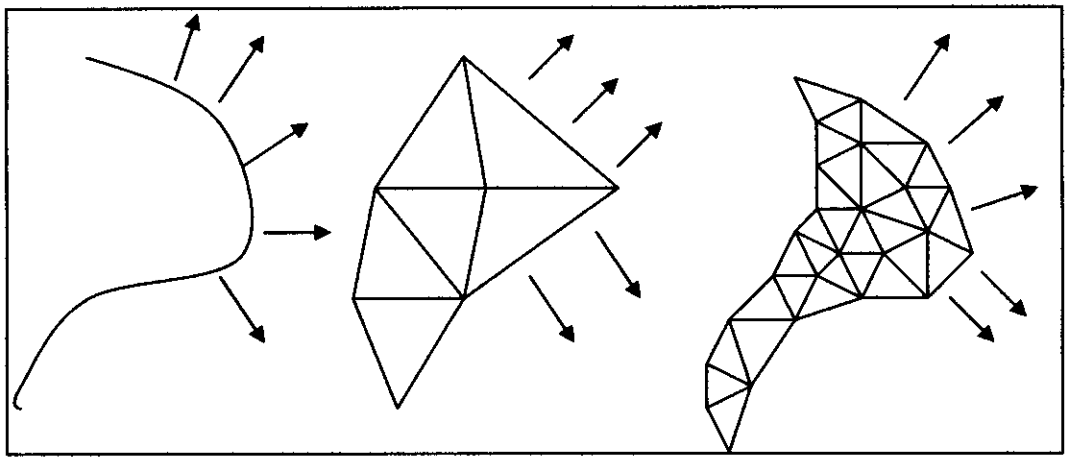

Figure 6.1: Influence of mesh refinement on load representation

6.2.3. Imposition of boundary conditions

In many of the problems one encounters situations where portions of boundaries were forces are specified has points in common with points of the boundaries where displacements are specified. A case then arise where some of the nodes in the mesh are subjected to both force and displacement degrees of freedom. It is obvious that both boundary conditions may not be imposed on the same node. As a rule one should therefore impose the displacement boundary conditions at the singular points and disregard the force boundary condition.

Singularity problems also come in the form of two different boundary conditions which are specified at the same point. Two options are available to the analyst in such a case. Either a weighted average of the two conditions can be imposed on the point or the larger value of the two should be imposed.

The guidelines described above merely serves as a guideline in the generation of a finite element model of a structure and the final decision regarding the modelling lies with the analyst. It is however important that the analyst must keep these guidelines in mind during the modelling of the structure.

6.3. Model generation

Generation of a numerical model which accurately will describe the tailplane was done with the use of the basic outlines of model generation as described by Matthews et al. (1998:65). These outlines are:

1. Geometry specifications,
2. mesh generation,
3. element types and
4. material properties.

Each of these outlines will be discussed briefly.

6.3.1. Geometry specifications

The tailplane needs to be generated as distinct regions. All the different lay-ups schedules had to be looked at globally and the tailplane then had to be divided into these distinct regions. Any region had to consist of only one single lay-up schedule. This was done to simplify the process of element generation later on.
As described by Matthews et al. (1998:65) the regions have to join seamlessly with one another so that artificial cracks and other discontinuities are avoided. To ensure that the geometrical model is imported easily into ANSYS all discontinuities have to be eliminated in CAD.

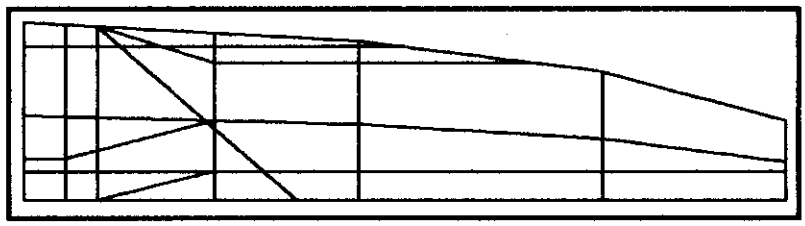

Figure 6.2: Tailplane area divisions

Figure 6.2 illustrates the divisions made to the top skin of the tailplane. The position of the shear web needed to be taken into account as well. The areas indicating the

shear web is created in ANSYS using the split lines as the basis for the position. The areas indicated in Figure 6.2 are then imported into ANSYS.

With the use of geometry manipulation and verification tools the final surfaces are created and checked before the mesh is generated. The final verified geometrical model of the tailplane is illustrated in figure 6.3. The coloured regions indicate different lay-up schedules for the individual areas.

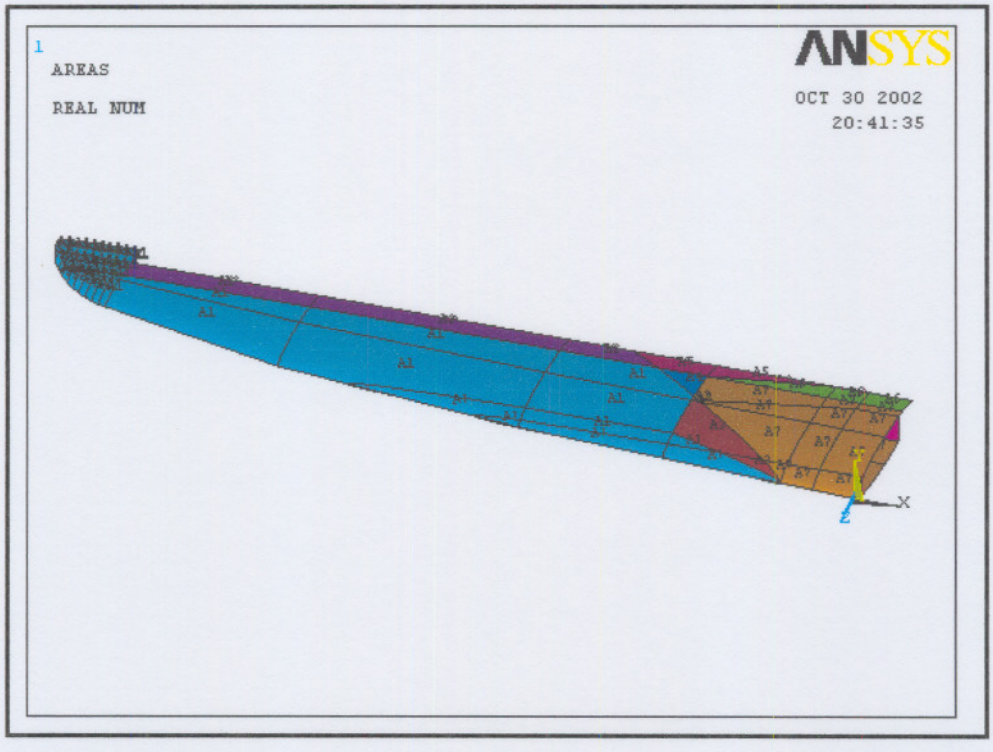

Figure 6.3: Geometrical model of tailplane in ANSYS

6.3.2. Element types

A large variety of types of elements are available with which to analyse the tailplane. ANSYS has the capabilities of modelling the tailplane as a solid. This analysis would however be computationally extremely costly. Special plate elements have been developed for the analysis of these models which simplifies the model to a 3D shell.

The 3D shell elements in ANSYS designed for this purpose are SHELL91 and SHELL99. Both of these elements are 8-node elements with 6 degrees of freedom at each node. A SHELL91 element however also come with an option for the analysis of structures taking into account the influences of sandwich structures and is capable of analysing non-linear materials.

For analysis of sandwich structures a symmetrical lay-up is however assumed. This does not comply with the lay-up schedule of the tailplane. We will therefore be using SHELL99 elements. The reason for this is the fact that calculation time is minimized dramatically with the use of these elements, especially when the lay-up of the structure being analysed consist of more than three layered materials.

SHELL99 elements are higher-order elements. Higher-order elements are defined as elements which have nodes not only at the element corners but also have mid-side nodes. These elements improve the accuracy of element bending and therefore soften the elements. In general for a mesh with a set number of nodes, the more nodes per single element the more accurate the solution.

6.3.3. Material properties

The properties of the materials used in the tailplane need to be inserted into the finite element model. ANSYS has the capability of modelling virtually any type of material that can be used. These include linear, non-linear, isotropic, anisotropic and orthographic materials.

The model chosen for the depiction of the materials used in the tailplane was linear orthographic materials. In the finite element modelling of the tailplane the mechanical properties needed to be specified for all three individual directions.

The data obtained from the experimental testing is used as basis for the modelling of the materials data. The transformed values obtained using the techniques explained are used. As ANSYS considers the whole 3 dimensional model, all the 3 dimensional properties of the materials were required and not just the 2 dimensional values as used in the laminate analysis. The extra properties were obtained by making the following

assumption. The properties of the composite in the z-direction are the same as the matrix material.

All the composite material properties were characterized using this linear orthographic model. The only exception made was for the foam material used as core in the structure. The foam material is a linear isotropic material and was modelled as such in the finite element model. This could be done as ANSYS has the capability of using different material models for the same analysis.

6.3.4. Mesh generation

The next step after the tailplane has been divided into the various areas is to specify the real constants for the various areas. The real constants describe the type of material used, thickness of individual layers and the orientation of the layers used in the analysis. Different real constants can be assigned to different regions of the tailplane. It is therefore in the real constants that the various lay-up schedules used in the tailplane is specified. Figure 6.3 illustrates the different lay-ups on the tailplane in different colours. Each of the coloured regions indicates a different real constant set.

After the real constants for all the areas have been specified the model can be meshed. There are two basic types of meshing options available to the analyst when using ANSYS. The first of these is mapped meshing. A mapped mesh is restricted to the element shape used and the pattern of the mesh. Irregular areas like some of the areas found in the tailplane can not be map meshed.

The second type of meshing possible is free meshing. In free meshing there is no predefined element shape or mesh pattern. Any irregular surface can be meshed with this option. It must however be insured that the aspect ratio of the elements used in the mesh does not become to large as this will influence the analysis adversely. The tailplane is therefore meshed using the free mesh option.

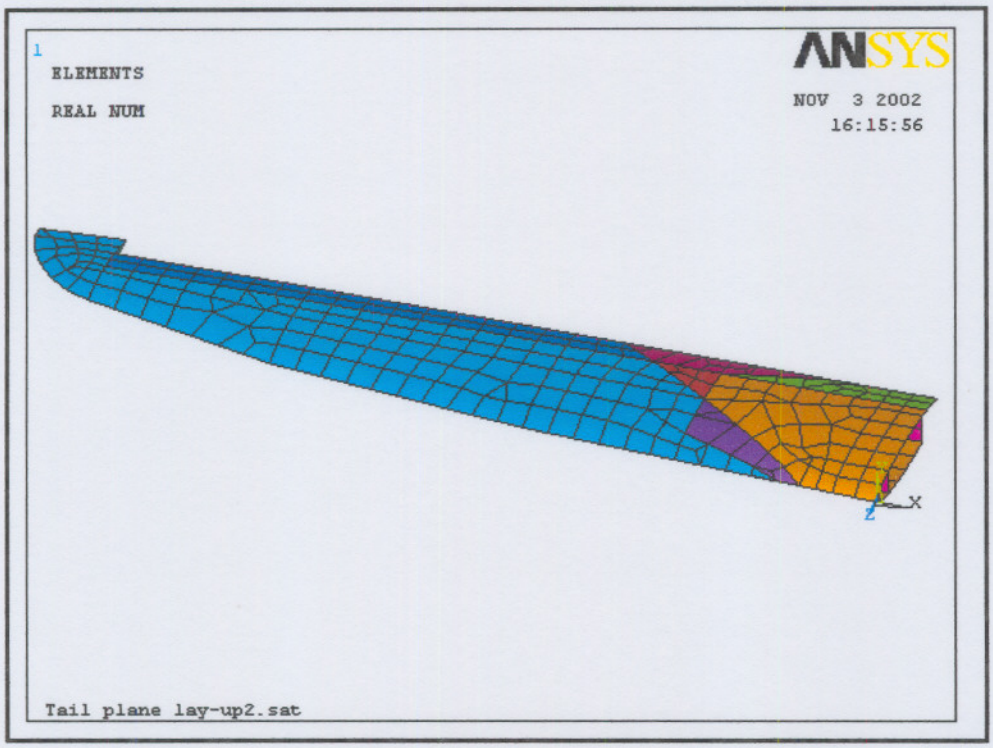

Figure 6.4: Tailplane coarse mesh

Illustrated in Figure 6.4 is the coarse mesh generated of the tailplane model. The element shapes used is quadrilateral higher order elements. This is however only the first basis mesh, as there will be made a number more to check whether the element size has an influence on the accuracy of the model.

The meshing of the model is the final step in the preparation of the finite element model. Different load scenarios can now be simulated using this model.

6.4. Static analysis

The first of the analyses that will be done on the model is a static analysis. A static analysis is used to determine the displacements, stresses, strains, etc. The static analysis will therefore serve as the basic verification of the analytical methods used in the previous chapter for the tailplane lay-up schedule.

The forces acting on the tailplane can however not be calculated all at once. Two analysis need to be done separately. The first hereof is the verification of the bending

and shear structures. Secondly the integrity of the structure due to the twisting moments acting thereon is calculated.

Before the loads and constraints can be applied to the tailplane it should also be noted that there are two distinct ways of applying loads and boundary conditions to a model in ANSYS. The first is to apply them directly on the nodes themselves. If the mesh of the model is however to change, all the loadings and constraints need to be reapplied to the new elements and nodes. The second option is applying the loads to the solid model. The mesh can be changed at any time without the need arising to define new loadings. The solid loads are transferred to the mesh by the program itself. Solid modelling is therefore used in the definition of the loads acting on the tailplane.

6.4.1. Pressure modelling

The loading exerted on the tailplane during normal operating conditions can be seen as variable pressure acting over the whole surface of the tailplane. An assumptions is made in the analysis process is that the air load pressure is constant. The air load will therefore be proportional to the chord length. This is not a true reflection of the loading exerted on the tailplane.

The true loading is calculated by means of equation 6.1. This equation is the definition of the dimensionless lift force coefficient C_L. The lift coefficient C_L varies over the length of the tailplane. Using this formula and the true C_L distribution over the tailplane the true air loading can be calculated.

$$C_L = \frac{L}{q_\infty S} \quad \text{where} \quad q_\infty = \frac{1}{2}\rho_\infty V_\infty^2 \qquad \text{...(6.1)}$$

The lift coefficient distribution of the tailplane is calculated using a panel method, and is calculated for 50 stations along half of the length of the tailplane. The force acting on the tailplane is then distributed over the different stations according to ratio calculated using equation 6.1 and the actual area of the different stations. Assuming that the air load pressure over the tailplane is constant the area can be normalized.

Normalizing the true lift distribution and comparing the different values against one another produces Figure 6.5.

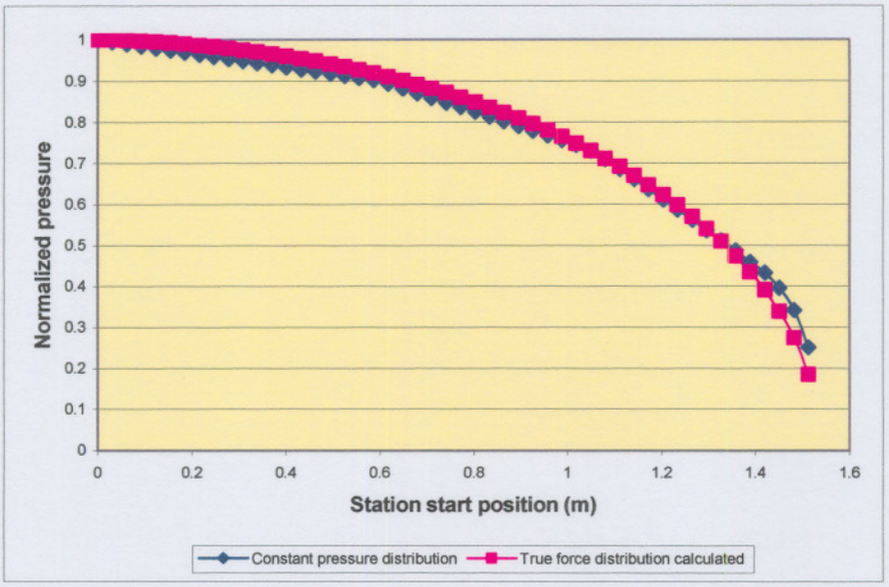

Figure 6.5: Normalized pressure distribution

It can be seen from Figure 6.5 that the assumption that the air load pressure acting on the tailplane can be assumed to be constant without sacrificing great accuracy.

This new constant pressure is then calculated as 0.0064 N/mm^2. This pressure is then applied over the whole top section of the tailplane. The next step is the application of the displacement boundary conditions followed by the symmetry boundary conditions.

The tailplane is supported only at the centre where it is attached to the fuselage. A connection interface exists here which is designed separately. This connection mechanism attaches to the tailplane at two points, one at the front of the tailplane and one at the rear thereof.

The web and shear connections found in the centre of the tailplane are added to aid in the transferring of the forces from the shear web to the fuselage. These two webs,

represented as two areas in the model, are therefore constricted against displacement in all degrees of freedom possible. These constrictions include linear as well as rotational displacements.

As described in the previous chapter the tailplane is symmetric around its centre. In the modelling of the tailplane we need to take advantage of this geometrical characteristic. Taking into account that the tailplane is symmetric, only half of the number of elements is needed for the same analysis. This translates into great savings into computational costs. We will therefore be applying symmetry boundary conditions at the centre of the tailplane.

Having applied all the various loadings and constraints to the model a static analysis of the tailplane can be done.

6.4.2. Results

The techniques listed below are used to verify that the solution of the model is correct:

1. displaced shape,
2. comparing model with a finer meshed model,
3. element sensitivity and
4. comparison with analytical data.

These different points will be discussed briefly below.

6.4.2.1. Displacement shape

The displaced shape of the tailplane is obtained from the ANSYS modelling. The tailplane displacement is illustrated in Figure 6.6. The maximum displacement of the tailplane is 100mm. Any discrepancies in the geometrical model, area connectivity etc., is observed using this displacement plot. The displacement plot also serves as the basis for checking whether the loadings and boundary conditions where applied correctly to the model.

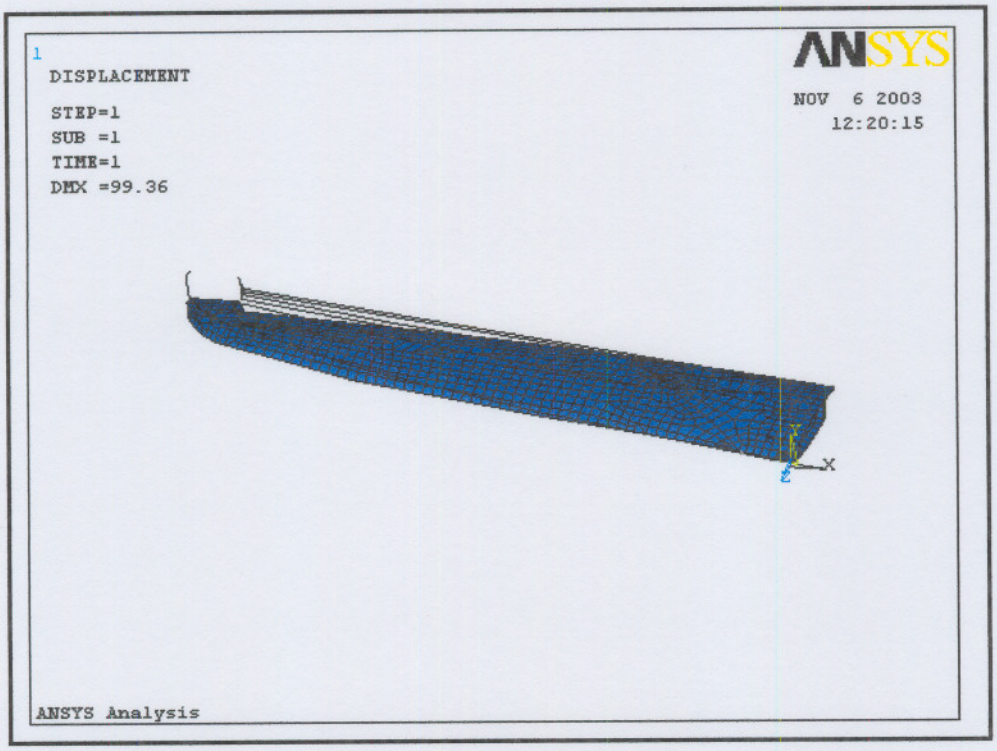

Figure 6.6: Displacement of tailplane

6.4.2.2. Finer mesh model

Comparison between the model used for the analysis and a model using finer elements is probably the most important part of the verification process of the tailplane. Noting that the finite element method is based on the principal of virtual displacements it will tend to underestimate displacements and strains. The solution is considered to be over stiff (Matthews, 1998:70). The stresses are therefore expected to converge from below. The answers obtained are not conservative; this must always be kept in mind.

The tailplane model is meshed a number of more times using increasingly smaller elements. The magnitude of the stress intensities did not change significantly with the increase of elements. As verification the deflections of the tailplane using different size elements were calculated and fell within 2% of each other. This is an indication that the model of the tailplane is not element size dependant.

6.4.2.3. Element sensitivity

The sensitivity of the model regarding the influences of different element shapes and orders also need to be inspected. These two aspects are inspected separately.

Firstly the shapes of the elements were inspected. Ensuring that the same amount of nodes are used for a mesh consisting of triangular elements as the number of nodes used in the quadratic mesh the model was analysed. Comparison of the stresses in the tailplane using triangular and quadrilateral elements shows a direct correlation. The different results obtained from the different analysis fall within extremely close proximity. The model of the tailplane is therefore not influenced by element shape.

This is however not true if the model is generated using lower-order elements. These lower-order elements only have nodes placed on their corners. The same size of element therefore has only half the number of nodes of the higher-order elements. Using these elements for the evaluation of the tailplane produces a result for the model analysis which is significantly lower than that of the higher-order elements. Lower-order elements are not capable of accurately predicting the bending of the elements. The model is therefore a lot stiffer and the stresses and strains are lower than what is expected.

The tailplane model is therefore influenced adversely when using lower-order elements for the evaluation of the model. Only higher order elements are used in the analysis to ensure that the model is depicted as accurately as possible.

6.4.2.4. Analytical verification

The final phase in the verification of the tailplane model is the comparison of the data obtained using the finite element model with the data calculated using analytical methods.

This is done by comparing the values for the individual layers used in the lay-up. It should be kept in mind that the analytical stresses must be recalculated for the lay-up of the individual sections as a whole. Using the analytical methods as described in the previous chapter the new stresses can be calculated for the individual layers. These

values can then be compared to the values calculated using the finite element program.

The individual values of the stresses and strains found in the finite element model of the tailplane are slightly lower than those calculated using the analytical methods. A number of reasons are responsible for this result. The first is the fact that the methods used in the analytical calculation only apply to flat plates. The complex shape of the tailplane should aid in the mechanical characteristics of the structure.

The second is the fact that the finite element method is over stiff. This equates to lower strains in the tailplane structure and in turn to lower internal stresses. A separate analysis of a simply supported I-beam was made to verify the influence of the finite element method on the stresses. Comparing the values obtained from the finite element analysis to analytical methods illustrated this by constantly returning values 4 percent lower than that of the analytical methods. It must therefore be kept in mind that the values of the tailplane model will also return values which are lower than that of the model.

The third role player in the lower stresses found in the finite element model of the tailplane is the influence that all the different sub-structures have on the tailplane as a whole. The influence of the lateral ribs and additional shear structures can not be analyzed using analytical methods. The structure becomes to complex to analyse with hand calculations. In the analytical design an assumption was also made that only certain of the sub-structures carry the different loadings individually.

Taking into account all these different aspects the values obtained using the finite element model are expected to be lower than the values obtained using the analytical plate theory. As an example the axial stresses found in the 6^{th} layer of the lay-up are illustrated in Figure 6.7. The position where the additional layer of unidirectional carbon fibre is added can be clearly seen. As expected the highest stresses are found in the bottom section where the chord length is at its lowest. The stresses here reach a maximum of 792 MPa. The values calculated using the analytical methods are 811.31 MPa.

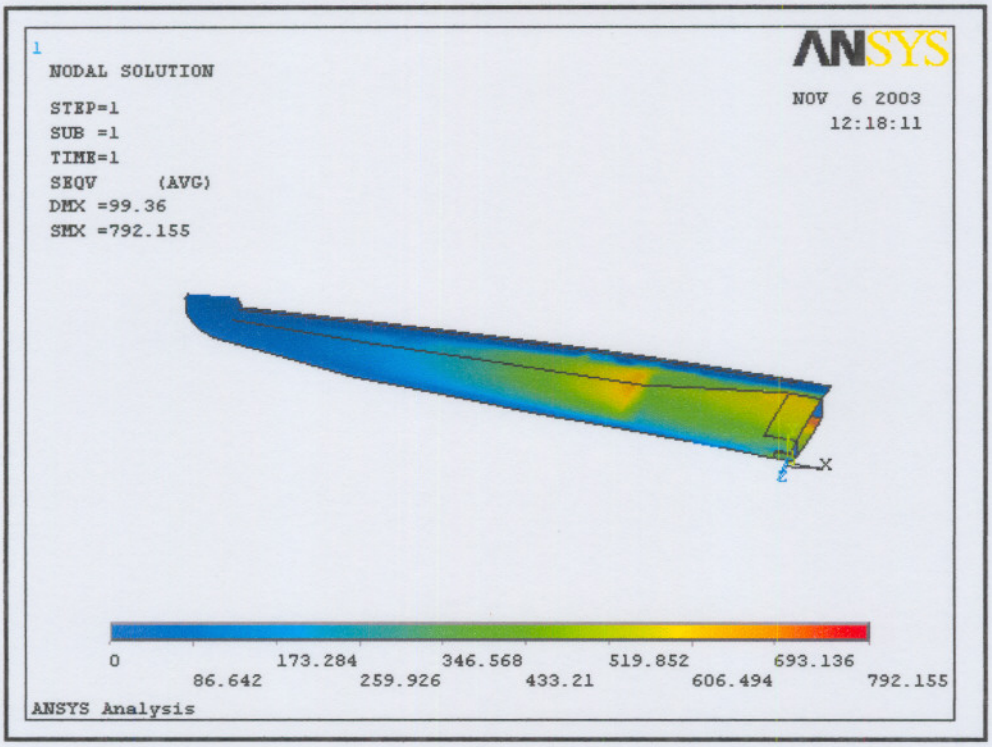

Figure 6.7: Stress intensity distribution over tailplane

All the different substructures where analyzed individually and all fell within extremely close proximity to those calculated using the analytical methods, taking into account the different factors influencing the magnitude of the values. It should however be noted that a number of stress concentrations arose on the boundaries of the model where the tailplane is fixed. These stresses were expected as the boundary conditions imposed on the model do not represent the actual attachments. The elements in the vicinity of these stresses were ignored in this analysis. It is however recommended that a full analysis be done on the tailplane attachments separately. The analysis results of all the substructures are found in the appendix of this report.

The values obtained using the finite element model can therefore be used with confidence in the analysis of the tailplane structure. A report generated using ANSYS on the numerical analysis is found in Appendix B.

6.5. Buckling analysis

The static analysis of the tailplane revealed that the internal stresses found in the tailplane due to the air loads fall well within the design specifications of the materials. This is however not the only analysis that needs to be done on the tailplane. Buckling can also occur in the structure. Buckling loads are the loads at which the structure becomes unstable.

A totally different analysis needs to be done in ANSYS to analyse the buckling characteristics of the structure. The analysis technique used is based on the normal Euler buckling approach. Eigenvalue buckling analysis predicts the theoretical buckling strength of an ideal linear elastic structure.

The values obtained do not take into account any non-linear characteristics or any imperfections in either the materials or the structure. It must therefore be kept in mind that the critical loads are slightly higher than what is expected in practice.

In a buckling analysis it is assumed that the materials can withstand any internal stresses. The loading is increased up to a point where the structure becomes unstable and the displacement at a specific point starts to diverge.

The loading that is exerted on the structure at the moment of this structural divergence is considered to be the buckling load. To ensure that buckling does not pose a problem the buckling load needs to be higher than the loading exerted on the tailplane before fracture occurs.

The first buckling occurs at the bottom skin of the tailplane. This is illustrated in Figure 6.8. The displacement at the point of buckling is exaggerated for illustration purposes.

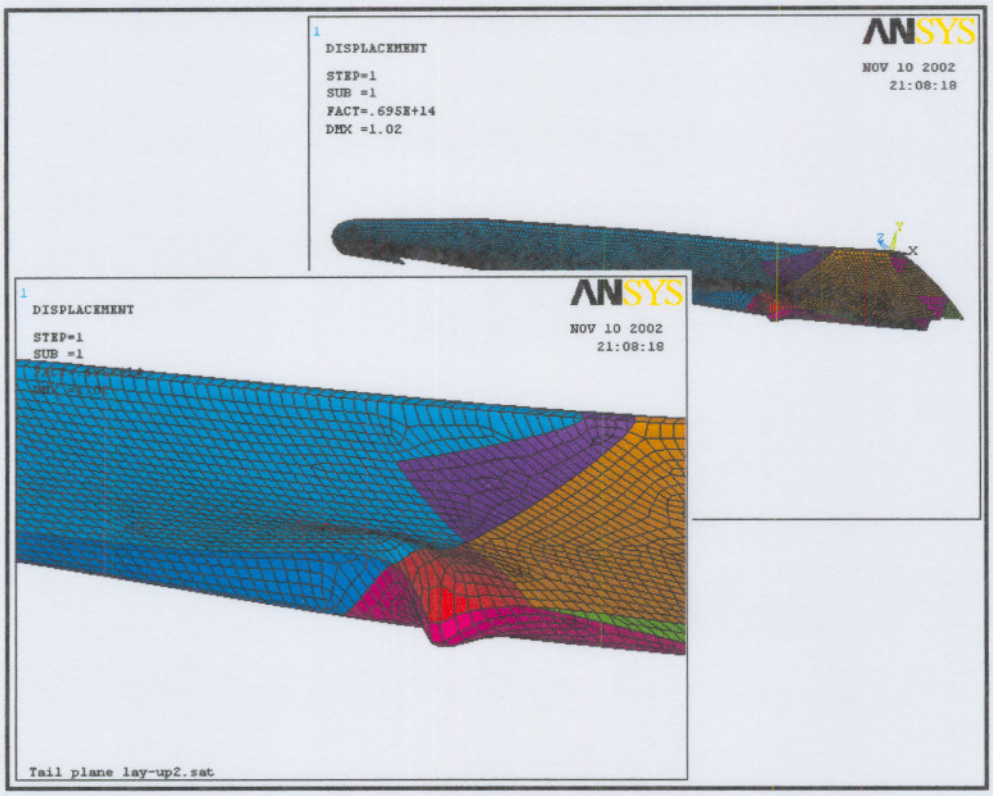

Figure 6.8: Buckling failure of tailplane

The buckling analysis returned a buckling load 8.6 times the loading of the air loads on the tailplane. This is 4 times higher than the value of the loading that can be exerted on the tailplane before structural fracture occurs. The structure therefore will fracture before buckling occurs.

The full ANSYS report concerning the tailplane is found in the appendix of this report.

6.6. Result comparison

The stresses throughout the tailplane and its substructures have now been calculated using the ANSYS (finite element method). These stresses can now be compared to those calculated using the empirical methods described in the previous chapter. The various substructures will be compared separately.

6.6.1. Tailplane flanges

If one where to compare the results of the numerical analysis of the tailplane flanges to that of the empirical calculations one would expect the values obtained using the numerical method to be lower than that of the values obtained using the empirical calculations.

This is due to two main reasons. The first of these is the fact that the tailplane flanges were designed with the empirical method as only the layers which are to carry the bending loads. In the final product the flanges are not the only layers found in the tailplane skins. The other layers added to carry the twisting moments and aid in the manufacturing of the tailplane also aid in carrying the bending loads. An LAP analysis using the empirical formulae is therefore done taking into account all these different layers. The LAP results for this calculation revealed lower internal stresses in the carbon flanges. These results are expected. The LAP analysis of the whole skins of the tailplane is given in the Appendix A of this study. The internal stresses in the tailplane flanges fell from 930 MPa to 811 MPa at the centre of the tailplane.

The second reason is due the fact that the empirical formulae do not take into account the curvature of the skins. It is therefore expected that the values of the internal lamina stresses will be even lower than the above mentioned values because these curved skins add to the stiffness of the final structure. The values of the internal stress in the flanges calculated using ANSYS (finite element method) is shown as being 770 MPa.

Having therefore assumed that the flanges of the tailplane absorb all the generated bending moments, translates in the flanges being over designed.

The same can be shown for the bottom skins. The internal stresses inside the skins are however higher than that of the top skin due to the fact of the fitments that is found at the back of the tailplane. The flanges are therefore shorter translating to higher internal stresses when subjected to the same loading.

6.6.2. Shear web

A similar comparison was done for the different shear webs as calculated. It was however not expected that the results would be the same as in the case of the flanges. The values expected for the stresses in the tailplane shear webs was expected to be lower than that in the analytical design. The reason being the presence of two webs (shear and elevator web), and the additional layer of 92110 woven glass which aids in the manufacturing process.

The internal stresses found in the shear web calculated with the analytical formulae yielded a value of 360 MPa. The value of the stress intensities as calculated using ANSYS was up to 300 MPa. A number of stress concentration points were seen at the elements bordering on the boundaries of the model. The full analysis of the webs found on the tailplane is found in the Appendix B of this document.

6.7. Conclusion

Having compared the different results of the two analysis techniques to one another all values changed according to what was expected. It was decided to keep the lay-up schedules of the tailplane of the glider the same as the one used in the numerical analysis using ANSYS.

The tailplane will be built using this lay-up schedule and will then be mechanically tested after which a conclusive decision can be made regarding the different analysis techniques.

7. ANALYSIS VERIFICATION

7.1. Introduction

Verification of the tailplane design forms an integral part of the total design and analysis of the newly designed tailplane. It also serves as the final process in the designing of the new tailplane. The testing of the tailplane is done by statically loading the tailplane, measuring the various displacements and then comparing these results to the values obtained using the finite element analysis program.

7.2. Manufacturing of the tailplane

The first step in the verification process is the manufacturing of a tailplane for which a finite element analysis has been done. Due to various restrictions on the availability of reinforcement material needed as specified in the initial design. An alternative tailplane was therefore manufactured by substituting the reinforcement material which was not available.

The reason that this was allowed was due to the fact that the initial tailplane was only to be used for testing and design process verifications. It did however necessitate the reanalysis of the tailplane with the finite element analysis program using the materials used in the manufacturing of the tailplane.

7.2.1. Altered Design

The major change which was made to the initial design was the usage of 200g/m^2 unidirectional carbon for the flanges instead of the suggested 120g/m^2. Using this material translates into much larger bending moment capacities.

7.2.2. Moulds

The first step in the manufacturing of the new tailplane is to manufacture the moulds which are to be used. A full 3-dimensional model of the tailplane was created in CAD program. Using this model and an additional program the G-codes are generated which are then transferred to a CNC milling machine.

The initial moulds are cut form SuperWood. The Super-Wood is used because of the relative consistent density throughout its thickness. It is also an extremely inexpensive method of creating these types of moulds.

After these moulds have been cut, the Super-Wood is sanded down slightly. This sanding is done to smooth out the roughness caused by the cutter path. After the sanding has been completed the mould is sealed using an epoxy. A number of layers of this epoxy are added in stages to the mould. Special care should was taken to ensure that the epoxy painted onto the moulds were applied in thin layers to prevent any streaking.

After allowing the epoxy time to cure it is again sanded down using extremely fine sanding paper to obtain a high gloss finish. A number of layers of polish are then added. These layers of polish are added to aid in the final extraction of the tailplane from the moulds.

7.2.3. Composite Lay-ups

After the application of the final layer of polish to the moulds the lay-up of the tailplane can be begun. The first step in the laying-up of the tailplane is the application of the gel-coat to the polished moulds.

Gel-coat forms the outer layer of the tailplane. This outer coating is added for the following reasons. Firstly it acts as a protective coating over the reinforcing material which isolates the reinforcing from harmful ultraviolet light. Ultraviolet light breaks down the structure of the epoxy bonding the reinforcing materials to one another.

Secondly the gel-coat acts as a surface which could be easily sanded own and polished on the final tailplane. Along with this the gel-coat acts as a filling material between the first layer of reinforcement material and the outer surface of the tailplane. The gel-coat is sprayed onto the surfaces of the moulds and need to be left for a period to start to thicken before the first layer of reinforcement is laid down.

After the gel-coat layer has reached the proper viscosity the first layer of reinforcement can be applied to the mould. A mixture of cotton flocks and epoxy resin is spread over the gel-coat. The first layer of the reinforcement material is then added and coated with epoxy resin. The following layers are then added consecutively to the moulds up until the foam layer.

Vacuum film is added over the foam layer and a vacuum is applied. The vacuum which is then created inside the vacuum bagging creates a positive pressure on the foam layer which ensures proper bonding of the stiff foam core material to the reinforcement material. The vacuum is kept until such a time as the epoxy resin has hardened.

The vacuum film can then be removed and the rest of the reinforcement material can be added to the moulds. On the application of the final layer to the moulds the vacuum bagging is added again to the moulds. A vacuum is again added to the moulds and sufficient time is given for the epoxy resins to harden.

7.2.4. Tailplane Assembly

The two parts of the tailplane can then be removed carefully from the tailplane moulds. The process of tailplane assembly can then be started. The first step in this process is to manufacture the attachment fittings of the horizontal tailplane onto the vertical tailplane.

The second step is the manufacturing of the front lip of the tailplane which is used to attach the two parts of the tailplane to one another on the front lip. A lip moulds is manufactured, which fits to the front of one of the moulds. This mould is manufactured to give a shape which approximately takes the shape of the other mould. This is illustrated in Figure 7.1.

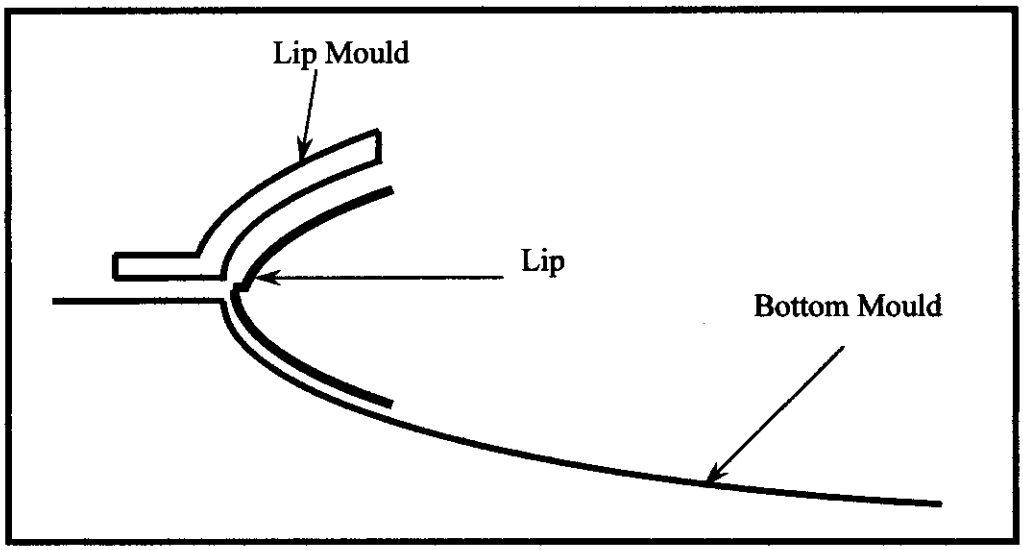

Figure 7.1: Lip mould set up

The next step in the manufacturing process is to manufacture the shear and flap web of the tailplane. These webs are manufactured in the form of a C shape. Firstly the reinforcement layers are laid over a wooden shape in the form of the shear web. The foam layer is then added and the final layers of the shear web are added. This is illustrated in Figure 7.2.

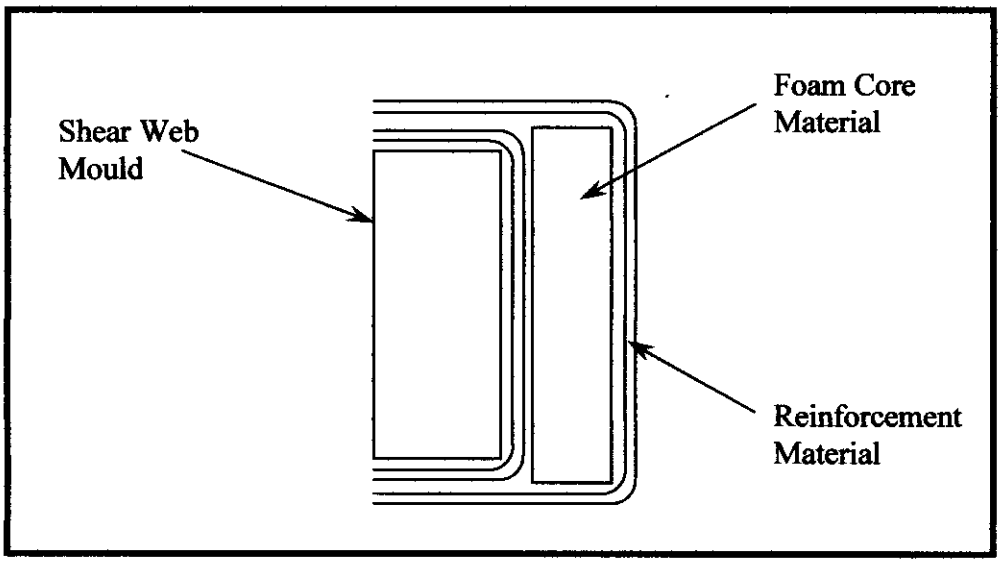

Figure 7.2: Shear web manufacturing

The webs are then attached to the bottom mould of the tailplane by means of a cotton flocks mixture. They are kept aligned by means of supports which are attached to the

mould structure. This ensures that they are in the correct position for when the tailplane is finally assembled.

Having built the lip mould onto the bottom mould as well as having attached the webs to the bottom mould the tailplane can be assembled. The surfaces of the lip mould and the webs which are to attach to the top mould during assembly is sanded down and coated with a layer of cotton flocks and epoxy resin which is used to bond the surfaces together. The top mould is then placed on top of the bottom mould and clamped down. Adequate time is then given for the epoxy resin to cure.

The tailplane can then be removed from the moulds and the final finishing thereof can be done. Due to the fact that this first tailplane extracted from the moulds will merely be used for testing purposes it will not be finished in the same manner as the tailplane which will be used on the gliders themselves.

The tailplane can therefore now be tested to verify the accuracy of the process used for the design of the tailplane.

7.2.5. Testing Mythology

A procedure for the testing of the tailplane needed to be designed. Due to the fact that it would be virtually impossible to apply the exact loading conditions experienced by the tailplane during flight conditions it was decided to apply a simplified loading.

The bending stresses in the tailplane are the most critical of the loading stresses. It was therefore decided to test the tailplane for these bending stresses. The bending displacements of the tailplane are also the easiest of the various displacements to measure.

A further simplification was made to the actual loading of the tailplane. During flight conditions the loading on the tailplane is distributed across the whole area of the tailplane. This would be extremely difficult to simulate. It was therefore decided that the loading on the tailplane will be done by using two point loadings per tailplane halve.

The loading would be done through a system of beams with a single point of origin. The points of contact of the loadings on the tailplane was chosen to ensure that the bending moments experienced by the tailplane. The bending moment exerted on the tailplane due to normal flight conditions and the bending moments exerted by the two point loadings are shown in Figure 7.3.

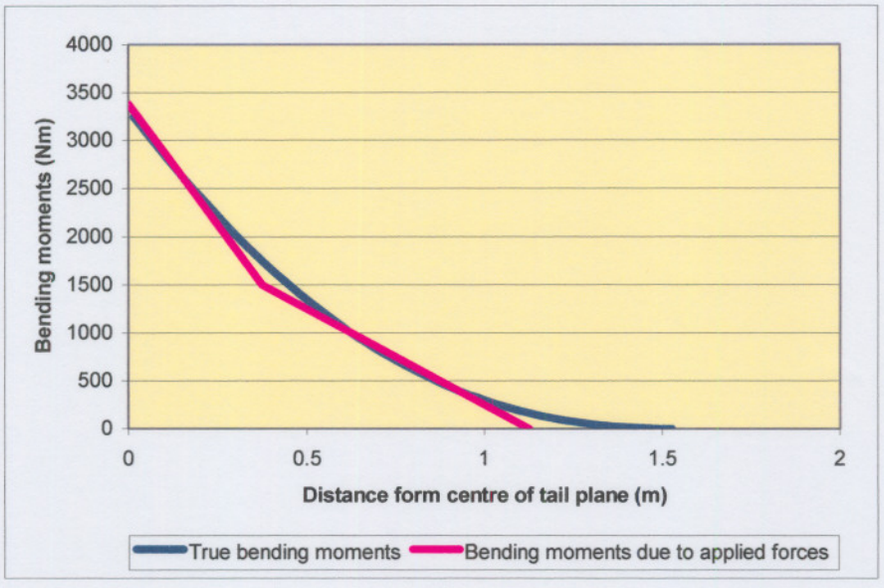

Figure 7.3: Comparison between true bending moments and bending moments due to applied forces

As seen in the graph above the bending moments created due to the point loading matches the bending moments of the normal loadings closely. This simplification will therefore subject the tailplane to the adequate loading set up.

This loading set up shown in Figure 7.4 will also be analysed using the finite element analysis technique. The displacements obtained from the mechanical testing and that obtained using ANSYS can then be compared. This comparison will then form the basis of the verification process of the tailplane design.

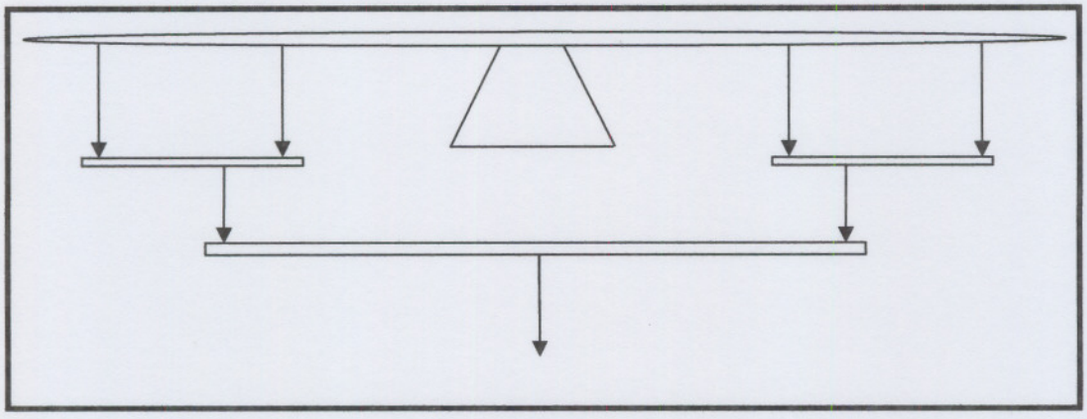

Figure 7.4: Whiffle tree set up

7.2.6. Mechanical Testing

The mechanical testing of the tailplane is done using the set up illustrated in Figure 7.4. The loading of the tailplane is done by attaching a chain block and load cell to the bottom beam.

The load cell is placed in between the beam and the chain block. Load is then slowly applied by shortening the chain block. The value of the load applied is then measured by means of the load cell.

The value of the loading applied and the deflection measured at the tip of the tailplane can then be obtained and tabled. These values are then used in conjunction with the values obtained from the finite element. The values which are obtained from the mechanical testing are however expected to differ from the values calculated using the finite element analysis program.

These differences are expected due to the various additional pieces of reinforcement. These additional pieces of reinforcement are found at the leading edged of the tailplane where the two halves are attached together and at the various positions where the webs are attached to the skins.

These additional pieces of reinforcing stiffen the tailplane and the true deflection of the tailplane is expected to be less than the values obtained using the finite element analysis program.

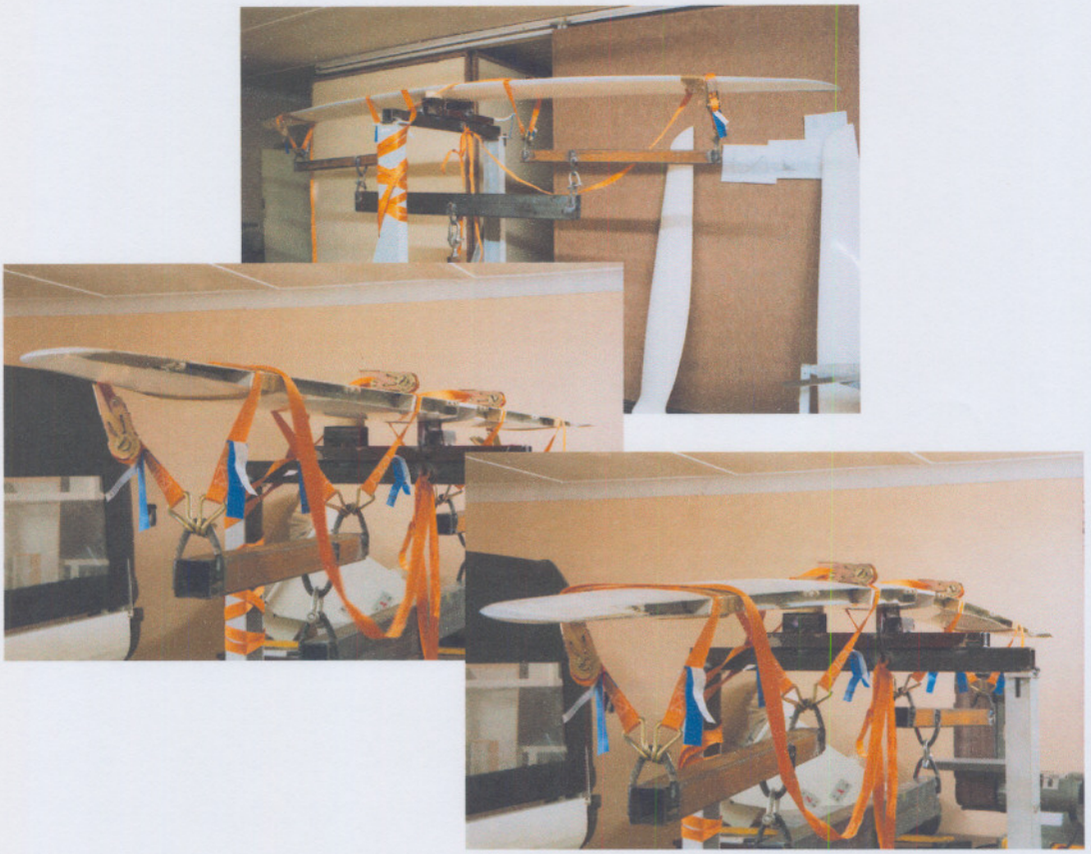

Figure 7.5: Mechanical loading set up

7.2.7. Deflection comparison

The deflections of the tip of the tailplane were measured at various loadings to obtain a trend. This trend was then also obtained using the same loadings in ANSYS. These two separate trends were then plotted together to verify the accuracy of the tailplane deflections simulated in ANSYS. The graph illustrated in Figure 7.6.

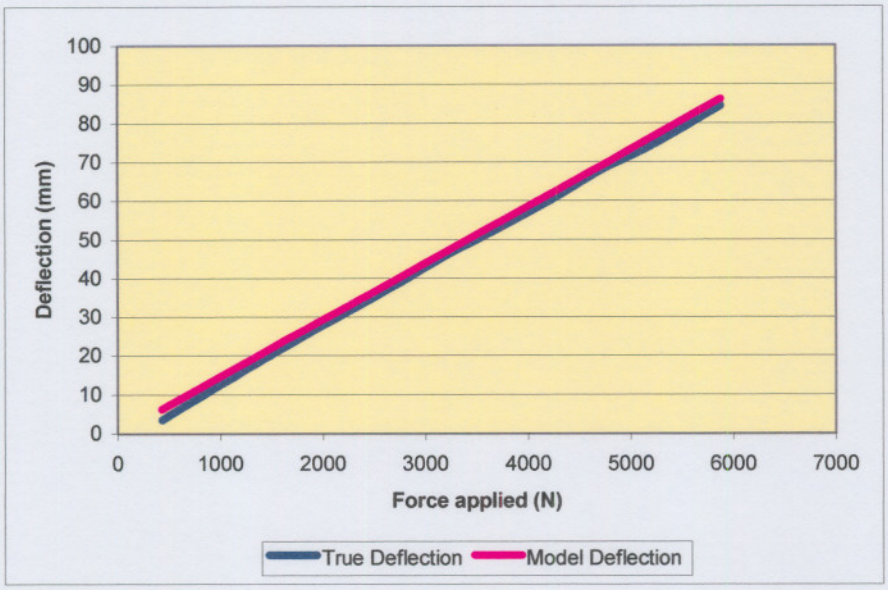

Figure 7.6: Comparison between true deflection of tailplane and deflections of model

The deflections obtained using the ANSYS model is slightly higher throughout the various loading conditions. This falls in line with the expected values. On average the deflections of the tailplane was found to be 3.5% lower than that of the model.

From the Figure 7.6 it can be seen that the difference between the deflection of the model and the true deflections are slightly higher at the lower forces. This can be explained due to the additional glass fibre reinforcements which are added on to the tailplane at the lip and on the contact surfaces between the web and the tailplane skins. These additional pieces of glass fibre reinforcement are not modelled in ANSYS. As the forces on the tailplane increases the role of these pieces of reinforcement become less which would mean that the true deflections would come more in line with the deflections modelled in ANSYS.

7.3. Conclusion

The verification of the tailplane was done by loading the tailplane with various different loadings. These loadings were then reproduced in the ANSYS model. Using the data obtained from the experimental testing and the ANSYS model the accuracy of the model was determined. The experimental and the model data correlated within 3.5% for the deflection due to loadings. It can therefore be said that the finite element model used in ANSYS accurately represents the true tailplane.

The comparison of the ANSYS modelling deflections and the actual mechanical testing deflections indicate that the method of analysis is correct. It can therefore be assumed that the tailplane which was designed for the new glider will also be correct.

8. CONCLUSION

8.1. Conclusion

A process for the design and analysis of new composite material parts for use on gliders were compiled and tested. The process starts at the phase of the design process where the composite material properties are obtained and tested.

The second step in the process is the empirical design of the specific part. This is done using a number of classical formulas compiled for composite materials. These formulas however have a number of limitations. The most important of these limitations is the lack to adequately represent the complex shapes of the structures used in gliders. The empirical design is therefore merely a tool with which to obtain an initial reference for the design.

To address these problems a numerical analysis technique, in the form of a finite element analysis code, was used to change the design to better suit the application in the glider.

Due to limitations on the availability of certain of the reinforcement materials a variation of the true tailplane was manufactured. This tailplane was also modelled in ANSYS to determine whether the finite element models generated in ANSYS accurately represents the tailplane designed.

This physical model is then loaded to obtain the deflections of the tailplane. These loadings were reproduced on the finite element model of the tailplane in ANSYS. A comparison between the deflections of the true and the model deflections revealed an accuracy of the model of 3.5% according to the expected displacements compared to the true displacements.

The model therefore accurately represents the tailplane which was manufactured. It can therefore be assumed that the initial model generated for the tailplane which will be used on the glider also will accurately represent its physical counterpart.

The method used for the design and analysis of composite material structures used for this design can therefore be assumed to be accurate and successful. It can therefore be assumed that the tailplane which was initially designed for the JS1 glider will also fulfil the requirements of the design, as indicated in the analysis.

8.2. Recommendations for further studies

Due to the complexity of the modelling of composite materials the basic mechanical properties of the various constituents need to be obtained and verified as this forms the basis of the whole design process. It is therefore suggested that a full study be done of all the various materials which are going to be used on the manufacturing of the glider. All these different reinforcement materials (various types and weights) need to be analysed separately. All these various mechanical properties need to be used to compile a database of all the various constituents used. This will aid in design process and shorten the design time.

Another aspect which needs to be investigated is the numerical modelling of the dynamic movement of the tailplane. To be more precise the flutter characteristics of the composite structures need to be determined to ensure that the stiffness of the structure is sufficient for all operating conditions.

9. BIBLIOGRAPHY

GIBSON, R.F. 1994. Principles of composite materials mechanics. Singapore: McGraw-Hill, Inc. 425p.

ANDERSON, J.D. Jr. 1991. Fundamentals of aerodynamics. Singapore: McGraw-Hill, Inc 772p.

SHIGLEY, J.E. 1989. Mechanical engineering design. Singapore: McGraw-Hill, Inc. 779p.

SWANSON, S.R. 1997. Advanced Composite materials. Upper Saddle River: Prentice-Hall, Inc. 249p.

HOLLMANN, M. 1996. Modern aircraft design, Volume 1 4th Edition. Monterey: Hollmann 239p.

HERAKOVICH, C.T. 1998. Mechanics of fibrous composites. New York: John Wiley & Sons, Inc. 460p.

WINDOW, A.L. & HOLISTER, G.S. 1983. Strain gauge technology. New York: Elsevier Science Publishing CO., Inc. 356p.

BERG, J.S. & ADAMS, D.F. 1989. An evaluation of composite material compression test methods. *Journal of composite technology and research*, 11(2):41-46, Summer.

SCHOEPPNER, G.A. & SIERAKOWSKI, R.L. 1990. Review of compression test methods for organic matrix composites. *Journal of composite technology and research*, 12(1):3-12, Spring.

MEGSON, T.H.G. 1982. Aircraft structures for engineering students. London: Edward Arnold Ltd. 485p.

Skin Lay-up

Layer Number	Material Type	Material Thickness	Material Direction
1	Woven Glass	0.06417	0
2	Woven Glass	0.06417	0
3	Woven Glass	0.06417	0
4	Woven Kevlar	0.04236	45
5	Foam Core	5	-
6	Unidirectional Carbon	0.12222	0
7	Unidirectional Carbon	0.12222	0
8	Unidirectional Carbon	0.12222	0
9	Woven Kevlar	0.04236	45
10	Woven Glass	0.06417	0
11	Woven Glass	0.06417	0
12	Woven Glass	0.19444	45

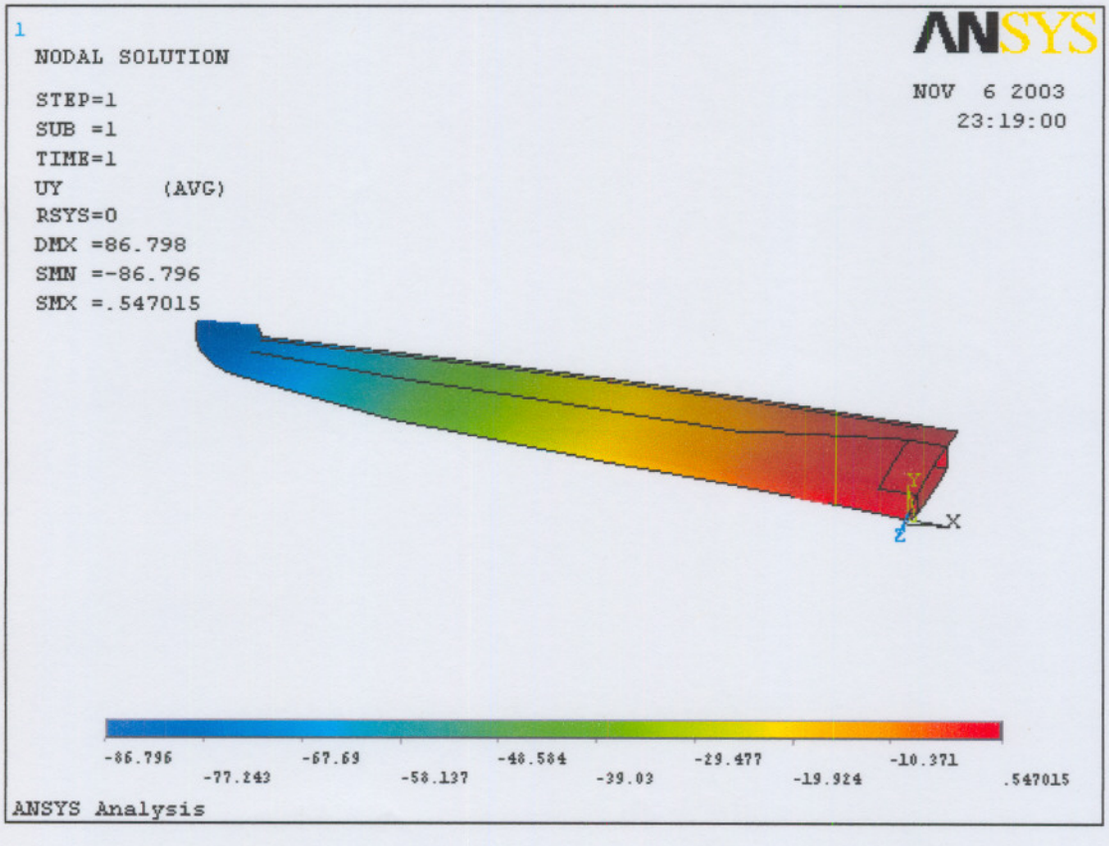

Translation

LOKEN, H. & HOLLMANN, M. 1988. Designing with core. Monterey: Aircraft Designs, Inc. 123p.

OCHOA, O.O. & REDDY, J.N. 1992. Finite element analysis of composite laminates. Dordrecht: Kluwer Academic Publishers 206p.

MATTHEWS, F.L., DAVIES, G.A.O., HITCHINGS, D. & SOUTIS, C. 1998. Finite element modelling of composite materials and structures. London: University of London. 201p.

THOMAS, F. 1999. Fundamentals of sailplane design. Maryland: College Park Press. 274p.

TARNOPOL'SKII Yu. M. & KULAKOV V.L. 1998. Handbook of composites. London: Chapman & Hall. 1135p.

WHITNEY, J.M., DANIEL, I.M. & PIPES, R.B., 1982. Experimental mechanics of fibre composite materials, *Society for experimental mechanics*, Bethel.

LEE, S. & MUNRO, M., 1986. Evaluation of In-Plane shear test methods for advanced composite materials by decision analysis technique. *Composites*. 17(1):13-22.

CREMER, M., 1995. Konstruktion des flügels für das segelflugzeug AFH26. Universität Hannover. 112p.

WEBER, K.F. & DIRKS, W., 2002. Construction rules and standards for the construction of sailplanes. 5p.

JOINT AVIATION AUTHORITIES, 2001. JAR22: Sailplanes and powered sailplanes.

APPENDIX A:

LAMINATE ANALYSIS PROGRAM RESULTS

The results of the laminate analysis program for the various critical section of the tailplane are presented in this section. The order of the results is listed below:

1. Tailplane flange - centre section,
2. Tailplane flange – 215 mm from centre section,
3. Tailplane shear web – centre section,
4. Tailplane skin – centre section and the
5. Tailplane skin – 400 mm from centre section.

Report TAILPLANE - FLANGE - CENTRE
Laminate analysis program analysis of flange sections in centre of tail plane
Data File : C:\Documents and Settings\Christoff\Desktop\Tail plane.ld
Units : mm N deg °C -
Volume fraction correction method : Halpin-Tsai
Failure tracked by : Tsai-Wu Tsai-Hill Hoffman Max.stress

Material properties for lay-up FLANGE-CENTRE :

Material : CARBON UD

E11	= 188000	N/mm²
E22	= 18000	N/mm²
G12	= 500	N/mm²
v12	= 0.05	
a11	= (undefined)	
a22	= (undefined)	
ß11	= (undefined)	
ß22	= (undefined)	
E resin	= (undefined)	
v resin	= (undefined)	
Vf nom.	= (undefined)	
Vf act.	= (undefined)	
S11T	= 2150	N/mm²
S22T	= 180	N/mm²
S11C	= 1280	N/mm²
S22C	= 100	N/mm²
S12	= 250	N/mm²
F12	= auto	

Selected Lay-up : FLANGE-CENTRE
Lay-up is not symmetric Total number of layers = 2
Total thickness: nominal = 0.1534 mm actual = 0.1534 mm
Curing Temperature = 0 °C Room Temperature = 0 °C

Layer	material name	thickness (nominal, mm)	angle (deg)
	- - - top - - -		
1 :	CARBON UD	0.0767	0
2 :	CARBON UD	0.0767	0
	- - bottom - -		

Selected Loading : FLANGE-CENTRE (ref: Operating Conditions)

			order	steps
X Strain	= -0.004315	-	1	1
Y Strain	= 0.000116	-	1	1
XY Load	= 0	N/mm	1	1
X Moment	= 0	N	1	1
Y Moment	= 0	N	1	1
XY Moment	= 0	N	1	1
Top Temperature	= 0	°C		
Bottom Temperature	= 0	°C		
Moisture Content	= 0	% weight		

ABD Matrix : [N/mm N ; N N mm]

28846.1	138.093	0	0	0	0
138.093	2761.86	0	0	0	0
0	0	76.7	0	0	0
0	0	0	56.5662	0.270795	0
0	0	0	0.270795	5.41591	0
0	0	0	0	0	0.150406

Layer Stress list :

All Directions, Mechanical
Units : N/mm²

Layer	XX	YY	XY	11	22	12
1	-811.310	-1.796	0.000	-811.310	-1.796	0.000
	-811.310	-1.796	0.000	-811.310	-1.796	0.000
2	-811.310	-1.796	0.000	-811.310	-1.796	0.000
	-811.310	-1.796	0.000	-811.310	-1.796	0.000

Layer Strain list :

All Directions, Mechanical
Units : -

Layer	XX	YY	XY	11	22	12
1	-0.004	0.000	0.000	-0.004	0.000	0.000
	-0.004	0.000	0.000	-0.004	0.000	0.000
2	-0.004	0.000	0.000	-0.004	0.000	0.000
	-0.004	0.000	0.000	-0.004	0.000	0.000

Failure index list :
(The energy-based criteria are shown square-rooted)

Layer	Tsai-Wu	Tsai-Hill	Hoffman	Max.Stress	Max.Strain
1	0.705	0.633	0.709	0.634	0.634
	0.705	0.633	0.709	0.634	0.634
2	0.705	0.633	0.709	0.634	0.634
	0.705	0.633	0.709	0.634	0.634

Report TAILPLANE - FLANGE 215MM
Laminate analysis program analysis of flange sections in centre of tail plane
Data File : C:\Documents and Settings\Christoff\Desktop\Tail plane.ld
Units : mm N deg °C -
Volume fraction correction method : Halpin-Tsai
Failure tracked by : Tsai-Wu Tsai-Hill Hoffman Max.stress

Material properties for lay-up FLANGE-CENTRE :

Material : CARBON UD

E11	= 188000	N/mm²
E22	= 18000	N/mm²
G12	= 500	N/mm²
v12	= 0.05	
a11	= (undefined)	
a22	= (undefined)	
ß11	= (undefined)	
ß22	= (undefined)	
E resin	= (undefined)	
v resin	= (undefined)	
Vf nom.	= (undefined)	
Vf act.	= (undefined)	
S11T	= 2150	N/mm²
S22T	= 180	N/mm²
S11C	= 1280	N/mm²
S22C	= 100	N/mm²
S12	= 250	N/mm²
F12	= auto	

Selected Lay-up : FLANGE-CENTRE
Lay-up is not symmetric Total number of layers = 2
Total thickness: nominal = 0.1534 mm actual = 0.1534 mm
Curing Temperature = 0 °C Room Temperature = 0 °C

Layer	material name	thickness (nominal, mm)	angle (deg)
	- - - top - - -		
1 :	CARBON UD	0.0767	0
2 :	CARBON UD	0.0767	0
	- - bottom - -		

Selected Loading : FLANGE - 215MM (ref: Operating Conditions)

			order	steps
X Strain	= -0.00549	-	1	1
Y Strain	= 0.001	-	1	1
XY Load	= 0	N/mm	1	1
X Moment	= 0	N	1	1
Y Moment	= 0	N	1	1
XY Moment	= 0	N	1	1
Top Temperature	= 0	°C		
Bottom Temperature	= 0	°C		
Moisture Content	= 0	% weight		

ABD Matrix : [N/mm N ; N N mm]

28846.1	138.093	0	0	0	0
138.093	2761.86	0	0	0	0
0	0	76.7	0	0	0
0	0	0	56.5662	0.270795	0
0	0	0	0.270795	5.41591	0
0	0	0	0	0	0.150406

Layer Stress list :

All Directions, Mechanical
Units : N/mm²

Layer	XX	YY	XY	11	22	12
1	-1031.467	13.062	0.000	-1031.467	13.062	0.000
	-1031.467	13.062	0.000	-1031.467	13.062	0.000
2	-1031.467	13.062	0.000	-1031.467	13.062	0.000
	-1031.467	13.062	0.000	-1031.467	13.062	0.000

Layer Strain list :

All Directions, Mechanical
Units : -

Layer	XX	YY	XY	11	22	12
1	-0.005	0.001	0.000	-0.005	0.001	0.000
	-0.005	0.001	0.000	-0.005	0.001	0.000
2	-0.005	0.001	0.000	-0.005	0.001	0.000
	-0.005	0.001	0.000	-0.005	0.001	0.000

Failure index list :
(The energy-based criteria are shown square-rooted)

Layer	Tsai-Wu	Tsai-Hill	Hoffman	Max.Stress	Max.Strain
1	0.851	0.814	0.818	0.806	0.806
	0.851	0.814	0.818	0.806	0.806
2	0.851	0.814	0.818	0.806	0.806
	0.851	0.814	0.818	0.806	0.806

Report TAILPLANE - SHEAR WEB - CENTRE
Laminate analysis program analysis of flange sections in centre of tail plane
Data File : C:\Documents and Settings\Christoff\Desktop\Tail plane.ld
Units : mm N deg °C -
Volume fraction correction method : Halpin-Tsai
Failure tracked by : Tsai-Wu Tsai-Hill Hoffman Max.stress

Material properties for lay-up SHEAR WEB - CENTRE :

Material : GLASS WOVEN

E11	= 45300	N/mm²
E22	= 45300	N/mm²
G12	= 10800	N/mm²
v12	= 0.28	
a11	= (undefined)	
a22	= (undefined)	
ß11	= (undefined)	
ß22	= (undefined)	
E resin	= (undefined)	
v resin	= (undefined)	
Vf nom.	= (undefined)	
Vf act.	= (undefined)	
S11T	= 746	N/mm²
S22T	= 746	N/mm²
S11C	= 540	N/mm²
S22C	= 540	N/mm²
S12	= 165	N/mm²
F12	= auto	

Selected Lay-up : SHEAR WEB - CENTRE
Lay-up is not symmetric Total number of layers = 2
Total thickness: nominal = 0.38888 mm actual = 0.38888 mm
Curing Temperature = 0 °C Room Temperature = 0 °C

Layer	material name	thickness (nominal, mm)	angle (deg)
	- - - top - - -		
1 :	GLASS WOVEN	0.19444	45
2 :	GLASS WOVEN	0.19444	45
	- - bottom - -		

Selected Loading : SHEAR WEB - CENTRE (ref: Operating Conditions)

			order	steps
X Strain	= -0.0004315	-	1	1
Y Strain	= 0.000116	-	1	1
XY Load	= 140	N/mm	1	1
X Moment	= 0	N	1	1
Y Moment	= 0	N	1	1
XY Moment	= 0	N	1	1
Top Temperature	= 0	°C		
Bottom Temperature	= 0	°C		
Moisture Content	= 0	% weight		

ABD Matrix : [N/mm N ; N N mm]

16433.4	8033.61	0	0	0	0
8033.61	16433.4	0	0	0	0
0	0	6881.35	0	0	0
0	0	0	207.099	101.242	0
0	0	0	101.242	207.099	0
0	0	0	0	0	86.7209

Layer Stress list :

All Directions, Mechanical
Units : N/mm²

Layer	XX	YY	XY	11	22	12
1	-15.838	-4.012	360.008	350.083	-369.933	5.913
	-15.838	-4.012	360.008	350.083	-369.933	5.913
2	-15.838	-4.012	360.008	350.083	-369.933	5.913
	-15.838	-4.012	360.008	350.083	-369.933	5.913

Layer Strain list :

All Directions, Mechanical
Units : -

Layer	XX	YY	XY	11	22	12
1	-0.000	0.000	0.020	0.010	-0.010	0.001
	-0.000	0.000	0.020	0.010	-0.010	0.001
2	-0.000	0.000	0.020	0.010	-0.010	0.001
	-0.000	0.000	0.020	0.010	-0.010	0.001

Failure index list :
(The energy-based criteria are shown square-rooted)

Layer	Tsai-Wu	Tsai-Hill	Hoffman	Max.Stress	Max.Strain
1	0.988	0.961	0.988	0.685	0.867
	0.988	0.961	0.988	0.685	0.867
2	0.988	0.961	0.988	0.685	0.867
	0.988	0.961	0.988	0.685	0.867

Report TAILPLANE - SKIN - CENTRE
Laminate analysis program analysis of flange sections in centre of tail plane
Data File : C:\Documents and Settings\Christoff\Desktop\Tail plane.ld
Units : mm N deg °C -
Volume fraction correction method : Halpin-Tsai
Failure tracked by : Tsai-Wu Tsai-Hill Hoffman Max.stress

Material properties for lay-up SKIN - CENTRE :

Material : GLASS WOVEN

E11	= 45300	N/mm²
E22	= 45300	N/mm²
G12	= 10800	N/mm²
v12	= 0.28	
a11	= (undefined)	
a22	= (undefined)	
ß11	= (undefined)	
ß22	= (undefined)	
E resin	= (undefined)	
v resin	= (undefined)	
Vf nom.	= (undefined)	
Vf act.	= (undefined)	
S11T	= 746	N/mm²
S22T	= 746	N/mm²
S11C	= 540	N/mm²
S22C	= 540	N/mm²
S12	= 165	N/mm²
F12	= auto	

Material : KEVLAR WOVEN

E11	= 86000	N/mm²
E22	= 86000	N/mm²
G12	= 4430	N/mm²
v12	= 0.185	
a11	= (undefined)	
a22	= (undefined)	
ß11	= (undefined)	
ß22	= (undefined)	
E resin	= (undefined)	
v resin	= (undefined)	
Vf nom.	= (undefined)	
Vf act.	= (undefined)	
S11T	= 1086	N/mm²
S22T	= 1086	N/mm²
S11C	= 753	N/mm²
S22C	= 753	N/mm²
S12	= 55	N/mm²
F12	= auto	

Selected Lay-up : SKIN - CENTRE
Lay-up is not symmetric Total number of layers = 3
Total thickness: nominal = 0.27964 mm actual = 0.27964 mm
Curing Temperature = 0 °C Room Temperature = 0 °C

Layer	material name	thickness (nominal, mm)	angle (deg)
	- - - top - - -		
1 :	GLASS WOVEN	0.19444	45
2 :	KEVLAR WOVEN	0.0426	45
3 :	KEVLAR WOVEN	0.0426	45

- - bottom - -

Selected Loading : SKIN - CENTRE (ref: Operating Conditions)

			order	steps
X Load	= 0	N/mm	1	1
Y Load	= 0	N/mm	1	1
XY Load	= 86	N/mm	1	1
X Moment	= 0	N	1	1
Y Moment	= 0	N	1	1
XY Moment	= 0	N	1	1
Top Temperature	= 0	°C		
Bottom Temperature	= 0	°C		
Moisture Content	= 0	% weight		

ABD Matrix : [N/mm N ; N N mm]

13089.4	8134.59	0	123.687	229.214	0
8134.59	13089.4	0	229.214	123.687	0
0	0	6532.32	0	0	153.997
123.687	229.214	0	89.8013	61.3558	0
229.214	123.687	0	61.3558	89.8013	0
0	0	153.997	0	0	48.1757

Layer Stress list :

All Directions, Mechanical
Units : N/mm²

Layer	XX	YY	XY	11	22	12
1	-0.000	0.000	364.558	364.558	-364.558	-0.000
	-0.000	0.000	207.961	207.961	-207.961	-0.000
2	-0.000	0.000	426.455	426.455	-426.455	-0.000
	-0.000	0.000	356.099	356.099	-356.099	-0.000
3	-0.000	0.000	356.099	356.099	-356.099	-0.000
	-0.000	0.000	285.743	285.743	-285.743	-0.000

Layer Strain list :

All Directions, Mechanical
Units : -

Layer	XX	YY	XY	11	22	12
1	0.000	0.000	0.021	0.010	-0.010	-0.000
	0.000	0.000	0.012	0.006	-0.006	-0.000
2	0.000	0.000	0.012	0.006	-0.006	-0.000
	0.000	0.000	0.010	0.005	-0.005	-0.000
3	0.000	0.000	0.010	0.005	-0.005	-0.000
	0.000	0.000	0.008	0.004	-0.004	-0.000

Failure Index list :
(The energy-based criteria are shown square-rooted)

Layer	Tsai-Wu	Tsai-Hill	Hoffman	Max.Stress	Max.Strain
1	0.995	0.966	0.995	0.675	0.864
	0.568	0.551	0.568	0.385	0.493
2	0.817	0.793	0.817	0.566	0.671
	0.682	0.662	0.682	0.473	0.560

3	0.682	0.662	0.682	0.473	0.560
	0.547	0.531	0.547	0.379	0.450

Report TAILPLANE - SKIN - 400MM
Laminate analysis program analysis of flange sections in centre of tail plane
Data File : C:\Documents and Settings\Christoff\Desktop\Tail plane.ld
Units : mm N deg °C -
Volume fraction correction method : Halpin-Tsai
Failure tracked by : Tsai-Wu Tsai-Hill Hoffman Max.stress

Material properties for lay-up SKIN - 400MM :

Material : KEVLAR WOVEN

E11	= 86000	N/mm²
E22	= 86000	N/mm²
G12	= 4430	N/mm²
v12	= 0.185	
a11	= (undefined)	
a22	= (undefined)	
ß11	= (undefined)	
ß22	= (undefined)	
E resin	= (undefined)	
v resin	= (undefined)	
Vf nom.	= (undefined)	
Vf act.	= (undefined)	
S11T	= 1086	N/mm²
S22T	= 1086	N/mm²
S11C	= 753	N/mm²
S22C	= 753	N/mm²
S12	= 55	N/mm²
F12	= auto	

Selected Lay-up : SKIN - 400MM
Lay-up is not symmetric Total number of layers = 2
Total thickness: nominal = 0.0852 mm actual = 0.0852 mm
Curing Temperature = 0 °C Room Temperature = 0 °C

Layer	material name	thickness (nominal, mm)	angle (deg)
	- - - top - - -		
1 :	KEVLAR WOVEN	0.0426	45
2 :	KEVLAR WOVEN	0.0426	45
	- - bottom - -		

Selected Loading : SKIN - 400MM (ref: Operating Conditions)

			order	steps
X Load	= 0	N/mm	1	1
Y Load	= 0	N/mm	1	1
XY Load	= 44	N/mm	1	1
X Moment	= 0	N	1	1
Y Moment	= 0	N	1	1
XY Moment	= 0	N	1	1
Top Temperature	= 0	°C		
Bottom Temperature	= 0	°C		
Moisture Content	= 0	% weight		

ABD Matrix : [N/mm N ; N N mm]

4872.65	4117.78	0	0	0	0
4117.78	4872.65	0	0	0	0
0	0	3091.65	0	0	0
0	0	0	2.94756	2.49093	0
0	0	0	2.49093	2.94756	0
0	0	0	0	0	1.8702

Layer Stress list :

All Directions, Mechanical
Units : N/mm²

Layer	XX	YY	XY	11	22	12
1	-0.000	0.000	516.432	516.432	-516.432	-0.000
	-0.000	0.000	516.432	516.432	-516.432	-0.000
2	-0.000	0.000	516.432	516.432	-516.432	-0.000
	-0.000	0.000	516.432	516.432	-516.432	-0.000

Layer Strain list :

All Directions, Mechanical
Units : -

Layer	XX	YY	XY	11	22	12
1	0.000	0.000	0.014	0.007	-0.007	-0.000
	0.000	0.000	0.014	0.007	-0.007	-0.000
2	0.000	0.000	0.014	0.007	-0.007	-0.000
	0.000	0.000	0.014	0.007	-0.007	-0.000

Failure index list :
(The energy-based criteria are shown square-rooted)

Layer	Tsai-Wu	Tsai-Hill	Hoffman	Max.Stress	Max.Strain
1	0.989	0.961	0.989	0.686	0.813
	0.989	0.961	0.989	0.686	0.813
2	0.989	0.961	0.989	0.686	0.813
	0.989	0.961	0.989	0.686	0.813

APPENDIX B:

ANSYS ANALYSIS OF TAILPLANE

A report of the ANSYS analysis of the tailplane which was designed is attached in this section. The deflections of the tailplane as well as the stress intensities of all the layers of the various sections are illustrated.

TAIL PLANE - ANSYS ANALYSIS

By G.C. Kühn

November 07, 2003

Report Generated by ANSYS

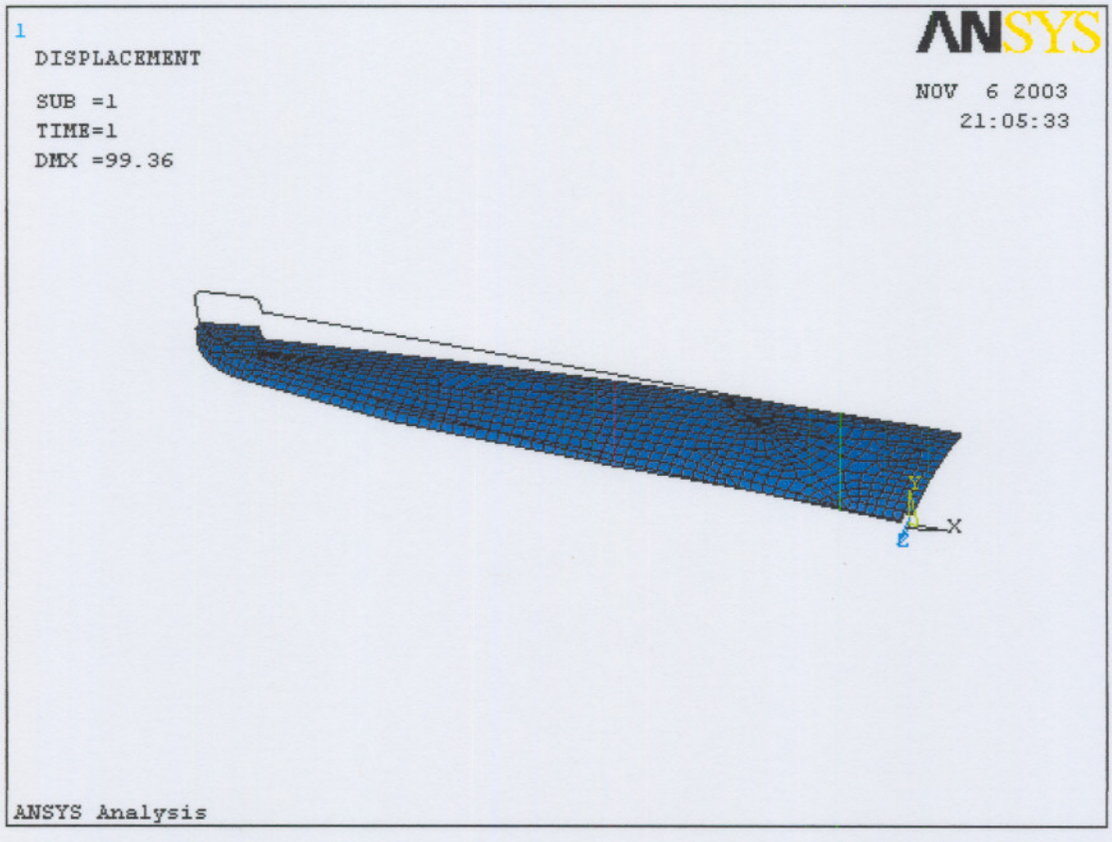

Deformed Shape

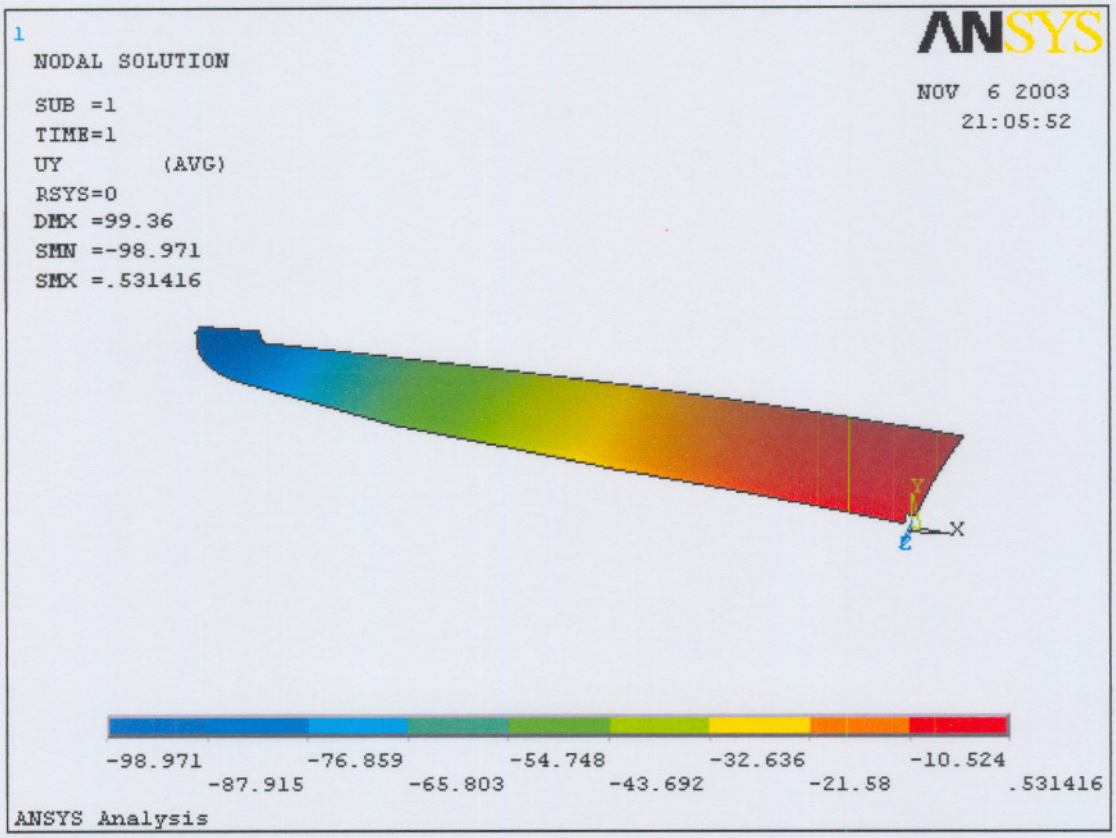

Translation

Skin Lay-up

Layer Number	Material Type	Material Thickness	Material Direction
1	Woven Glass	0.06417	0
2	Woven Glass	0.06417	0
3	Woven Glass	0.06417	0
4	Woven Kevlar	0.04236	45
5	Foam Core	5	-
6	Unidirectional Carbon	0.0767	0
7	Unidirectional Carbon	0.0767	0
8	Unidirectional Carbon	0.0767	0
9	Woven Kevlar	0.04236	45
10	Woven Glass	0.06417	0
11	Woven Glass	0.06417	0
12	Woven Glass	0.19444	45

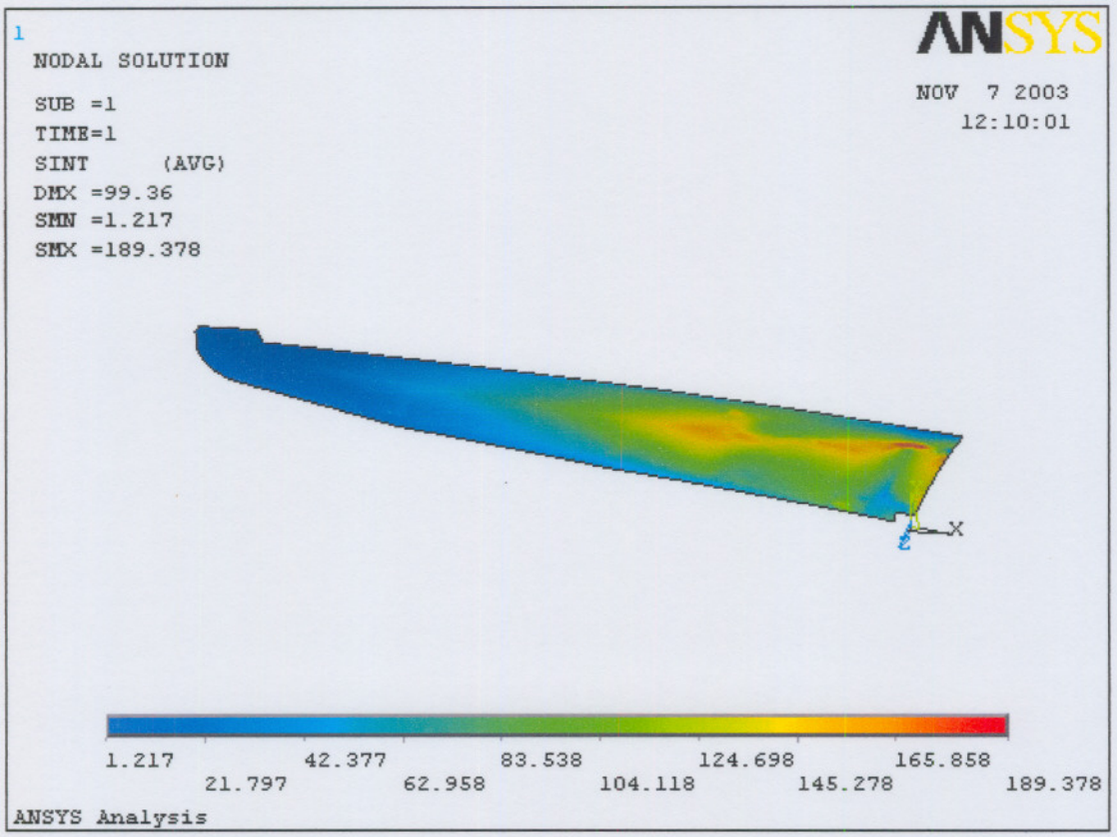

Stress Intensities - Top Skin Layer 1

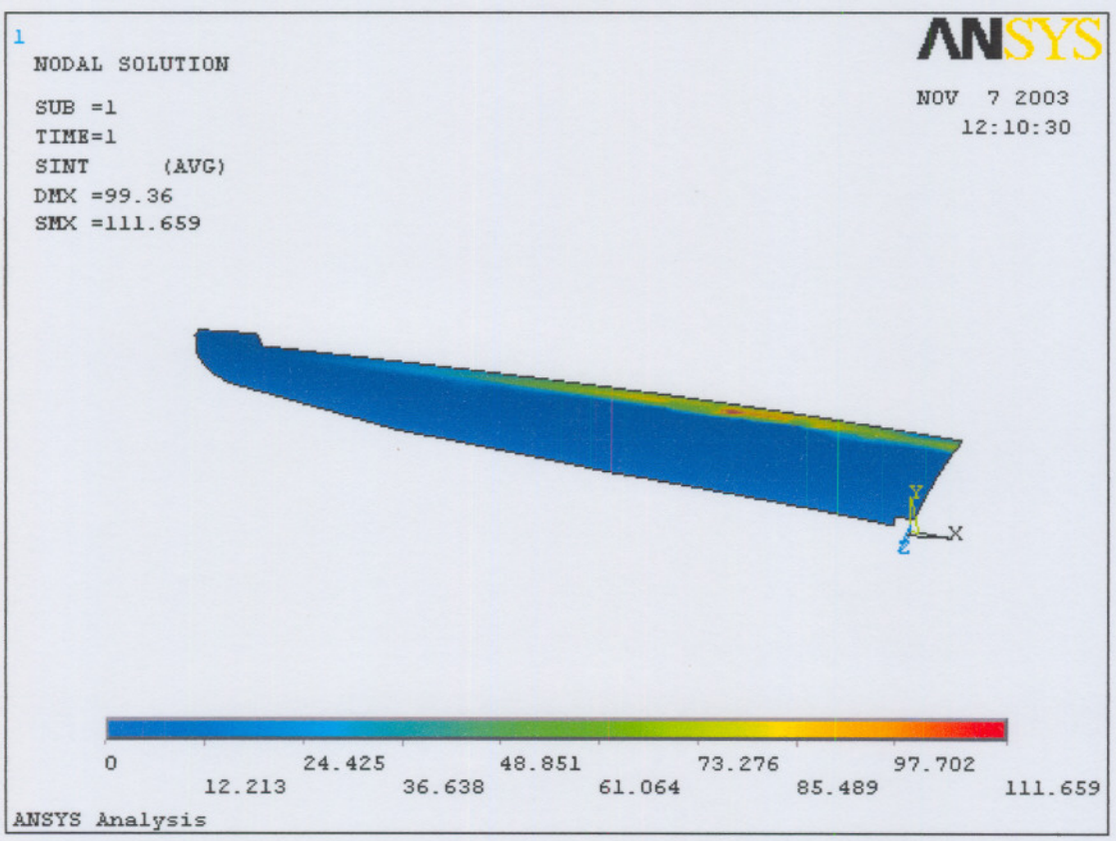

Stress Intensities - Top Skin Layer 2

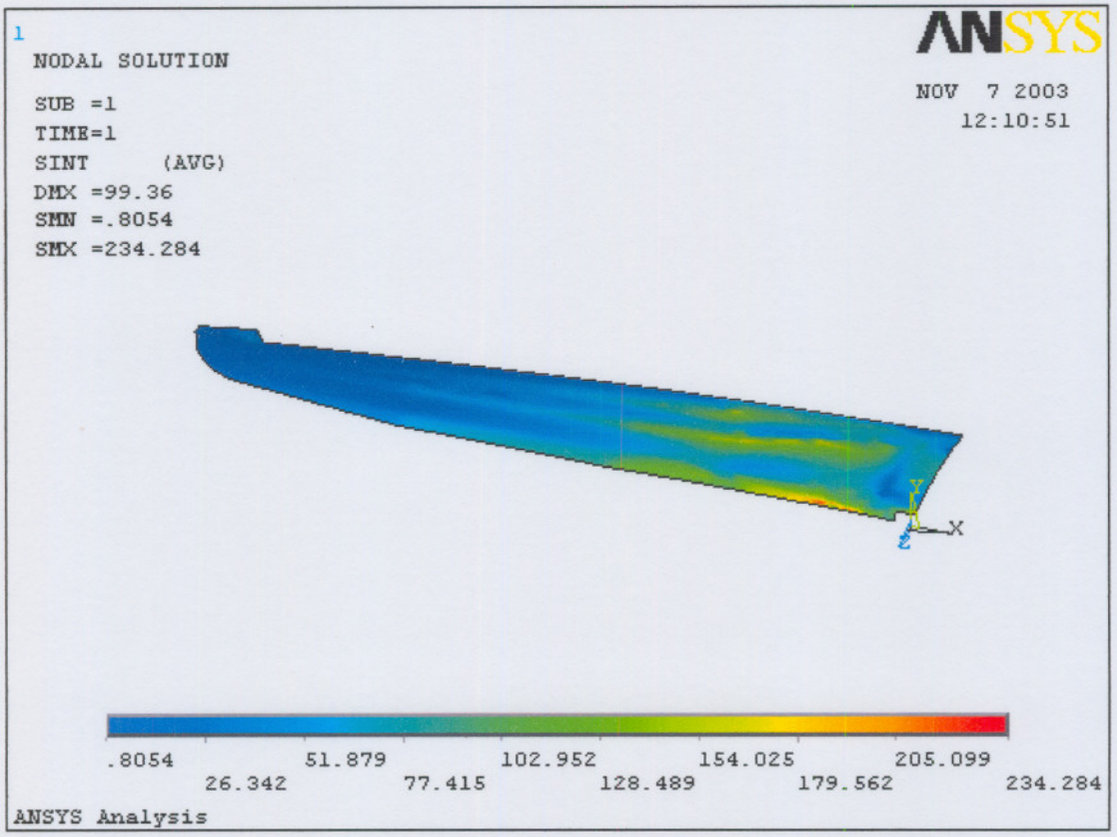

Stress Intensities - Top Skin Layer 4

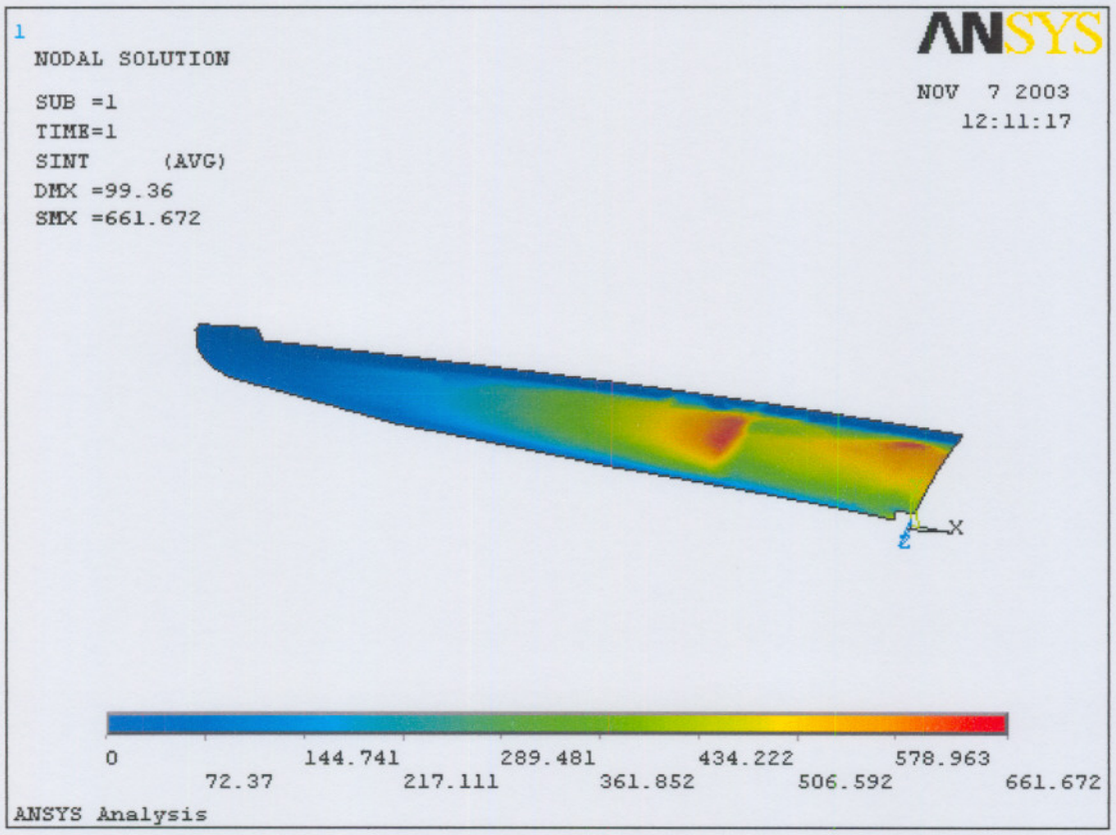

Stress Intensities - Top Skin Layer 6

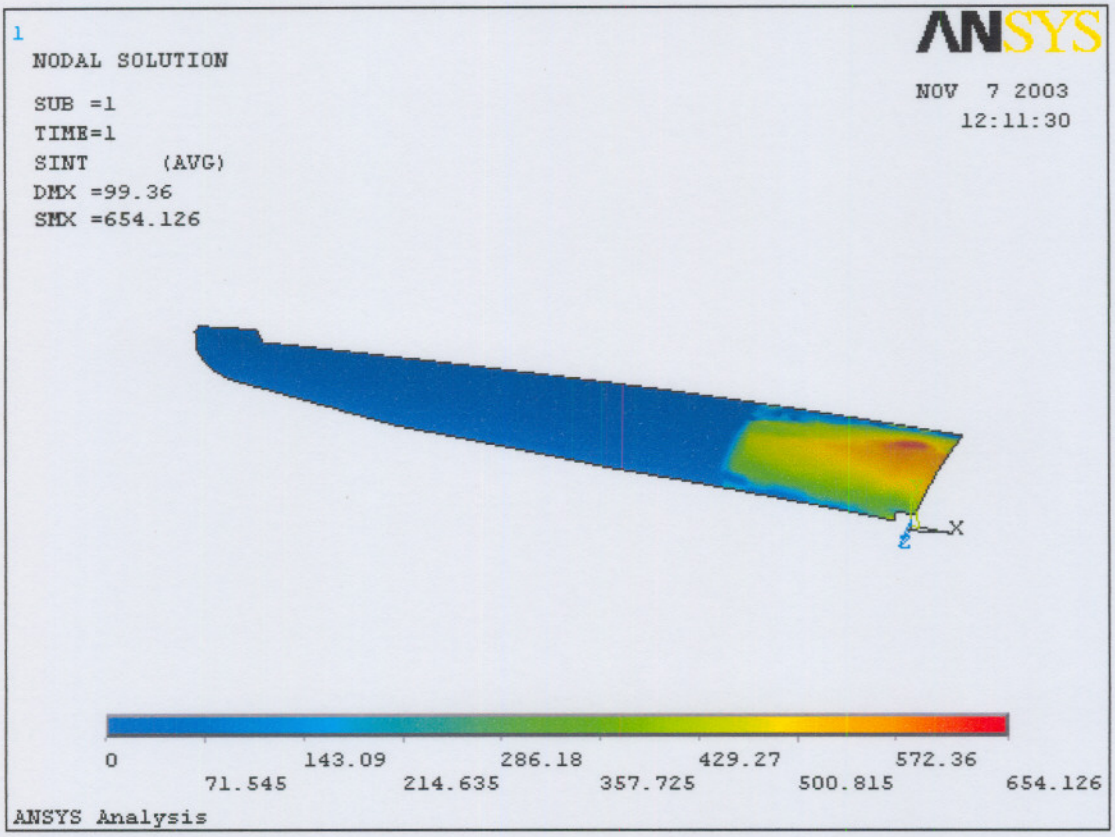

Stress Intensities - Top Skin Layer 8

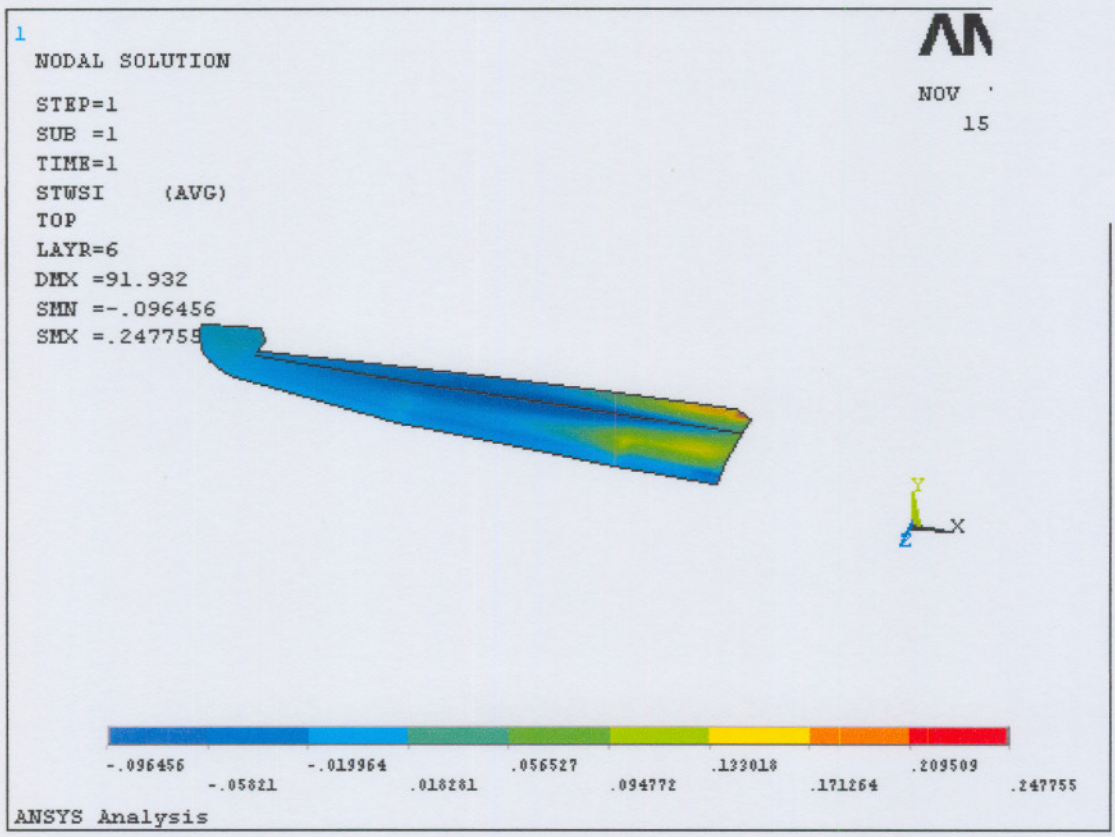

Tsai-Wu Failure Criteria - Top skin Carbon Flange

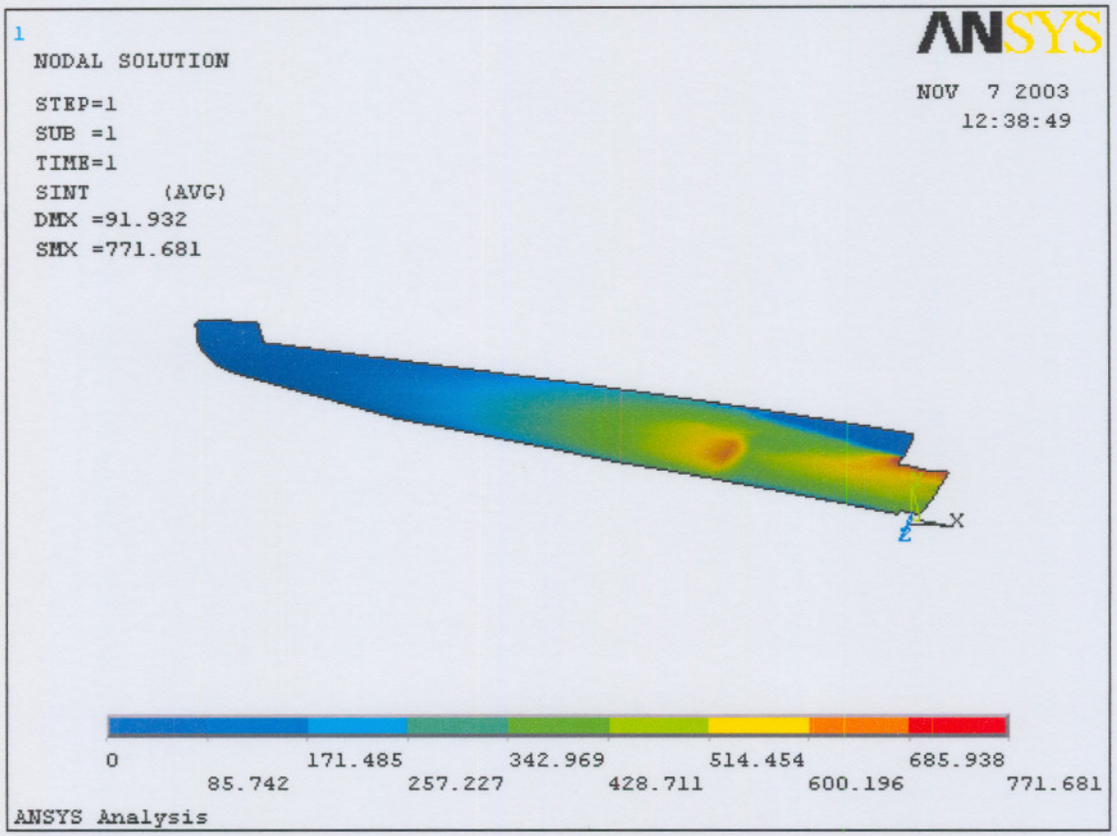

Stress Intensities - Bottom Skin Layer 6

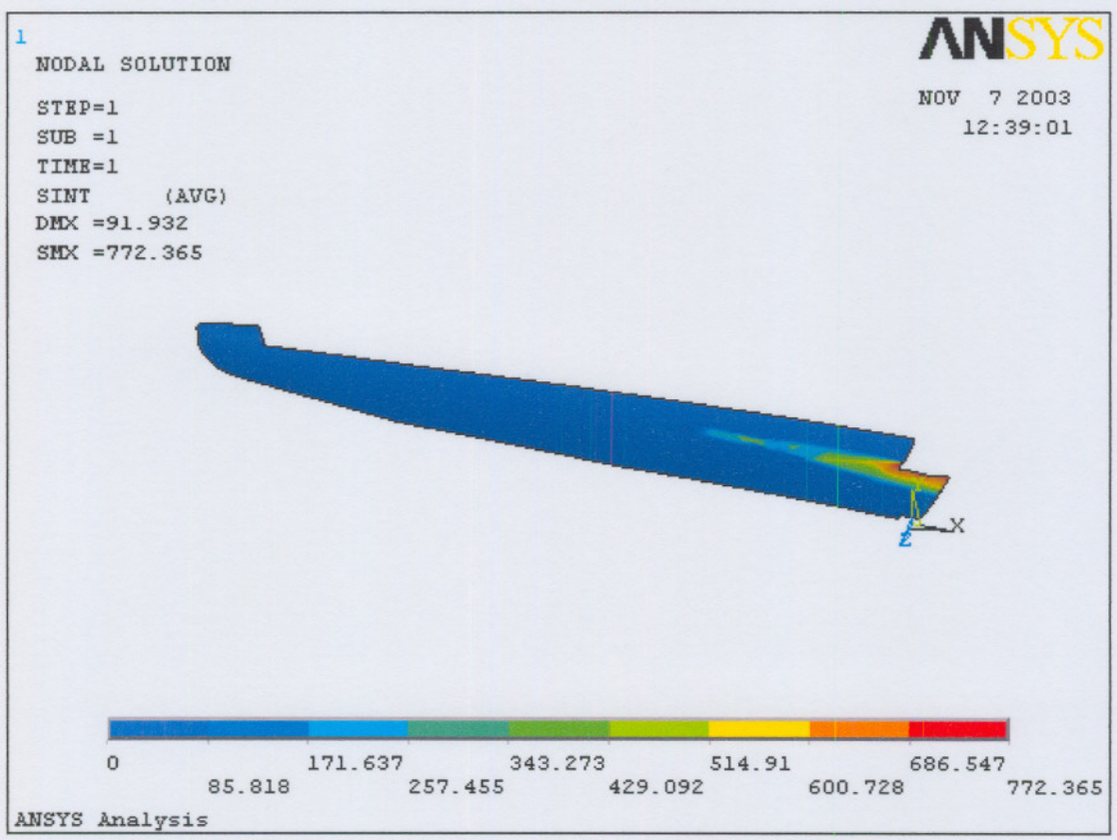

Stress Intensities - Bottom Skin Layer 7

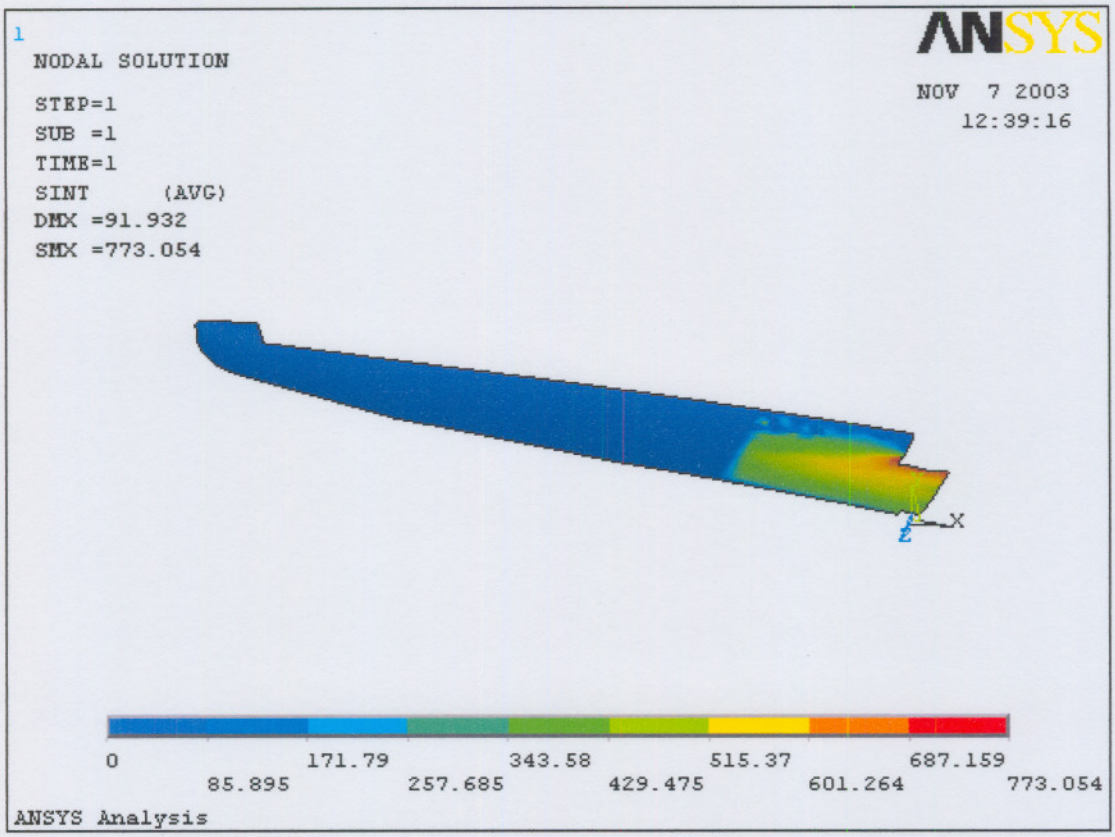

Stress Intensities - Bottom Skin Layer 8

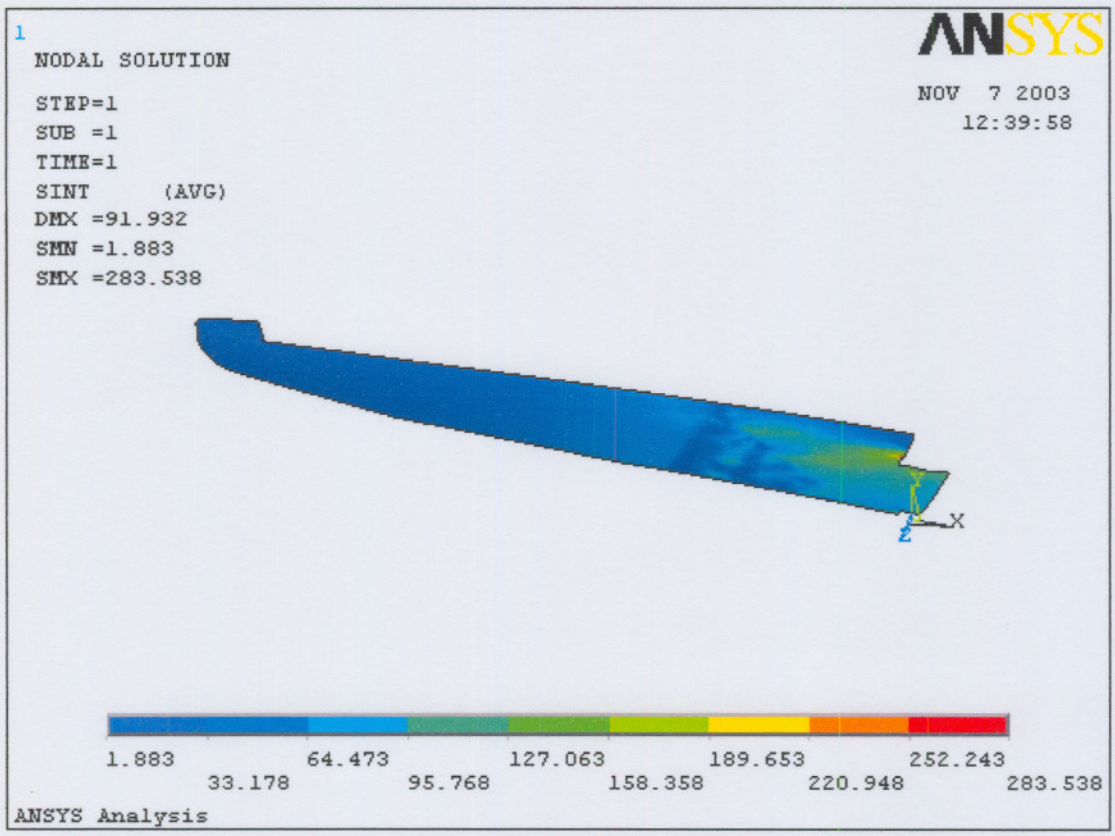

Stress Intensities - Bottom Skin Layer 12

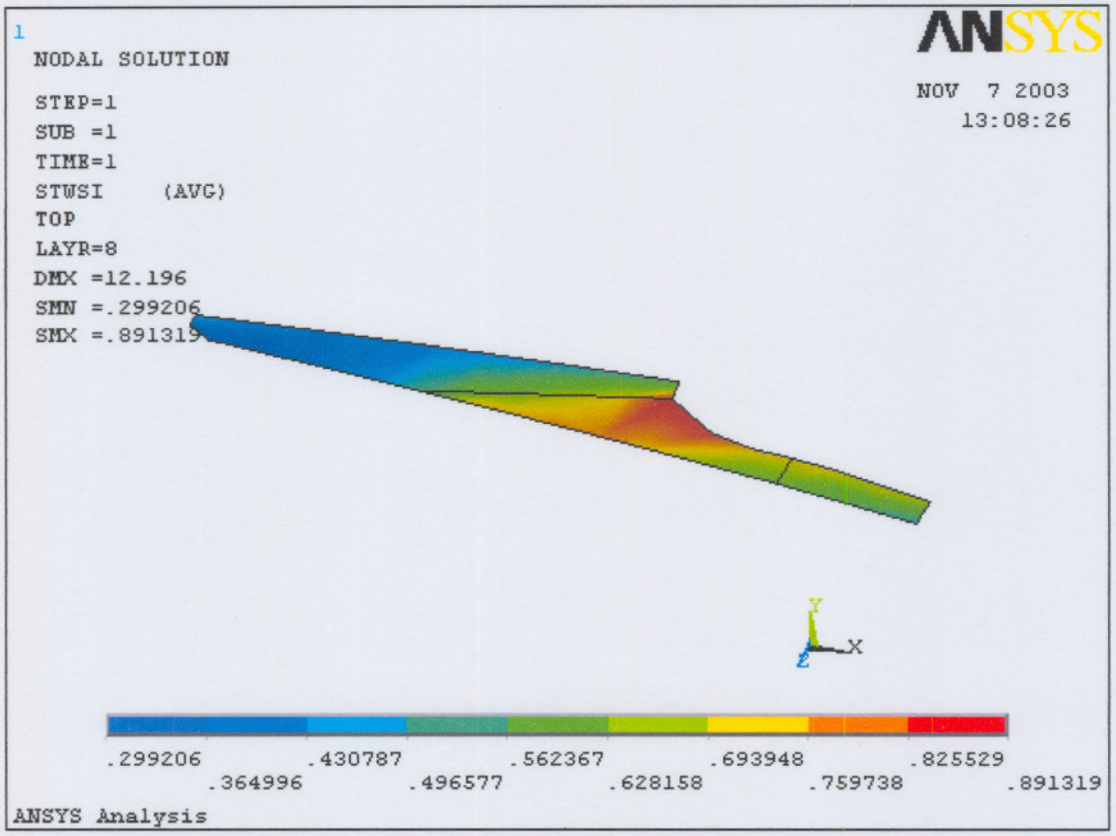

Tsai-Wu Failure Criteria - Bottom Skin Carbon Flange

Shear Web Lay-up

Layer Number	Material Type	Material Thickness	Material Direction
1	Woven Glass	0.06417	0
2	Woven Glass	0.19444	45
3	Foam Core	5	-
4	Woven Glass	0.19444	45
5	Woven Glass	0.06417	0

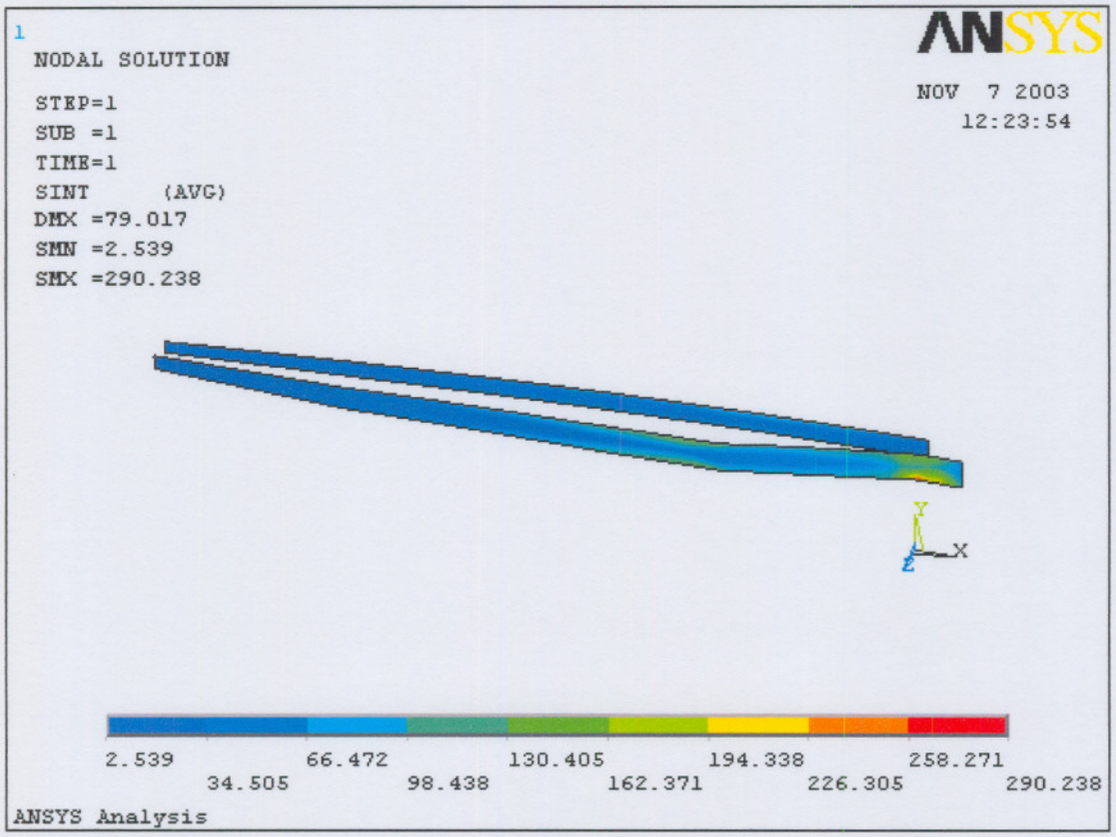

Stress Intensities - Shear Web Layer 1

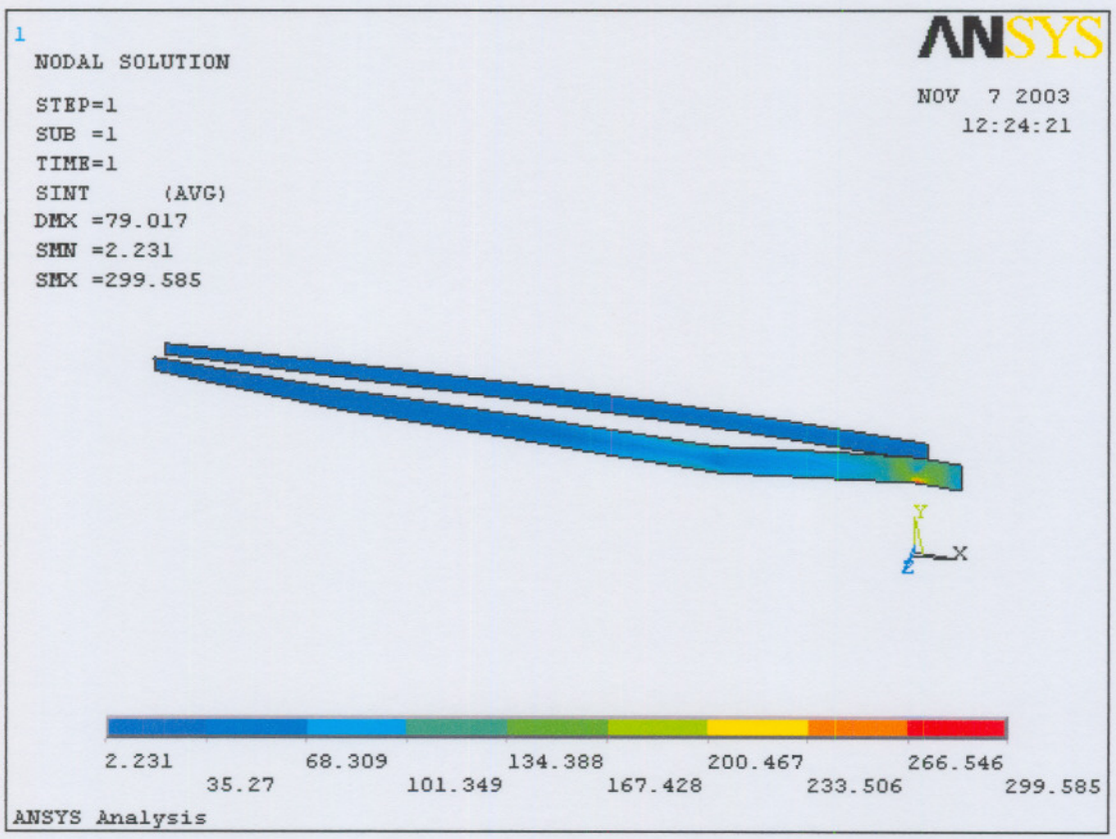

Stress Intensities - Shear Web Layer 2

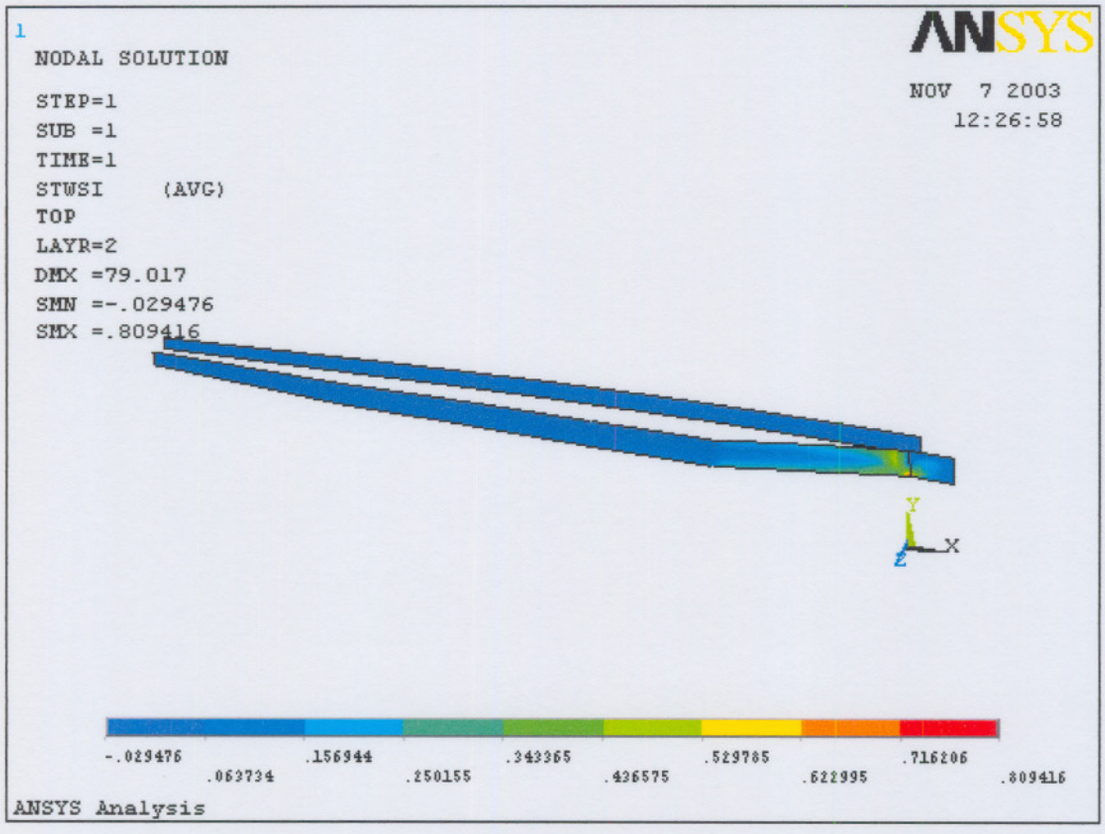

Tsai-Wu Failure Criteria - Shear Web Layer 2

APPENDIX C:

ANSYS ANALYSIS OF MANUFACTURED TAILPLANE

A brief report on the tailplane which was manufactured for the verification of the analysis process is given in this section.

TAIL PLANE FOR VERIFICATION - ANSYS ANALYSIS

By G.C. Kühn

November 06, 2003

Report Generated by ANSYS

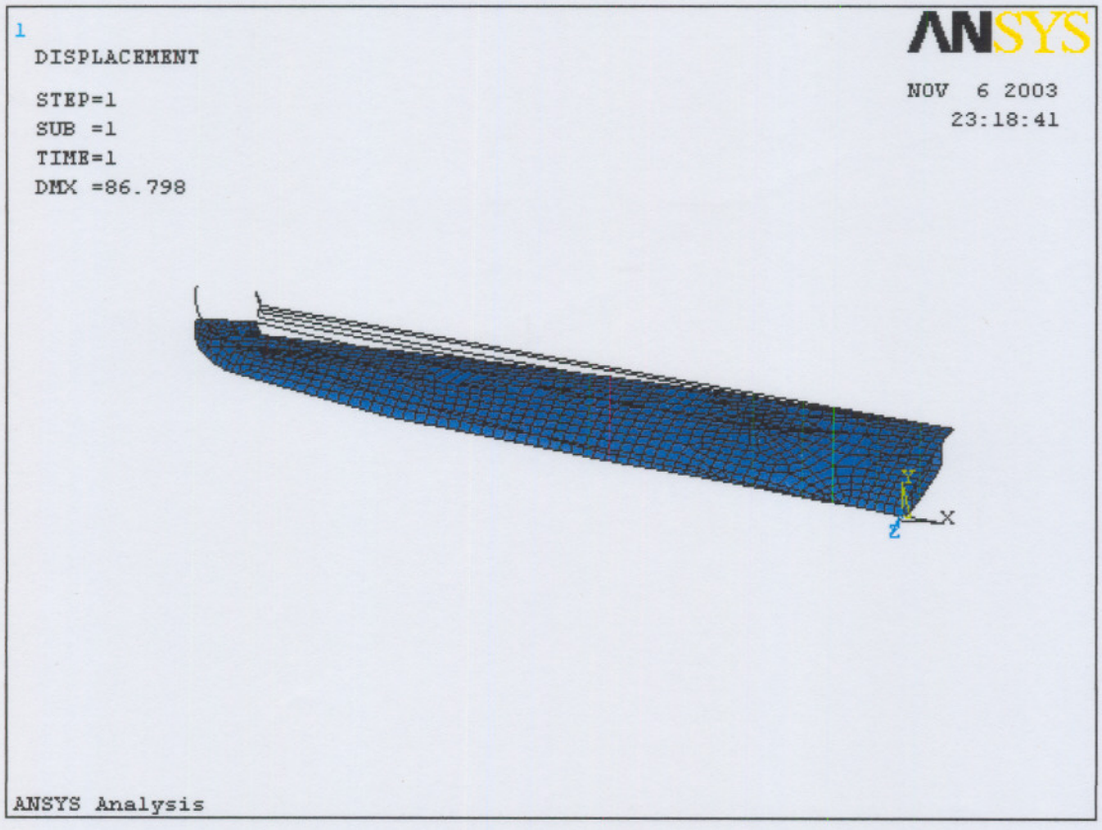

Deformed Shape

Skin Lay-up

Layer Number	Material Type	Material Thickness	Material Direction
1	Woven Glass	0.06417	0
2	Woven Glass	0.06417	0
3	Woven Glass	0.06417	0
4	Woven Kevlar	0.04236	45
5	Foam Core	5	-
6	Unidirectional Carbon	0.12222	0
7	Unidirectional Carbon	0.12222	0
8	Unidirectional Carbon	0.12222	0
9	Woven Kevlar	0.04236	45
10	Woven Glass	0.06417	0
11	Woven Glass	0.06417	0
12	Woven Glass	0.19444	45

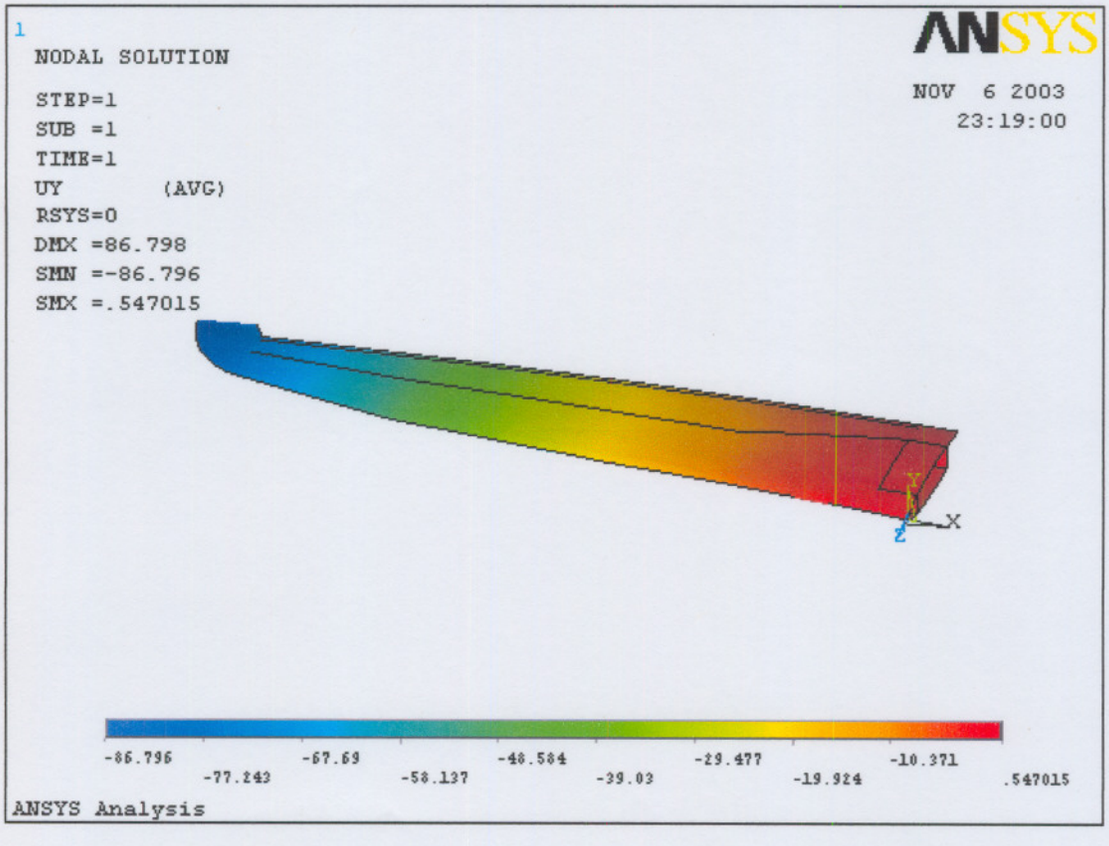

Translation